ELECTRICALLY CONDUCTIVE POLYMERS FOR THE USE AS NOVEL PIGMENTS IN ADVANCED COATINGS

A Dissertation
Submitted to the Graduate Faculty
of the
North Dakota State University
of Agriculture and Applied Science

By

Joseph Robert Byrom

In Partial Fulfillment of the Requirements
for the Degree of
DOCTOR OF PHILOSOPHY

Major Department:
Coatings and Polymeric Materials

April 2017

Fargo, North Dakota

North Dakota State University
Graduate School

Title

ELECTRICALLY CONDUCTIVE POLYMERS FOR THE USE AS NOVEL PIGMENTS IN ADVANCED COATINGS

By

Joseph Byrom

The Supervisory Committee certifies that this ***disquisition*** complies with North Dakota State University's regulations and meets the accepted standards for the degree of

DOCTOR OF PHILOSOPHY

SUPERVISORY COMMITTEE:

Dr. Victoria Johnston Gelling
Chair

Dr. Erik Hobbie

Dr. Andriy Voronov

Dr. Dean Webster

Approved:

April 24, 2017
Date

Dean Webster
Department Chair

ABSTRACT

With the push to more environmentally friendly materials to solve some of the biggest challenges in the coatings industry, electrically conductive polymers (ECPs) are seen as a flexible solution due to their unique properties. ECPs are seen as an attractive substitute to the current metallic materials used in applications such as printable electronics, anti-static protection, and corrosion mitigation. Polypyrrole (PPy) is seen as a popular class of ECPs due to its inherent high electrical conductivity, resistance to environmental degradation, and ease of synthesis.

The first part of this work was to study the ability of polypyrrole to be synthesized through a novel photochemical process. This method eliminated the need to stabilize particles in a suspension and deposit an electrically conductive film onto a variety of substrates. The second part of this work was to synthesize functional versions of PPy that could further be crosslinked into the coating matrix to improve bulk physical properties through better interaction between the functional filler and the organic coating matrix. The last part of this work is based off prior work at NDSU on AL-flake/PPy composites. This study took the development of these pigments further by incorporating organic anions known to inhibit corrosion and study their efficacy.

Advanced analytical methods such as Conductive Atomic Force Microscopy was used to study the electrical properties of PPy. In addition, advanced electrochemical tests such as Electrical Impedance Spectroscopy (EIS), Scanning Vibrating Electrode Technique (SVET), Linear Polarization (LP), and Galvanic Coupling (GP) were conducted alongside traditional accelerated weathering techniques such as ASTM B117 and GM 9540 to determine the corrosion resistance of the synthesized coatings.

ACKNOWLEDGEMENTS

First and foremost, I would like to thank Dr. Victoria Gelling for giving me the opportunity to join her lab as a graduate student, her advice and guidance over the years has helped me become more knowledgeable in the field of polymers and coatings.

Secondly, I would like to thank my committee members for setting aside time to thoroughly critique my work and push me to better understand the research I conducted. Their dedication to challenging me throughout this experience has paid off immensely.

Thirdly, I would like to thank Heidi Docktor, Scott Payne, and Jayma Moore for all of their assistance in the characterization studies performed to complete this dissertation. I would also like to thank the rest of the Gelling lab: Abhijit Suryawanshi, Niteen Jadhav, Kiran Bhat Kashi, Drew Pavlacky, Chris Vetter, and Kenneth Croes for all of their help in my studies.

Lastly, I would like to thank my family for pushing me achieve this degree, Stacy Sommer for giving me the motivation to apply at NDSU after my wonderful experience in the CPM's Summer SURE program, and my undergraduate advisor Dr. John Texter at Eastern Michigan University for helping build a solid foundation of knowledge in polymers and coatings.

TABLE OF CONTENTS

LIST OF TABLES

LIST OF FIGURES

CHAPTER 1. INTRODUCTION

1.1. Introduction

Polymeric materials have exploded in use over the past 110 years due to their ability to be tailored to the situation. In the coatings world, solvent borne alkyd coatings have been replaced by epoxy-amine, urethane, melamine-formaldehyde, and other types for drastically improved performance and operational properties. In addition, more environmentally friendly coating systems have been developed resulting in less volatile organic compound (VOCs) containing coatings even down to zero VOC coating systems such as UV-curable and powder coating technologies.

In addition to improving coating technologies, polymeric materials have been utilized to replace conventional materials in various applications. Polymers have been used great extent to replace metal components due to the higher strength to weight ratio, resistance to corrosion, and overall cost reduction. Advanced polymeric composites now replace metal in areas such body armor and structural components in the aerospace industry just to name a few examples.

While the physical properties are advantageous for many applications, the electrically resistive nature of most polymeric materials limits their uses in the electronic industry. Since the first electrically conductive polymer (ECP), polyacetylene was discovered by Shirakawa et al. accidentally in the 1970s, rapid advancement in the development of electrically conductive polymers has been accomplished.[1] For Shirakawa's work pioneering the development of ECP's he was awarded the Nobel Prize in 2000. Since the discovery of doped polyacetylene, other ECPs have been discovered and researched extensively. Of these, the most popular today due to ease of synthesis, high conductivity, and long-term stability are polypyrrole, polyaniline, and polythiophene. The structures for these ECPs are shown in Figure 1.1.

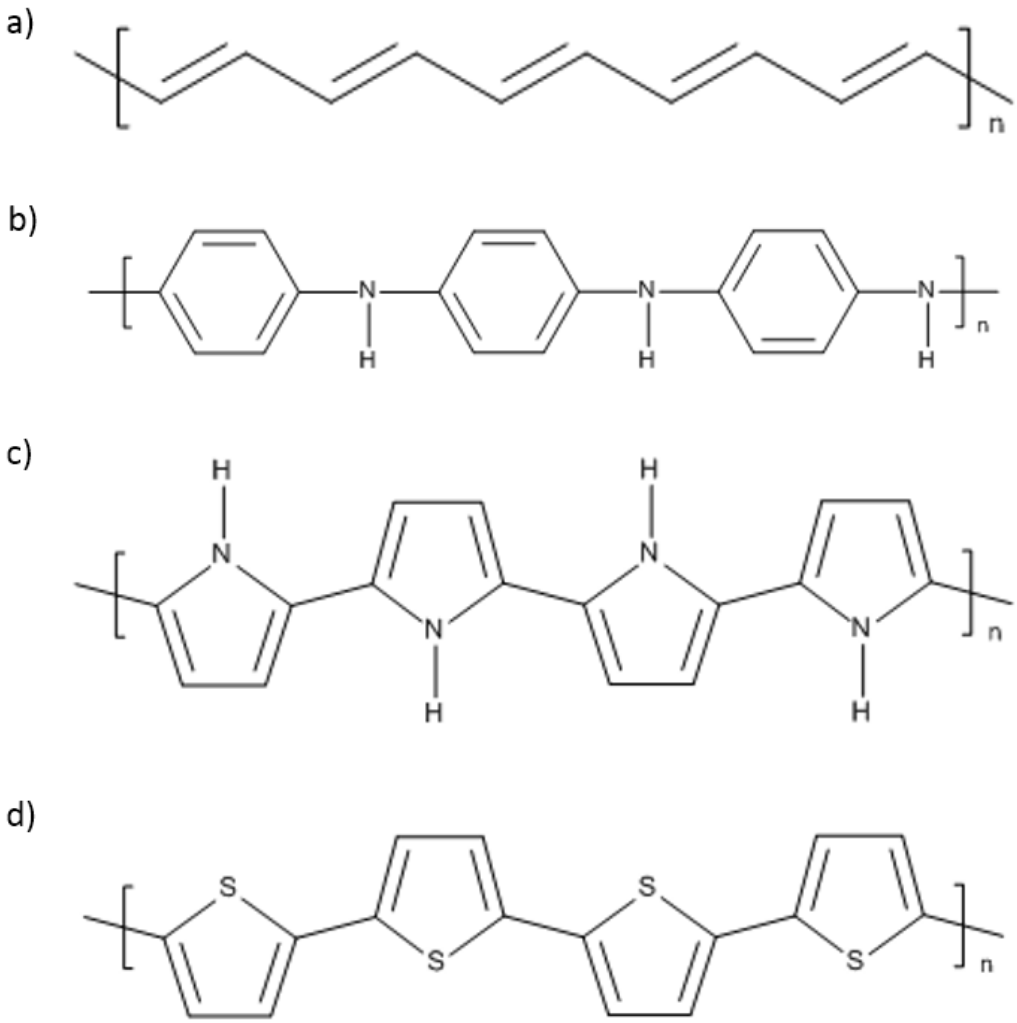

Figure 1.1: Common ECPs under investigation: a) polyacetylene, b) polyaniline, c) polypyrrole, and d) polythiophene.

ECPs can be synthesized via two mechanisms: electrochemical polymerization or through chemical oxidation.[2, 3] Electrochemical polymerization of ECPs yields high molecular weight films of conductive polymers that display high levels of conductivity. Electrochemical synthesis is extremely effective in coating metal parts in uniform ECP films. Chemical oxidation of ECP monomers is a simple, inexpensive process that can be used to synthesize ECPs in a variety of morphologies and particle sizes. Common chemical oxidants such as ammonium persulfate and

ferric chloride are extremely effective at oxidizing ECP monomers to form high molecular weight ECPs that can be further used in various applications.[4]

The mechanism of polymerization of ECPs is unlike the conventional polymerization methods of free radical and step growth polymerization.[5] Below, in Figure 1.2, the mechanism of polymerization of polypyrrole is shown. This mechanism begins with an oxidizing agent abstracting an electron from the pyrrole monomer forming a pyrrole cation radical. These cation radicals can further combine with one another forming a dimer. The dimer can further be oxidized into pyrrole dimer cation radical. This process continues to repeat until high molecular weight polypyrrole is formed.

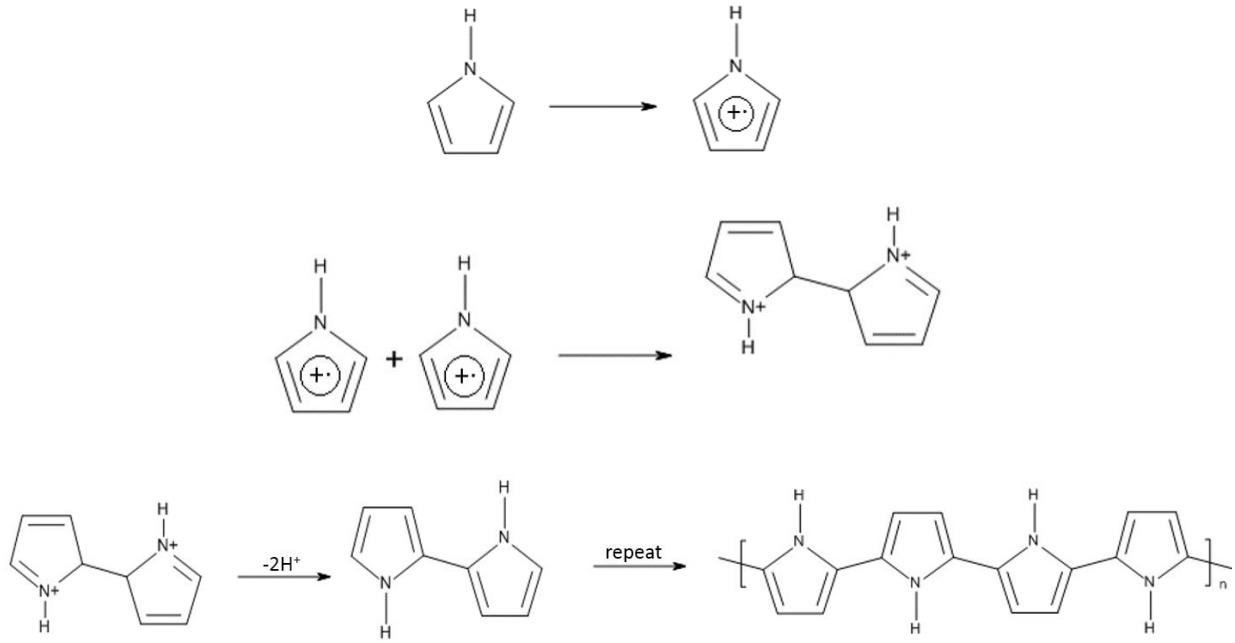

Figure 1.2: Mechanism of the polymerization of pyrrole.

ECPs can exist in three different states, neutral, oxidized, and reduced forms.[6] Reduced forms of ECPs are either resistive or show a semiconductor like nature. This ability to exist as a semiconductor is due to the long range conjugation within the polymer backbone. To act as a semiconductor in this neutral form the molecular weight is fairly large. The oxidative form is

accomplished by the removal of electrons (oxidation) from the π backbone, a process also known as p-doping.[6] This process was first used to dope polyacetylene with iodine resulting in an electrically conductive polymer with a conductivity of 10^{-5} to 10^{3} S·cm depending on the level of oxidation.[1] The two different states of polypyrrole are depicted in Figure 1.3. To achieve this doping effect, the presence of counterions in solution during polymerization is needed. These counteranions (NO_3^- for example) form a ionic interaction with the positive charges that result in being in a bipolaron state.

The electrical conductivity of ECPs has been thoroughly studied to determine how electrons move on the backbone of the polymer.[7-10] Polypyrrole, for example, relies on the existence of polarons and bipolarons to act as the charge carriers to allow electrical conduction. Electron spin resonance studies by Scott et al. showed evidence of bipolarons existing in the oxidized state of polypyrrole. This theory was later expanded upon to include evidence of polarons also existing within the polypyrrole backbone.[8] The polaron state is an intermediate state that coexists in oxidized polypyrrole.[11] These structures are shown in Figure 1.3.

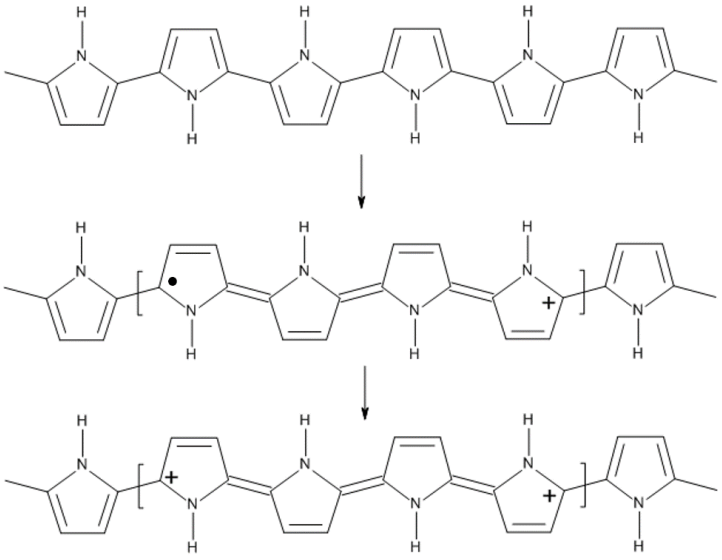

Figure 1.3: Different states of polypyrrole. Top: reduced, middle: polaron, and bottom: bipolaron.

Within the past three decades. these studies have helped map the intrinsic properties of these conductive polymers. ECPs have since been then explored as possible replacements in a variety of electronic applications including: printable electronics, photovoltaics, electrical sensors, antistatic and electromagnetic interference (EMI) coatings, and corrosion inhibition.[12-22] Of these ECPs, polypyrrole has shown great promise on the areas of printable electronics, antistatic and EMI coatings, as well as corrosion inhibition. Polypyrrole shows great promise in these areas due to long term environmental stability of the electrical properties, great temperature stability, ease of synthesis, and tailorable conductive properties based on reaction parameters.[2, 23-26]

1.2. Electrically Conductive Polymers for Printable Electronics

One of the areas where ECPs have grown momentum is in the development of printable electronics. Rapid printing of electronics is seen as the next generation in computer chip manufacturing due to the possibility of rapid production, lower cost substrate availability, and overall economics.[27] Current electronic chip manufacturing is only economically friendly with mass production of simplistic chip design. Printable electronics based on an ink-jet platform would allow an economical option to small volume production as well.

Currently, the traditional method of production for computer chips is based on "subtractive technology" as illustrated in Figure 1.4. This subtractive technology is inferior to the idea of "additive technology" (illustrated at the bottom of Figure 1.4). Subtractive technology requires multiple steps and the use of expensive materials/processes to get the finished product. Additive technology only requires the addition of the appropriate materials in the right pattern/places. The elimination of the extra steps is extremely attractive from a manufacturing standpoint, due to reduction in overall manufacturing time. In addition, eliminating the need for extra raw materials

limits the waste per each computer chip manufactured, as well as eliminating the use toxic etching materials used in the current process.

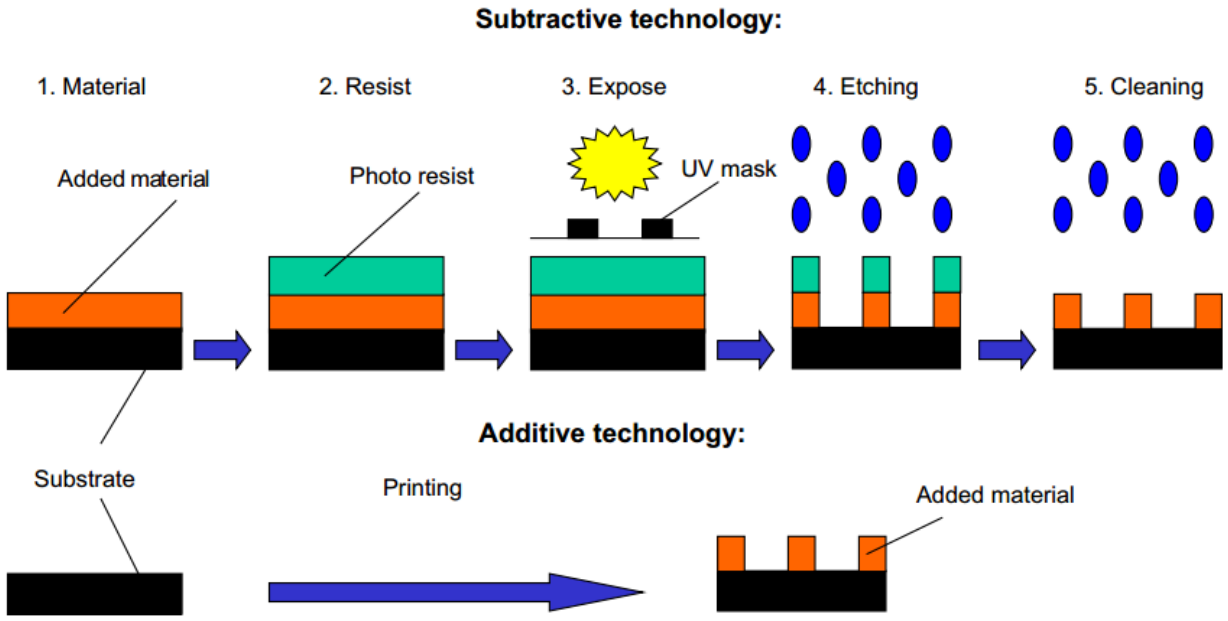

Figure 1.4: Subtractive (top) and additive (bottom) technologies currently being used in computer chip manufacturing. Reprinted from Ref [27] (Journal of Cleaner Production, 17(9) Kunnari, E., J. Valkama, M. Keskinen and P. Mansikkamäki, Environmental evaluation of new technology: printed electronics case study. (791-799, 2009). with permission from Elsevier

Printable electronics, through this additive technology method, require the deposition of an electronically conductive material in a predefined pattern. Initial printable electronics focused on the development of silver inks, which consisted of silver nanoparticles suspended in water/solvent solution. Silver inks have been successfully demonstrated as suitable printing inks for printable electronics.[28, 29] Silver inks, however have disadvantages as well, including the high cost, poor long term stability of the silver dispersions, and the long term inertness of silver nanoparticles.[30] Other materials such as copper nanoparticles, graphene, and even liquid metal alloys have also been studied and have seen reasonable success.[31-33]

ECPs are seen as an attractive substitute to conventional metal nanoparticle dispersions for printable electronics due to stability of their dispersions, as well as lack of high temperature needed to form a uniform conductive network. For example, silver inks require a sintering temperature of over 400°C, which is not feasible for printing on most substrates that printable electronics are designed from. Stable, polyaniline nanoparticle dispersions have been synthesized in the presence of dodecyl-benzenesulfonic acid.[34] When printed onto paper substrates, these nanoparticle dispersions were shown to be able form high resolution patterns in a standard ink-jet printer and the resulting dried inks had bulk conductivity of 0.8 $mS \cdot cm^{-1}$. Polythiophene dispersions have also been studied as a suitable conductive material in the development of printable gas sensors.[35]

The current drawback of ECPs for printable electronics, however, is the ability to achieve conductivity similar to metals as well as long term stability of ECP dispersions. New synthesis methods involving ozone has allowed the ability to synthesize controlled PPy dispersions of nanoparticles that have shelf lives greater than a month.[36] Other methods such as deposition of pyrrole solutions on substrates and then polymerizing them has also been studied and could show promise as this alleviates the dispersion issue entirely.[37, 38]

1.3. Electrically Conductive Polymers for Electrical Protection

As electronics are being pushed into more and more devices, the market of effective anti-static coatings has grown considerably. Static electricity can be extremely damaging to sensitive electronics, due to the buildup of electrons on a non-conductive surface due to the triboelectric effect. A common example of static electricity damage is the destruction of navigation equipment on air planes. Planes can routinely see surface charges of upwards of 1 million volts appear during flight, thus sufficient protection is needed. Conventional protection against static electricity discharge and lightning strike protection revolves around the use of copper and other metal meshes

to protect the aircraft.[39] Major drawbacks for this tech exist, the first is the high density of metals (8.96 g/cm^3 for copper) as well as the ability for the copper mesh to cause galvanic corrosion. This issue is the most significant as it requires the mesh to be embedded into an organic resin to ensure it does not come into contact with the metal substrate. Advancements into lower the overall density of suitable materials as well as combat the corrosion issues has developed carbon fiber based materials, but the cost of these limits it from an economical advantage.[40]

ECPs are heavily being investigated for replacement of these traditional materials as anti-static coatings require bulk resistances in the semiconductor range compared to printable electronics which requires a much higher bulk conductivity. Since 1990, patents involving ECPs have been issued in regard to the development of organic coatings that provide anti-static protection.[41-44] In addition, conductive polymers such as polypyrrole and polyaniline have shown promise as conductive additives to epoxy resin in having the ability to effectively bleed off charges from simulated lightning strikes.[45, 46]

Anti-static coatings have shown even greater promise for ECPs. Polyaniline infused thermoplastic composites have shown anti-static behaviors even at loadings around 10 wt%.[47] PPy has also been successfully embedded in thermoplastic composites for anti-static protection, although levels required for effective anti-static protection was in the range of 17 weight%.[48] PPy has also been incorporated in the development of conductive latex coatings by encompassing latex particles in a thin PPy shell.[49] This method requires only around 1 wt% of PPy in the final polymer composition yet the surface resistance of the cured latex film is 1E6Ω, which is in the realm of efficient static discharge.

ECPs have also shown great promise as coatings or coating additives in electromagnetic interference (EMI) coatings.[50] EMI shielding is becoming more important with technology

continuing to take a more central role in society. EMI shielding requires an effective electrically conductive "shield" to protect the sensitive electronics underneath.[51] ECP based coatings and composites can display surface conductivities suitable for EMI shielding application. PPy coated fabrics have shown to ability to offer protection up to 80db.[52] This level of protection is suitable for military EMI shielding.

1.4. Electrically Conductive Polymers for Corrosion Protection

Possibly the most sought-after applications for conductive polymers not including OLED displays is in the realm of corrosion inhibition of metal and metal alloys. It is estimated that the United States alone spent an estimated 1.2 trillion dollars in 2002 alone either protecting metal and metal alloys from corrosion or replacing materials damaged from corrosion.[53] This correlates to about 11% of the total GDP in 2002. Corrosion is a naturally occurring phenomenon forcing metals into the more thermodynamically stable oxidized state. Metal oxides do not have the mechanical properties that the reduced metals do, thus it is not desirable for this to occur. Corrosion of metallic materials can lead to catastrophic failures such as the Minneapolis I-35W bridge collapse.[54]

There are two types of corrosion protection that materials can provide: active and inactive corrosion mitigation. Inactive corrosion mitigation primarily focuses on not allowing corrosive media from reaching the metals surface. Organic coatings deposited on metal offer protection by acting as a barrier from electrolytes reaching the substrate surface. While organic coatings offer excellent barrier protection, they are not impervious to moisture penetration. Once moisture penetrates the organic coating layer and reaches the metal surface, corrosion begins. Adhesion of organic coatings to metal oxides is poor thus resulting in coating delamination and further failure.

Inactive corrosion mitigation is the most popular method of corrosion protection due to the low cost.

Active corrosion mitigation focuses on hindering the chemical reactions that occur when metals corrode. This can be accomplished by a variety of means. Galvanic protection is an effective tool in long term protection of metal.[55] Galvanic protection forces the metal substrate being protected to act as the cathode in an electrochemical redox cell, thus hindering corrosion. This galvanic protection occurs when connecting the substrate in question to a less noble material. This less noble material acts as a sacrificial anode and sacrificially corrodes. As long as there is still a sacrificial anode, galvanic protection can still occur. This technique has been applied extensively in the protection of steel pipes along with traditional organic coatings to provide long term protection. Cathodic protection however, is quite expensive, due to either requiring a constant electrical current to protect the substrate, or through the means of using sacrificial anodes which need to be replaced at regular intervals of the lifetime of the system.

Galvanic protection can also be accomplished through the addition of sacrificial materials in organic coatings. Zinc-rich primers are extremely popular for the protection steel substrates.[56] Zinc-rich primers are epoxy coatings loaded above the critical pigment volume concentration. This ensures the zinc pigment forms a fully conductive network within the coating system allowing it to sacrifice itself instead of the underlying steel substrate. This methodology has also been applied to magnesium rich primers for the protection of aluminum alloys in the aerospace industry.[57, 58] While both effective methods to offer an active corrosion mitigation method, coatings derived from this technology are very expensive, and hazardous to produce.

Electrically conductive polymers have shown great promise in the protection of a variety of metals and metal alloys.[59-62] Polypyrrole has been especially studied extensively for the

protection of aerospace aluminum alloys.[21, 63] Polypyrrole is seen as a possible alternative to chromate based pigments for protecting aerospace aluminum alloys. With the increasing regulations on the use of chromates due to the carcinogenic nature of hexavalent chromates, there is a large demand for materials that can offer protection without the toxicity.

Electrodeposited polyoctylpyrrole (POP) showed improved active corrosion inhibition on Al-2024T3 substrates.[16] These primers while showing active corrosion protection, displayed little in terms of barrier properties, thus a topcoat was required to provide suitable long term protection. Electrochemical Impedance Spectroscopy (EIS) studies showed these primer-topcoat systems maintain a high impedance value even after 545 days of electrolyte immersion, which was comparable to the EIS spectra of a polyurethane-chromated epoxy system (see Figure 1.5).

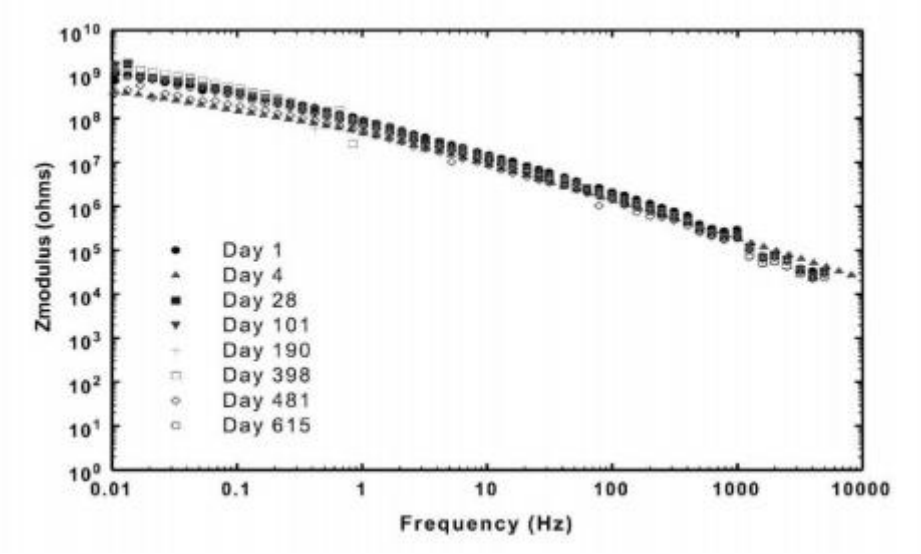

Figure 1.5: EIS spectra of polyurethane/POP coating system. Reprinted from ref [16] (Progress in Organic Coatings, 43(3), V.J. Gelling, M. Wiest, D.E Tallman, G.P. Bierwagen, G.G. Wallace, Electroactive-conducting polymers for corrosion control 4. Studies of poly(3-octyl pyrrole) and poly(3-octadecyl pyrrole) on aluminum 2024-T3 alloy, (149-157, 2001), with permission from Elsevier.

Unfortunately, ECPs by themselves have poor mechanical properties, thus, incorporating ECPs such as polypyrrole and polyaniline as corrosion inhibiting pigments has been extensively

studied.[64-67, 63] Multiple mechanisms for corrosion protection with ECPs have been proposed although the exact mechanism is not currently known. Mechanisms include anodic protection as well as the ability to release corrosion inhibiting anions during reduction processes. Studies of coatings containing polyaniline based pigments showed a passivation effect of steel.[68] This phenomenon was confirmed via XPS and SEM experiments.

Composite based pigments of ECPs and other materials have allowed the development of multifunctional materials.[69, 70] Polypyrrole deposited onto nanoclays allowed the development of active corrosion inhibiting pigments, but also displayed improved barrier properties due to the high aspect ratio of the nanoclays.[71] Previous work by Jadhav et al. demonstrated the development of novel Al-flake PPy composite pigments. These pigments through both electrochemical and accelerated weathering techniques, demonstrated an effective method in protection of Al-2024T3 substrates. Scanning vibrating electrode studies (SVET) showed the ability of coatings containing these pigments to effectively protect an open defect when immersed in an electrolyte solution (see Figure 1.6).[72]

These Al-flake/PPy pigments were also successfully incorporated with inorganic corrosion inhibiting anions such as vanadate, molybdate, and tungstate. The resulting pigment's superiority over Al-flake/PPy composite pigments without these corrosion inhibiting anions indicating possible dopant release from the pigments helping prevent corrosion of the Al-2024T3 substrate. In addition to these findings, the morphology of the PPy deposited on the Al-flake was shown to have a profound effect on the corrosion protection of the underlying substrate.

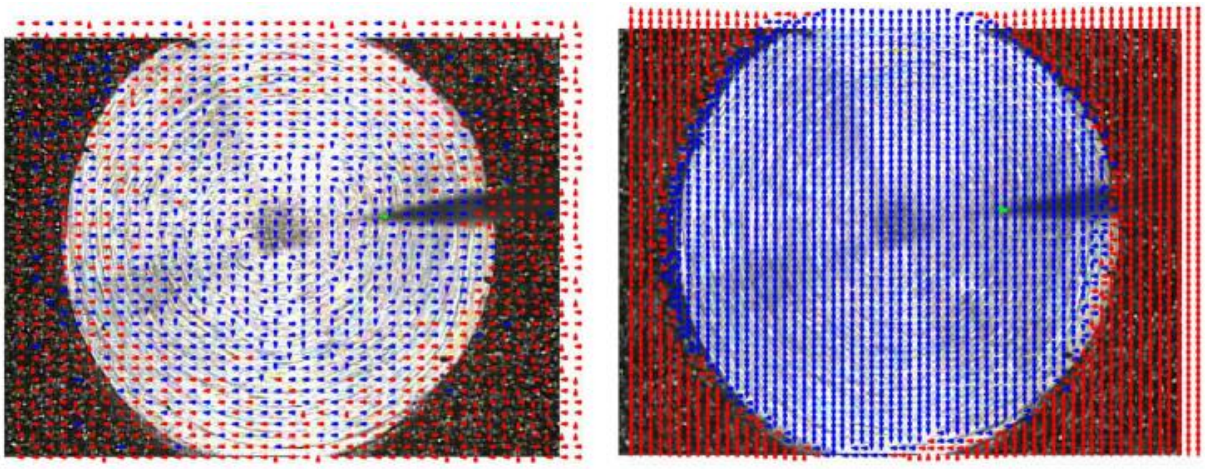

Figure 1.6: SVET Results (current density vectors overlaid onto optical micrographs of a defect in PPy/Al-Flake composite pigmented coatings.) Reprinted from ref [72] (Electrochemica Acta, 102, N. Jadhav, C.A. Vetter, V.J. Gelling, The effect of polymer morphology on the performance of a corrosion inhibiting polypyrrole/aluminum flake composite pigment, (28-43, 2013), with permission from Elsevier.

1.5. Conclusions

ECPs have shown great promise since their discovery three decades ago in supplanting traditional materials. As such there is still a great interest in studying a variety of uses for conductive polymers, especially polypyrrole. In this dissertation, the ECP, polypyrrole, was studied for a variety of uses including printable electronics, anti-statis/EMI shielding, and corrosion protection. In Chapter two, a novel photopolymerization technique of pyrrole to conductive polypyrrole was carried out in combination with UV-curable resins. This work was continued on from Kassi et al. to hopefully develop electrically conductive coatings that demonstrated adequate adhesion to substrates. The resulting work involved the use of a different solvent to obtain homogenous solutions. When these coatings were cured, the resulting coatings demonstrated superior adhesion and electrical properties compared to prior developments. The final properties with PPy content greater than 40% demonstrated the necessary surface resistance required for anti-static application.

Chapter three of this dissertation worked on developing more environmentally friendly versions of these coatings with 100% VOC formulations. Utilizing acrylonitrile, solvent free electrically conductive UV-curable coatings were developed that showed comparable electrical properties to the previously developed solvent borne predecessors. Corrosion studies via accelerated weathering showed poor corrosion inhibiting properties, which were associated with the residual silver nanoparticles that develop during the photo-oxidation of pyrrole to polypyrrole.

Chapter four focused on the ability to improve the corrosion protection of Al-2024 with UV-curable coatings containing crosslinkable polypyrrole. The technique of doping PPy with reactive surfmers allowed the UV-curable matrix to crosslink with the polypyrrole pigments to help improve the polymer-filler interaction which increased the barrier protection properties of the final coatings. Tensile tests demonstrated that coatings containing these surfmers improved the ultimate tensile strength of the final coating compared to coatings containing PPy pigment without surfmers indicating successful crosslinking had occurred.

Chapter five focused on the optimization of the reaction conditions for PPy_SEM, the pigment that showed the best properties when incorporated in the UV-curable matrix. pH during the synthesis showed to not have a profound effect on the resulting corrosion inhibiting processes of these pigments. Coatings containing the PPy pigments showed better corrosion protection than that of control clear coats, indicating the presence of PPy helped protect the Al-2024T3 substrate.

Chapter six focused on expanding upon the work of Jadhav et al. PPy/Al-Flake composite pigments. The new generation focused on the use of organic corrosion inhibitors instead of conventional inorganic corrosion inhibitors. Elemental analysis confirmed the addition of the organic corrosion inhibitors in the synthesized pigments. Coatings containing pigments doped with anthraquinone-2-sulfonate showed a galvanic coupling effect indicating sacrificial protection

was occurring. This was attributed due to the “wire-like” morphology observed on the Al-flake surface.

1.6. References

1. Chiang, C., C. Fincher, Y. Park, A. Heeger, H. Shirakawa, E. Louis, S. Gau and A. G. MacDiarmid, Electrical conductivity in doped polyacetylene. *Physical Review Letters* 1977, 39 (17), 1098-1101.

2. Myers, R. E., Chemical oxidative polymerization as a synthetic route to electrically conducting polypyrroles. *Journal of electronic materials* 1986, 15 (2), 61-69.

3. Yoneyama, H., Y. Shoji and K. Kawai, Electrochemical synthesis of polypyrrole films containing metal oxide particles. *Chemistry Letters* 1989, (6), 1067-1070.

4. Lee, J., D. Kim and C. Kim, Synthesis of soluble polypyrrole of the doped state in organic solvents. *Synthetic Metals* 1995, 74 (2), 103-106.

5. Sadki, S., P. Schottland, N. Brodie and G. Sabouraud, The mechanisms of pyrrole electropolymerization. *Chemical Society Reviews* 2000, 29 (5), 283-293.

6. MacDiarmid, A. G. and A. J. Epstein In “Synthetic metals”: A novel role for organic polymers, Makromolekulare Chemie. Macromolecular Symposia, 'Ed.'^'Eds.' Wiley Online Library: 1991; pp 11-28.

7. Salmon, M., A. Diaz, A. Logan, M. Krounbi and J. Bargon, Chemical modification of conducting polypyrrole films. *Molecular Crystals and Liquid Crystals* 1982, 83 (1), 265-276.

8. Bredas, J., J. Scott, K. Yakushi and G. Street, Polarons and bipolarons in polypyrrole: Evolution of the band structure and optical spectrum upon doing. *Physical Review B* 1984, 30 (2), 1023.

9. Scott, J., J. Bredas, K. Yakushi, P. Pfluger and G. Street, The evidence for bipolarons in pyrrole polymers. *Synthetic Metals* 1984, 9 (2), 165-172.

10. Sato, K., M. Yamaura, T. Hagiwara, K. Murata and M. Tokumoto, Study on the electrical conduction mechanism of polypyrrole films. *Synthetic Metals* 1991, 40 (1), 35-48.

11. Camurlu, P., Polypyrrole derivatives for electrochromic applications. *RSC Advances* 2014, 4 (99), 55832-55845.

12. Dhawan, S. and D. Trivedi, Thin conducting polypyrrole film on insulating surface and its applications. *Bulletin of Materials Science* 1993, 16 (5), 371-380.

13. Jonas, F. and G. Heywang, Technical applications for conductive polymers. *Electrochimica acta* 1994, 39 (8), 1345-1347.

14. Zhang, P., Z. Yang, D. Wang, S. Kan, X. Chai, J. Liu and T. Li, Electrochemical deposition and photovoltaic properties of Nano-Fe< sub> 2</sub> O< sub> 3</sub>-incorporated polypyrrole films. *Synthetic Metals* 1997, 84 (1), 165-166.

15. Pomposo, J., J. Rodrıguez and H. Grande, Polypyrrole-based conducting hot melt adhesives for EMI shielding applications. *Synthetic Metals* 1999, 104 (2), 107-111.

16. Gelling, V. J., M. M. Wiest, D. E. Tallman, G. P. Bierwagen and G. G. Wallace, Electroactive-conducting polymers for corrosion control: 4. Studies of poly (3-octyl pyrrole) and poly (3-octadecyl pyrrole) on aluminum 2024-T3 alloy. *Progress in Organic Coatings* 2001, 43 (1), 149-157.

17. Kim, M., H. Kim, S. Byun, S. Jeong, Y. Hong, J. Joo, K. Song, J. Kim, C. Lee and J. Lee, PET fabric/polypyrrole composite with high electrical conductivity for EMI shielding. *Synthetic Metals* 2002, 126 (2), 233-239.

18. Zhang, F., M. Johansson, M. R. Andersson, J. C. Hummelen and O. Inganäs, Polymer photovoltaic cells with conducting polymer anodes. *Advanced materials* 2002, 14 (9), 662-665.

19. Chen, M., Printed electrochemical devices using conducting polymers as active materials on flexible substrates. *Proceedings of the IEEE* 2005, 93 (7), 1339-1347.

20. Mabrook, M., C. Pearson and M. Petty, Inkjet-printed polypyrrole thin films for vapour sensing. *Sensors and Actuators B: Chemical* 2006, 115 (1), 547-551.

21. Tallman, D. E., K. L. Levine, C. Siripirom, V. G. Gelling, G. P. Bierwagen and S. G. Croll, Nanocomposite of polypyrrole and alumina nanoparticles as a coating filler for the corrosion protection of aluminium alloy 2024-T3. *Applied Surface Science* 2008, 254 (17), 5452-5459.

22. Jadhav, N., C. A. Vetter and V. J. Gelling, Characterization and Electrochemical Investigations of Polypyrrole/Aluminum Flake Composite Pigments on AA 2024-T3 Substrate. *ECS Transactions* 2012, 41 (15), 75-89.

23. Samuelson, L. A. and M. A. Druy, Kinetics of the degradation of electrical conductivity in polypyrrole. *Macromolecules* 1986, 19 (3), 824-828.

24. Maddison, D. and J. Unsworth, Optimization of synthesis conditions of polypyrrole from aqueous solutions. *Synthetic Metals* 1989, 30 (1), 47-55.

25. Omastová, M., S. Kosina, J. Pionteck, A. Janke and J. Pavlinec, Electrical properties and stability of polypyrrole containing conducting polymer composites. *Synthetic Metals* 1996, 81 (1), 49-57.

26. Hung, S.-L., T.-C. Wen and A. Gopalan, Application of statistical design strategies to optimize the conductivity of electrosynthesized polypyrrole. *Materials Letters* 2002, 55 (3), 165-170.

27. Kunnari, E., J. Valkama, M. Keskinen and P. Mansikkamäki, Environmental evaluation of new technology: printed electronics case study. *Journal of Cleaner Production* 2009, 17 (9), 791-799.

28. Lee, K. J., B. H. Jun, T. H. Kim and J. Joung, Direct synthesis and inkjetting of silver nanocrystals toward printed electronics. *Nanotechnology* 2006, 17 (9), 2424.

29. Perelaer, J., A. W. de Laat, C. E. Hendriks and U. S. Schubert, Inkjet-printed silver tracks: low temperature curing and thermal stability investigation. *Journal of Materials Chemistry* 2008, 18 (27), 3209-3215.

30. Delay, M., T. Dolt, A. Woellhaf, R. Sembritzki and F. H. Frimmel, Interactions and stability of silver nanoparticles in the aqueous phase: Influence of natural organic matter (NOM) and ionic strength. *Journal of Chromatography A* 2011, 1218 (27), 4206-4212.

31. Luechinger, N. A., E. K. Athanassiou and W. J. Stark, Graphene-stabilized copper nanoparticles as an air-stable substitute for silver and gold in low-cost ink-jet printable electronics. *Nanotechnology* 2008, 19 (44), 445201.

32. Torrisi, F., T. Hasan, W. Wu, Z. Sun, A. Lombardo, T. S. Kulmala, G.-W. Hsieh, S. Jung, F. Bonaccorso and P. J. Paul, Inkjet-printed graphene electronics. *Acs Nano* 2012, 6 (4), 2992-3006.

33. Zhang, Q., Y. Zheng and J. Liu, Direct writing of electronics based on alloy and metal (DREAM) ink: A newly emerging area and its impact on energy, environment and health sciences. *Frontiers in Energy* 2012, 6 (4), 311-340.

34. Ngamna, O., A. Morrin, A. J. Killard, S. E. Moulton, M. R. Smyth and G. G. Wallace, Inkjet printable polyaniline nanoformulations. *Langmuir* 2007, 23 (16), 8569-8574.

35. Chang, J. B., V. Liu, V. Subramanian, K. Sivula, C. Luscombe, A. Murphy, J. Liu and J. M. Fréchet, Printable polythiophene gas sensor array for low-cost electronic noses. *Journal of Applied Physics* 2006, 100 (1), 014506.

36. Vetter, C. A., A. Suryawanshi, J. R. Lamb, B. Law and V. J. Gelling, Novel synthesis of stable polypyrrole nanospheres using ozone. *Langmuir* 2011, 27 (22), 13719-13728.

37. He, F., M. Omoto, T. Yamamoto and H. Kise, Preparation of polypyrrole–polyurethane composite foam by vapor phase oxidative polymerization. *Journal of applied polymer science* 1995, 55 (2), 283-287.

38. Lock, J. P., S. G. Im and K. K. Gleason, Oxidative chemical vapor deposition of electrically conducting poly (3, 4-ethylenedioxythiophene) films. *Macromolecules* 2006, 39 (16), 5326-5329.

39. Black, S. (2013). Lightning strike protection stategies for composite aircraft. Composites World, Gardner Business Media Inc.

40. Gou, J., Y. Tang, F. Liang, Z. Zhao, D. Firsich and J. Fielding, Carbon nanofiber paper for lightning strike protection of composite materials. *Composites Part B: Engineering* 2010, 41 (2), 192-198.

41. Jonas, F., G. Heywang, W. Schmidtberg, J. Heinze and M. Dietrich (1991). Method of imparting antistatic properties to a substrate by coating the substrate with a novel polythiophene, Google Patents.

42. Krafft, W., F. Jonas, B. Muys and D. Quintens (1994). Antistatic plastic articles, Google Patents.

43. De Boer, J. (1995). Antistatic coating for, in particular, a cathode ray tube comprising latex particles of a polypyrole compound in a silicon dioxide matrix, Google Patents.

44. Cinquina, P., G. Magnone and G. Manciocco (1998). Anti-glare, anti-static coating for a reflective-transmissive surface, Google Patents.

45. Kilbride, M. and R. A. Pethrick, Enhancement of the surface electrical conductivity of thermoplastic composite matrices. *Proceedings of the Institution of Mechanical Engineers, Part L: Journal of Materials Design and Applications* 2012, 226 (3), 252-264.

46. Katunin, A., K. Krukiewicz, R. Turczyn, P. Sul, A. Łasica and M. Bilewicz, Synthesis and characterization of the electrically conductive polymeric composite for lightning strike protection of aircraft structures. *Composite Structures* 2017, 159, 773-783.

47. Soto-Oviedo, M. A., O. A. Araújo, R. Faez, M. C. Rezende and M.-A. De Paoli, Antistatic coating and electromagnetic shielding properties of a hybrid material based on polyaniline/organoclay nanocomposite and EPDM rubber. *Synthetic Metals* 2006, 156 (18), 1249-1255.

48. Omastová, M., J. Pavlinec, J. Pionteck and F. Simon, Synthesis, Electrical Properties and Stability of Polypyrrole-Containing Conducting Polymer Composites. *Polymer international* 1997, 43 (2), 109-116.

49. Huijs, F., F. Vercauteren and G. Hadziioannou, Resistance of transparent latex films based on acrylic latexes encapsulated with a polypyrrole shell. *Synthetic Metals* 2001, 125 (3), 395-400.

50. Wang, Y. and X. Jing, Electrically conducting polymers for electromagnetic interference shielding. *Polymers for Advanced Technologies* 2005, 16 (4), 344-351.

51. Li, N., Y. Huang, F. Du, X. He, X. Lin, H. Gao, Y. Ma, F. Li, Y. Chen and P. C. Eklund, Electromagnetic interference (EMI) shielding of single-walled carbon nanotube epoxy composites. *Nano Letters* 2006, 6 (6), 1141-1145.

52. Hong, Y., C. Lee, C. Jeong, J. Sim, K. Kim, J. Joo, M. Kim, J. Lee, S. Jeong and S. Byun, Electromagnetic interference shielding characteristics of fabric complexes coated with conductive polypyrrole and thermally evaporated Ag. *Current applied physics* 2001, 1 (6), 439-442.

53. Koch, G. H., M. P. Brongers, N. G. Thompson, Y. P. Virmani and J. H. Payer (2002). Corrosion cost and preventive strategies in the United States. *NACE International*, FHWA-RD-01-156.

54. Astaneh-Asl, A. In Progressive collapse of steel truss bridges, the case of I-35W collapse, Proceedings of 7th International Conference on Steel Bridges, Guimarães, Portugal, 'Ed.'^'Eds.' 2008.

55. Humble, R., Cathodic Protection of Steel in Sea Water With Magnesium Anodes★. *Corrosion* 1948, 4 (7), 358-370.

56. Knudsen, O. Ø., U. Steinsmo and M. Bjordal, Zinc-rich primers—Test performance and electrochemical properties. *Progress in Organic Coatings* 2005, 54 (3), 224-229.

57. Battocchi, D., A. Simoes, D. E. Tallman and G. Bierwagen, Electrochemical behaviour of a Mg-rich primer in the protection of Al alloys. *Corrosion Science* 2006, 48 (5), 1292-1306.

58. Simões, A., D. Battocchi, D. Tallman and G. Bierwagen, Assessment of the corrosion protection of aluminium substrates by a Mg-rich primer: EIS, SVET and SECM study. *Progress in Organic Coatings* 2008, 63 (3), 260-266.

59. Krstajić, N., B. Grgur, S. Jovanović and M. Vojnović, Corrosion protection of mild steel by polypyrrole coatings in acid sulfate solutions. *Electrochimica acta* 1997, 42 (11), 1685-1691.

60. Truong, V.-T., P. Lai, B. Moore, R. Muscat and M. Russo, Corrosion protection of magnesium by electroactive polypyrrole/paint coatings. *Synthetic Metals* 2000, 110 (1), 7-15.

61. He, J., D. E. Tallman and G. P. Bierwagen, Conjugated polymers for corrosion control: scanning vibrating electrode studies of polypyrrole-aluminum alloy interactions. *Journal of the electrochemical society* 2004, 151 (12), B644-B651.

62. Redondo, M. and C. Breslin, Polypyrrole electrodeposited on copper from an aqueous phosphate solution: Corrosion protection properties. *Corrosion Science* 2007, 49 (4), 1765-1776.

63. Yan, M., C. A. Vetter and V. J. Gelling, Corrosion inhibition performance of polypyrrole Al flake composite coatings for Al alloys. *Corrosion Science* 2013, 70, 37-45.

64. Armelin, E., R. Pla, F. Liesa, X. Ramis, J. I. Iribarren and C. Alemán, Corrosion protection with polyaniline and polypyrrole as anticorrosive additives for epoxy paint. *Corrosion Science* 2008, 50 (3), 721-728.

65. Kalendová, A., D. Veselý and J. Stejskal, Organic coatings containing polyaniline and inorganic pigments as corrosion inhibitors. *Progress in Organic Coatings* 2008, 62 (1), 105-116.

66. Armelin, E., Á. Meneguzzi, C. A. Ferreira and C. Alemán, Polyaniline, polypyrrole and poly (3, 4-ethylenedioxythiophene) as additives of organic coatings to prevent corrosion. *Surface and Coatings Technology* 2009, 203 (24), 3763-3769.

67. Mahmoudian, M., W. Basirun, Y. Alias and M. Ebadi, Synthesis and characterization of polypyrrole/Sn-doped TiO 2 nanocomposites (NCs) as a protective pigment. *Applied Surface Science* 2011, 257 (20), 8317-8325.

68. Li, P., T. Tan and J. Lee, Corrosion protection of mild steel by electroactive polyaniline coatings. *Synthetic Metals* 1997, 88 (3), 237-242.

69. Sathiyanarayanan, S., S. S. Azim and G. Venkatachari, A new corrosion protection coating with polyaniline–TiO< sub> 2</sub> composite for steel. *Electrochimica acta* 2007, 52 (5), 2068-2074.

70. Mahmoudian, M., W. Basirun, Y. Alias and M. Ebadi, Synthesis and characterization of polypyrrole/Sn-doped TiO< sub> 2</sub> nanocomposites (NCs) as a protective pigment. *Applied Surface Science* 2011, 257 (20), 8317-8325.

71. Hosseini, M., M. Raghibi-Boroujeni, I. Ahadzadeh, R. Najjar and M. Seyed Dorraji, Effect of polypyrrole–montmorillonite nanocomposites powder addition on corrosion performance of epoxy coatings on Al 5000. *Progress in Organic Coatings* 2009, 66 (3), 321-327.

72. Jadhav, N., C. A. Vetter and V. J. Gelling, The effect of polymer morphology on the performance of a corrosion inhibiting polypyrrole/aluminum flake composite pigment. *Electrochimica acta* 2013, 102, 28-43.

CHAPTER 2. ELECTRICALLY CONDUCTIVE UV-CURABLE HYBRID NETWORKS BASED ON ACRYLATED POLYESTERS AND POLYPYRROLE

2.1. Abstract

Polypyrrole (PPy) is a popular electrically conductive polymer being studied to supplant traditional metallic materials in a variety of technologies. Unfortunately, PPy suffers drawbacks which require it to be blended with traditional polymeric materials. In this study, electrically conductive composites were developed using a novel photopolymerization technique utilizing photosensitive oxidizing agents for pyrrole. This system was blended with traditional UV-curable acrylate resins and reactive diluents to improve the mechanical properties of the resulting films and create hybrid networks between the two systems. Coatings were applied on both aluminum 2024-T3 and glass substrates via draw downs and cured using a metal halide bulb. It was observed that as the coating was exposed to UV-light the coating turned from a clear yellow color to black upon curing, indicating the conversion of pyrrole to polypyrrole. Films containing polypyrrole showed decreased gloss, which was observed to be caused by a surface roughening. Hybrid networks containing 40% or more polypyrrole by weight showed bulk and local conductivity as characterized by four-point probe and conductive atomic force microscopy respectively. The electrical conductivity observed is sufficient for anti-static purposes. Photo-differential scanning calorimetry (P-DSC) did not provide insight into the amount of UV-light exposure needed to sufficiently polymerize pyrrole without degradation for the electrical properties. However, monitoring the electrical conductivity with respect to UV-exposure times allowed for optimization of electrical properties.[1]

[1] Submitted to Progress in Organic Coatings

2.2. Introduction

Since the first publication by Shirakawa et al., electrically conductive polymers (ECP's) have received attention in various fields such as photovoltaics, printable electronics, sensors, anti-corrosion additives, and anti-static technologies as possible replacements to traditional inorganic semi-conductor materials.[1-4] Polymers are advantageous due to their high strength-to-weight ratio, tailorable properties, and resistance to degradation in the environment. Traditional conductive composite materials used in these areas of technology typically involve metal fillers such as silver nanoparticles that are difficult to maintain in a stable suspension and require the use of surfactants that can have deleterious effects on the resulting composites.

Polypyrrole is one of the most popular ECPs currently being investigated due to its high conductivity, environmental stability, and ease of synthesis. Unfortunately, polypyrrole is an infusible black powder with poor mechanical properties. The mechanical properties of polypyrrole can be improved by blending with traditional thermoplastics and coatings.[5, 6] However, this retards the electrical properties of the polypyrrole as traditional coating resins and thermoplastics are insulating materials. Furthermore, polypyrrole is insoluble in common solvents thus requiring it to be dispersed as a pigment which can be troublesome as well.

Research into prepolymerizing porous structures and then polymerizing pyrrole in the pores is reported in literature[7, 8]. This technique does not require stabilization although it does increase processing time by adding additional steps. Methods to polymerize pyrrole alongside traditional coating resins have been limited due to the difference in reaction mechanism. ECPs can undergo polymerization through electrochemical means, such as chronoamperometry and chronopotentiometry, or by chemical oxidative polymerization involving chemical oxidizing agents.

In the 1990s it was discovered that polypyrrole could be polymerized to low yields by cationic photoinitiators.[9] Since then the use of other UV-sensitive materials has been employed to effectively photopolymerize pyrrole as well. Rinaldi et al. used ferrocenium salts to photopolymerize pyrrole in a polyvinyl chloride matrix.[10] The resulting composite showed very low conductivity which was attributed to loss of conjugation in the polypyrrole backbone. Photo-induced polymerization with silver salts has been reported in the literature over the past few years. These composites showed electrical conductivity in the range of 10^{-5} to 10^{-1} S/cm. Other materials such as ruthenium complexes and titanium dioxide have been used as photo-oxidative species for the photopolymerization of pyrrole.[11, 12]

Other ECP precursors have also been shown to undergo photopolymerization in similar conditions. De Barros et. al. successfully photopolymerized aniline using silver salts in acidic medium.[13] The resulting material showed conductivity in the range of 5 S/cm. Cationic photoinitiators have also been demonstrated to effectively polymerize thiophene into polythiophene.[14] The resulting polymer films showed conductivity in the range of 10^{-5} S/cm and morphologies different from the traditional polymerization procedures.

Photopolymerization of pyrrole while blended with thermoplastics has previously been reported.[10] However it is proposed that it would be advantageous to undergo photopolymerization of both the pyrrole and the resin system at the same time. Both acrylates and epoxy resins can undergo photopolymerization with suitable photoinitiators.[15] UV-curable resins are a fast growing industrial market due to fast cure times, lower energy costs, and the wide variety of industrially available resins.[16] UV-curable formulations can also be able to be formulated at higher solids levels using low viscosity reactive diluents thus eliminating the need for solvents. This method is also environmentally friendly, which is a bonus in a world where regulations on emissions are

becoming more stringent each year. Additionally, high solid coatings allow thicker film build at the same application thickness compared to traditional solvent borne coatings requiring a less number of coats to achieve desired film thickness. This reduces both the processing time and volume of a material needed thus lowering the cost of application and making it a greener alternative.

A literature review prior to this investigation discovered only one report of blending ECP's into UV-curable resins and studying the resulting properties.[17] There are, however, no reports on the photopolymerization of any conductive polymer precursors alongside either acrylates or epoxy systems. Thus, the authors suggest it important in investigating the resulting physical and electrical properties of the resulting coatings. In this report the first account of blending acrylate resins with pyrrole and photopolymerizing both at the same time is reported. The resulting films show promise in a variety of application such as anti-static coatings and corrosion protection coatings.

2.2. Experimental

2.2.1. Materials

All chemicals listed were used as received unless noted. EBECRYL® 436, is a blend of a chlorinated polyester acrylate diluted by 40% with the reactive diluent trimethylolpropane triacrylate (TMPA), was graciously supplied by Cytec industries. 2-Hydroxy-2-methyl-1-phenyl-propan-1-one (DAROCUR® 1173), a free radical photoinitiator was graciously supplied by BASF. Reagent grade acetonitrile and silver nitrate were purchased from Sigma Aldrich. Pyrrole was purchased from Alfa Aesar® and vacuum distilled prior to use. Aluminum 2024-T3 panels (3" x 6") were obtained from Q-Lab and sand blasted then degreased with hexane prior to coating

application. Glass panels (3” x 6”) were obtained from a local supplier and degreased with hexane prior to use.

2.2.2. Characterization of Coatings

Photo-differential scanning calorimetry was performed on a TA instruments Q-1000 differential scanning calorimeter equipped with a TA instruments Q-Series PCA photocalorimeter with a spectral output of 50 mW/cm^2 under a nitrogen atmosphere. Gloss measurements of the resulting films were recorded using the BYK gloss meter. König hardness measurements were performed on a BYK pendulum hardness apparatus. Cross-hatch adhesion was performed following the ASTM D3359 standard. Morphology of the coatings was studied with a JEOL JSM-6300 scanning electron microscope equipped with a field emission electron gun with a back-scattering electron detector. Thermal stability of the coatings was studied with a TA instruments Q-500 thermogravimetric analyzer (TGA) with a heating rate of 20°C/min up to 800°C under nitrogen. Bulk conductivity was measured using a Keithley® 2100 digital multimeter equipped with a four point probe assembly by Signatone®. Local conductivity and mapping was completed on a Veeco® 3100 atomic force microscope in contact mode with a current sensing probe with an applied potential of 1V at a scan rate 1.51Hz and 256 samples per line. Topography mapping was done on a Veeco® 3100 atomic force microscope in tapping mode.

2.2.3. Formulation and Curing of Coatings

Formulations were prepared varying in pyrrole content with respect to total mass of pyrrole and acrylates from 0% to 100% were created. Acetonitrile content was kept at 20% of the total mass of resin and pyrrole. Formulations were accomplished by first mixing half of the acetonitrile with the UV-curable resin and photoinitiator then left to mix for 15 minutes via magnetic stir bar. In a separate vial, the silver nitrate was dissolved in the second half of acetonitrile. Upon

dissolution of the silver nitrate in acetonitrile, pyrrole was added and shaken until mixed. Pyrrole to silver nitrate blend was maintained at 5:1 ratio. The contents of the vial containing the acrylates was then combined with the contents of the vial containing pyrrole and allowed to mix for 5 minutes. Draw downs onto aluminum 2024-T3 and glass panels were done at a wet-film thickness of 6 mils (approximately 152 μm) and exposed to ultraviolet light in 60 second intervals until tack free and no color change was observed. The UV-chamber setup used in this study was a DYMAX Model 5000-EC UV-Light Curing Flood System equipped with a metal halide bulb with a spectral intensity of 174 mW/cm^2. Spectral intensity of the bulb was measured with a UV Power Puck made by EIT instruments.

2.3. Results and Discussion

2.3.1. Coating Formulation and Curing Studies

Table 2.1 shows the formulation for each hybrid network studied. Pyrrole content was increased at increments of 20% from 0% to 100% . It was visibly apparent that upon the addition of pyrrole to the silver nitrate solution the solution slowly began to yellow. This is due to the slow oxidation process that pyrrole undergoes when exposed to silver salts at room temperature and no UV-light exposure. It should be noted that oxidative polymerization of pyrrole with silver salts with no UV-light exposure have been reported with reaction timelines upwards of 48 hours.[18] In these formulations the coatings were tack free within 180 seconds of UV-exposure, 960 times faster than without UV-exposure. It was noted that films on aluminum 2024-T3 cured slightly faster than films coating glass panels. This is attributed to possible reflection of ultraviolet light off the metal substrate back into the coating. As exposure time progressed the films containing pyrrole changed from a slight yellow color to a dark brown and finally a black color visually indicating the conversion of pyrrole to polypyrrole was complete.

Table 2.1: Coating formulations

Coating ID	Ebecryl® 436 (g)	Pyrrole (g)	Silver Nitrate (g)	DAROCUR® 1173 (g)	Acetonitrile (g)
0%_PPy	12.00	0.00	0.00	0.06	3.00
20%_PPy	9.60	2.40	1.21	0.048	3.00
40%_PPy	7.20	4.80	2.42	0.036	3.00
60%_PPy	4.80	7.20	3.62	0.024	3.00
80%_PPy	2.40	9.60	4.83	0.012	3.00
100%_PPy	0.00	12.00	6.04	0.00	3.00

Overlay of the photo-DSC plots obtained are displayed in Figure 2.1. The first minute of each scan was used to obtain a baseline. Exposure to UV-light began after the first minute and a large exotherm was observed in the formulation containing no pyrrole. This exotherm is attributed to the breaking of double bonds in acrylates during polymerization. It is noted that as the pyrrole content goes up the magnitude of this exotherm decreases and is nonexistent in the 100%_PPy sample. No observable exotherm for the polymerization of pyrrole can be attributed to the currently accepted mechanism in which pyrrole is polymerized.[19] These results lead to the conclusion that photo DSC is useful in determining the curing profile for the acrylate portion, but yields no information regarding the curing profile for the polypyrrole in these hybrid networks. It is also worth noting that the exposure time to reach the peak heat flow from the polymerization of the acrylates increases as the concentration decreases as well as a broadening of this exotherm. This indicates a possible retardation of polymerization of the acrylates with pyrrole existing in the formulations.

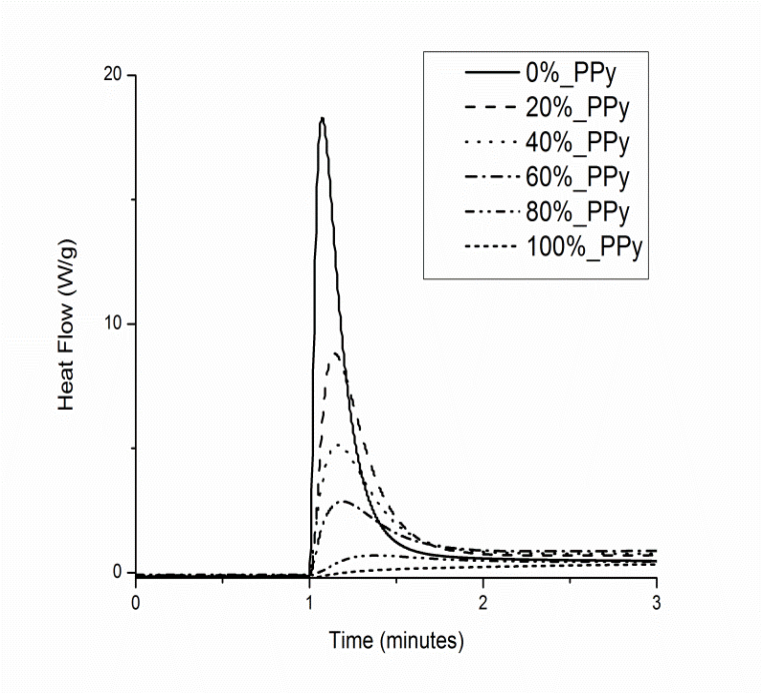

Figure 2.1: Photo-DSC curves of formulations.

2.3.2. Physical Property Testing and Morphology Studies

General coating properties of the composites are listed in Table 2.2. It was observed that there is a sharp decrease in the 85° gloss values when pyrrole content exceeds 20%. The roughening of the coating with increasing polypyrrole content is confirmed with SEM imaging as well. Polypyrrole due to its physical properties acts very much like a pigment thus reaching its critical pigment volume concentration (CPVC), when there is insufficient binder resin to coat the polypyrrole domains thus a rough surface will develop. A thorough literature search yielded no information regarding a value for the CPVC of polypyrrole. For this work, PPy can be regarded as a pigment particle due to the unsoluble like nature it has in coating resins However, literature suggests the CPVC of polyaniline, another conductive polymer is approximately 24% by volume, which is in line with what is observed in these coatings.[20] König hardness decreased with increasing pyrrole content. This softening of the coating could be possible plasticization of lower

molecular weight pyrrole oligomers. The coating comprised entirely of polypyrrole however displays a larger König hardness value. The "hardening" observed is believed to be caused by a smoother coating which correlates well with the slight increase in the gloss values as well with 80% PPy and 100% PPy coatings.

Table 2.2: Physical properties of hybrid networks

Coating ID	85° Gloss	König Hardness (s)	Cross-hatch Adhesion
0%_PPy	98.7	191	4B
20%_PPy	72.6	103	5B
40%_PPy	4.0	46	4B
60%_PPy	10.3	40	5B
80%_PPy	15.8	52	5B
100%_PPy	13.6	105	5B

Cross hatch adhesion was relatively unchanged throughout all levels of polypyrrole loading indicating polypyrrole content had no detrimental impact on the adhesion of these coatings to the aluminum 2024T3 surface. In addition, the coating comprising of 100% PPy demonstrated excellent adhesion to the aluminum 2024T3 surface. This is surprising, as polypyrrole films developed from other techniques tend to show poor adhesion to substrates. The slight improvement of adhesion observed in most formulations could be beneficial for the use of UV-curable coatings for corrosion resistant applications as conductive polymers have shown to anodically protect metals susceptible to corrosion.

Figure 2.2 are SEM images for the composite coatings. A back scattering electron detector was used to better observe where the silver particles were in the coating. Domains of polypyrrole and silver nanoparticles appear on the surface of these coatings at pyrrole content of 40%. As pyrrole content increases the domains with silver nanoparticles appear more frequently. Silver

nanoparticles should be embedded in the polypyrrole domains as they are being formed from the silver salt being reduced as pyrrole is oxidized to polypyrrole.

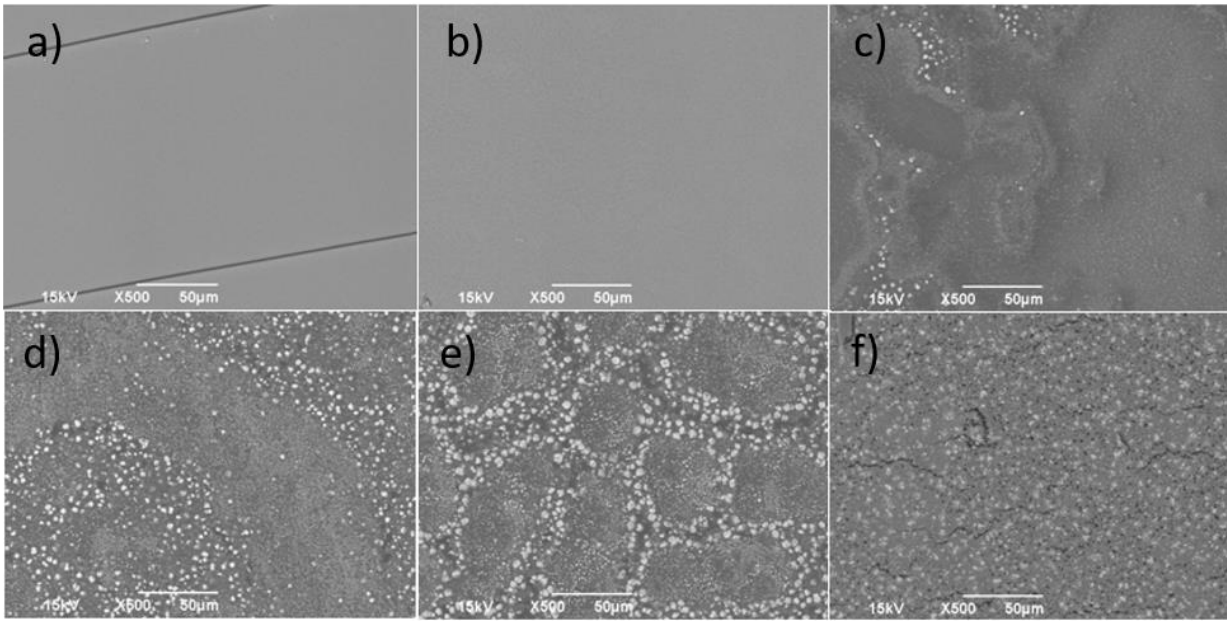

Figure 2.2: SEM images of cured hybrid networks. Top from left to right: 0%_PPy, 20%_PPy, 40%_PPy. Bottom from left to right: 60%_PPy, 80%_PPy, 100%_PPy.

It is also apparent of the cracks in the coating containing no polypyrrole. UV-curable coatings cure very rapidly and sometimes do not have adequate time to relieve stresses that build up within the cured film and fracturing in the coating occurs.[15] Similar observations were seen in the coating containing no polypyrrole. Coatings containing pyrrole showed no cracks except for 100%_PPy. This could be attributed to the longer curing time needed for coatings containing pyrrole thus having pyrrole and pyrrole oligomers acting as plasticizers of the UV-curable resin relieving the stresses being built up during photopolymerization. The morphology of the polypyrrole domains in the coatings are similar to other reports of photopolymerization of polypyrrole films.[21, 22]

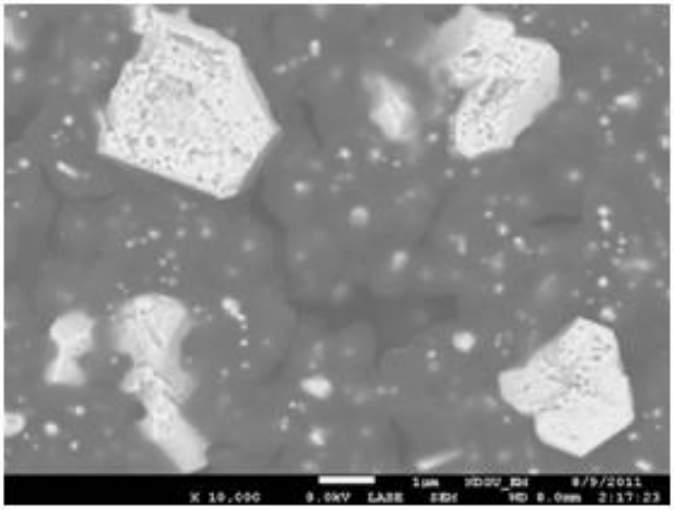

Figure 2.3: High resolution SEM of 100%_PPy.

A higher resolution image of the 100% PPy coating is presented in Figure 2.3. This image gives a better depiction of the size of the silver particles in the coating which range in size from approximately 100nm to 1µm. The sizes observed in this study of silver particles formed during the photopolymerization of pyrrole have been observed in other reports in the literature as well.[21, 22] Large macrostructures of silver found in the coatings are believed to be silver nitrate crystals. Energy dispersive spectroscopy indicates the presence of silver, nitrogen, and oxygen in these macrostructures.

Surface topography was analyzed using tapping mode atomic force microscopy. The height profiles for each of the formulations are presented in Figure 2.4. It is apparent that with increasing polypyrrole content in these hybrid networks the surface profile gets rougher up until 80%_PPy. Reports of polypyrrole films have shown surface roughness comparable to the values reported here.[23] The decline in surface roughness from 80% PPy to 100% PPy could be partially caused by the UV-curable resin curing so fast it locks the growing polypyrrole chains into place. Without the UV-curable resin the pyrrole monomers and oligomers have a low enough viscosity

to allow spreading during early stages of the photopolymerization. This correlated with the decrease in gloss with increasing pyrrole content up to 80% PPy followed by a gloss value increase from 80% PPy to 100% PPy. Surface roughness measurements (R_{ms}) are listed in Table 2.3.

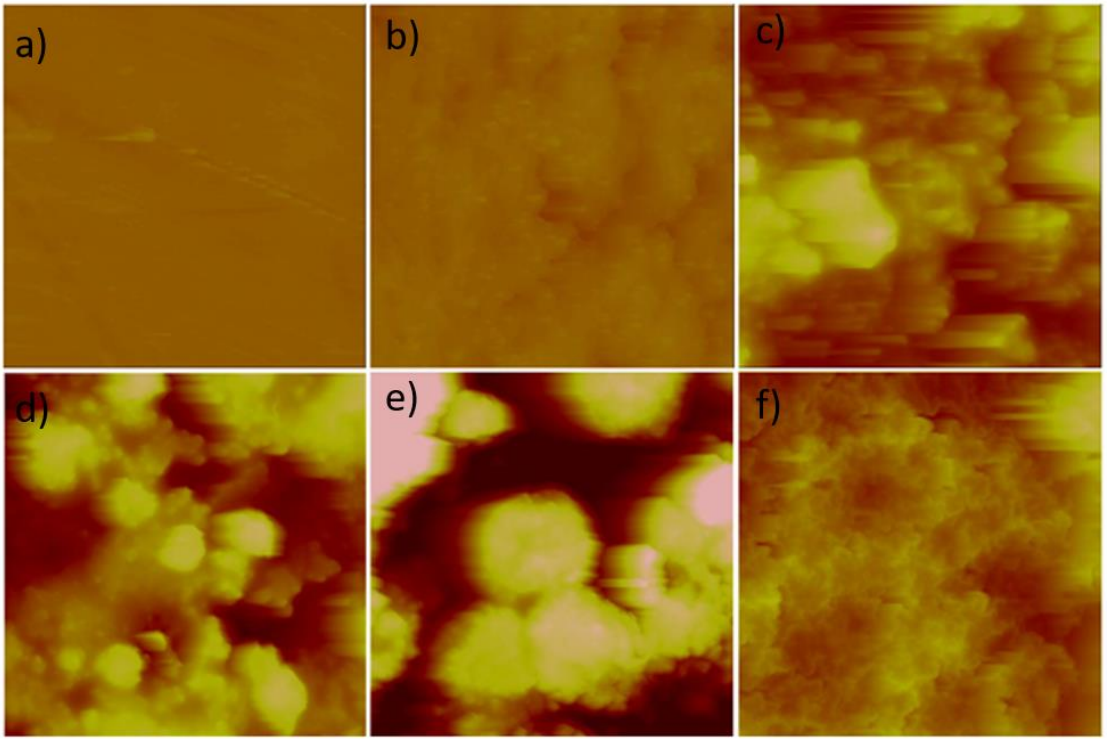

Figure 2.4: Height profiles of cured hybrid networks. Scan size is 20µm x 20µm. Top from left to right: 0%_PPy, 20%_PPy, 40%_PPy. Bottom from left to right: 60%_PPy, 80%_PPy, 100%_PPy.

Table 2.3: Surface roughness (root mean squared) of the hybrid networks

Coating ID	R_{RMS} (nm)
0%_PPy	16.5
20%_PPy	45.0
40%_PPy	335.0
60%_PPy	440.8
80%_PPy	1016
100%_PPy	214.3

2.3.3. Thermal Gravimetric Analysis of Coatings

Overlay of the TGA curves obtained for each coating is presented in Figure 2.5. The polyester resin displays three clear degradation regimes around 316°, 462°, and 610°C respectively. Photopolymerized polypyrrole shows two degradation regimes with one occurring around 190°C and 426°C. The sample 100% PPy displayed approximately a 1.5 wt% loss up to 100°C which is attributed to water absorption and or solvent remaining in the sample when exposed to the environment (the boiling points for water and acetonitrile are 100° and 81°C, respectively).[24]

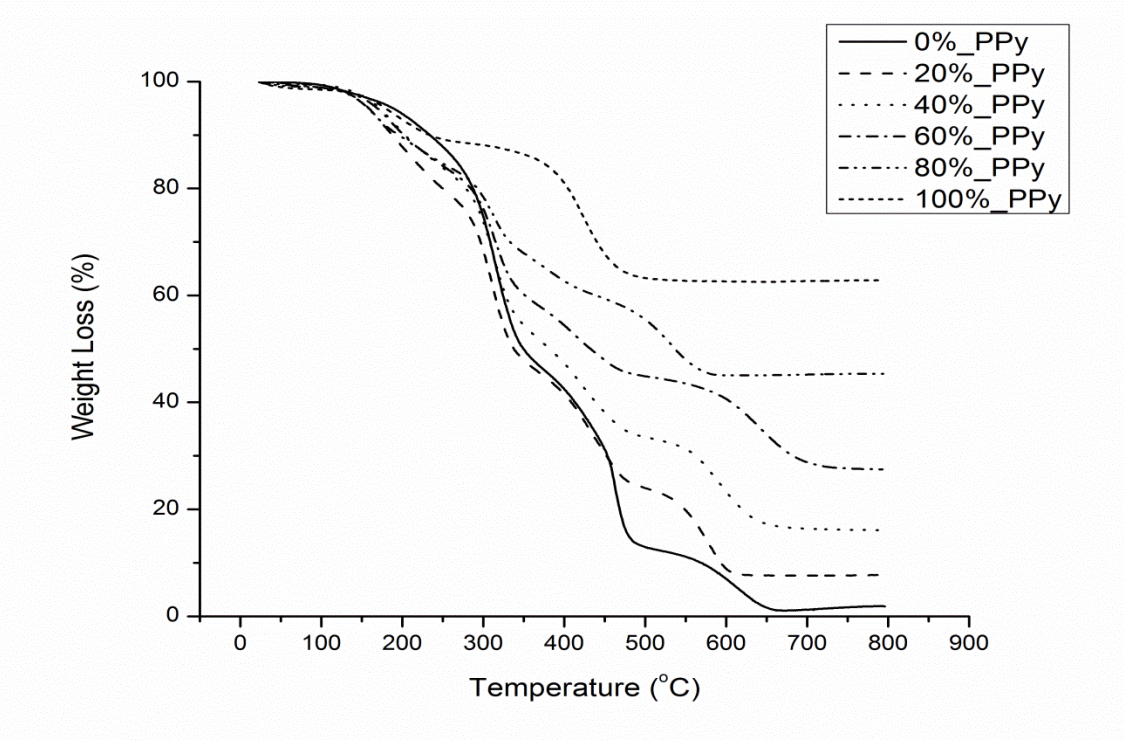

Figure 2.5: TGA plots at heating rate of 20°C/min under nitrogen atmosphere.

The first degradation phase around 190°C in 100% PPy has been attributed in literature to degradation of nitrate ions in nitrate doped polypyrrole.[25] The char yield in the 100%_PPy sample was approximately 63% and is attributed to a blend of silver and left over char from the

decomposition of polypyrrole. Literature on the thermal decomposition of polypyroles indicates a char yield of 35% for surfactant doped polypyrrole.[26] The char yield for the polyester acrylate is very low, on the order of 1-2 wt %. As pyrrole content increases so does the char yield indicating successful conversion of pyrrole to polypyrrole upon exposure to UV-light.

2.3.4. Electrical Properties Testing

Figure 2.6 shows the effect of pyrrole content with respect to the bulk conductivity of these coatings. It should be noted that resistance greater than 100 MΩ could not be measured by the four-point probe assembly in use. Concentrations below 40 wt% pyrrole displayed no measureable conductivity. It is noticed that as polypyrrole concentration increases so does the bulk conductivity up to a value around 1.4E-4 S/cm. This conductivity is in agreement of other reports for the conductivity of photopolymerized films, not just by silver salts but other metallic salts as well.[25, 27-29]

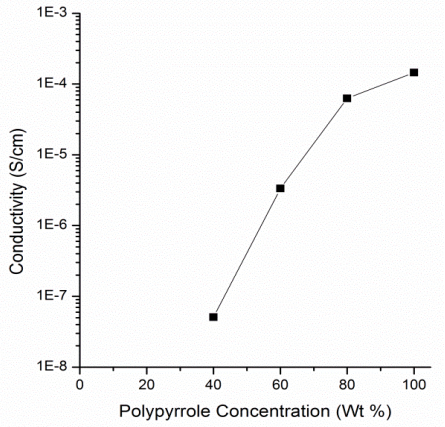

Figure 2.6: Plot of conductivity with respect to pyrrole content.

The first recordable resistance measurement at 40% PPy is in agreement in the first observance of the polypyrrole domains on the surface of the films from the SEM images. It should

be noted that in all formulations the silver content of the coating was kept below the percolation threshold of silver nanoparticles. Literature shows the percolation threshold of silver nanoparticles being in the vicinity of 5-6 volume %. The formulation containing the most silver, 100% PPy has a concentration of silver at approximately 3 volume %. Reports of blending silver nanoparticles with conventional resins as epoxy report conductivities about two orders of magnitude lower than the samples reported here confirming that the conductivity is attributed to the polypyrrole being formed during UV-exposure. According to the literature antistatic coatings need surface resistances in the range of 10^4 to 10^8 Ω to provide effective charge dissipation.[30] Coating formulations 40% PPy and 60% PPy showed surface resistances in this regime while higher polypyrrole content resulted in lower surface resistivities due to higher conductive content.

C-AFM is a useful tool in mapping conductivity at a much smaller scale and observing domains of local conductivity that might be present in a bulk system. Figure 2.7 are image maps of the current detected when passing 1V of potential through the base of the sample to the AFM tip. In these scans local conductivity measurements were first picked up on the 40% PPy sample just like in bulk conductivity measurements. It is noticeable that as the pyrrole content increases the current being measured also increases displaying increasing local conductivity in these samples. In addition to higher current being measured as pyrrole content increases so does the area of the scan showing conductivity further promoting the argument that successful photopolymerization of pyrrole is taking place.

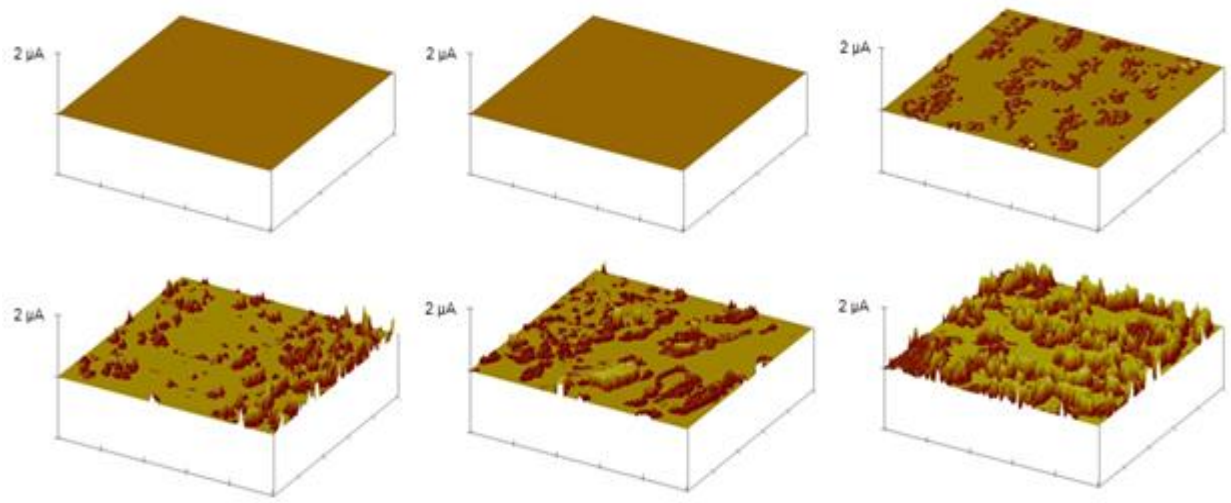

Figure 2.7: Local conductivity maps acquired through C-AFM. Scan size is 5µm x 5µm at an applied potential of 1V. Top from left to right (0%_PPy, 20%_PPy. 40%_PPy). Bottom from left to right (60%_PPy, 80%_PPy, and 100%_PPy).

Since photo-DSC results did not give any indication of the time it takes to effectively polymerize pyrrole with UV-light, a different method to monitor the polymerization is needed. For this experiment a new blend consisting of 70% pyrrole and 30% UV-curable resin was formulated to help determine the limit where these coatings display resistances lower than what is required for anti-static applications. Conductive polymers are known to degrade upon excessive exposure to ultraviolet light severely retarding the electrical properties thus determining the optimal exposure time would ensure high molecular weight polypyrrole being formed without destroying the conjugation in the polypyrrole backbone. At the same time sufficient UV-light will be needed to achieve high enough molecular weight polypyrrole with desired electrical properties. It is truly unfortunate no other reports on the photopolymerization of conductive polymers have investigated optimizing electrical properties with respect to exposure time.

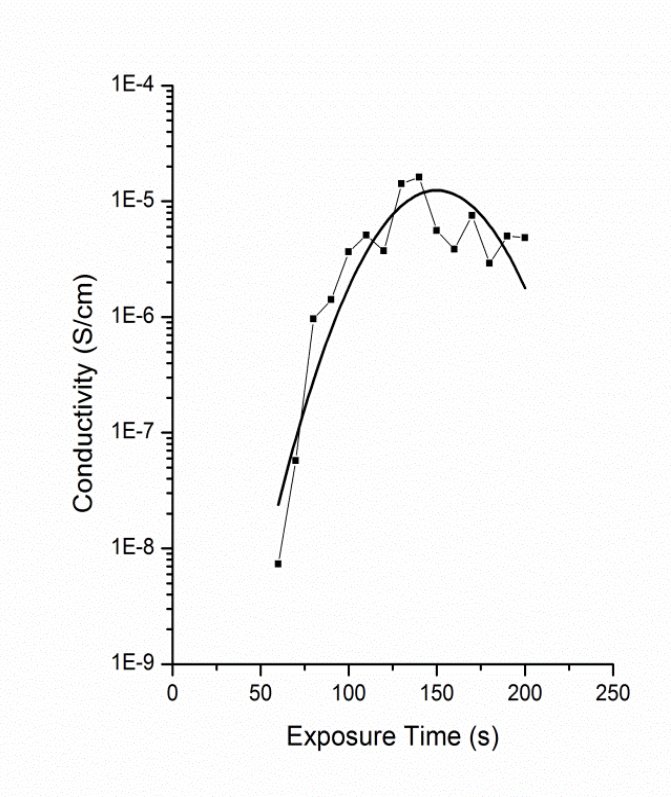

Figure 2.8: Plot of the effect of UV-light exposure on the resulting electrical conductivity of the coating.

In this experiment aluminum-2024 T3 panels were coated at 6 mil wet film thickness and exposed to UV-light for varying amounts of time ranging from 10 seconds to 200 seconds in increments of 10 seconds. Tack free coatings were then measured for bulk conductivity. Figure 2.8 above is the plot of conductivity with respect to UV-light exposure time. Less than 60 seconds exposure resulted in tacky-uncured coatings due to the presence of low molecular weight pyrrole oligomers still in the system. The highest conductivity recorded (approximately 3.0E-5 S/cm) was determined to be achieved at 140 seconds of UV exposure. Prior to 140 seconds of exposure the conductivity rises sharply in the range of 3 orders of magnitude indicating polymerization of pyrrole was ongoing. After 140 seconds of exposure a slight drop off in conductivity is noted.

This can be attributed to the loss of polarons and bipolarons in the polypyrrole backbone after excessive exposure to UV-light.[31]

The results indicate a clear difference in reaction speed for the curing rate for the polyester acrylate/TMPA blend and pyrrole. This technique provides an indirect method in studying the photo-polymerization of ECP's when traditional techniques such as photo-DSC falter. Unfortunately, the UV-intensity used in the photo-DSC testing was of much lower (approximately 50 mW/cm^2) compared to the experimental curing conditions used in this study and used in the curing of the films investigated in the previous section which were on the order of 174 mW/cm^2. This was due to the max UV-intensity available for the photo-DSC is lower than the spectral output for the metal-halide bulb used in the curing of the films.

2.4. Conclusions

A series of coating formulations with varying concentration of pyrrole were developed and cured using UV-light. Coatings showed diminished gloss and hardness with increasing pyrrole content indicating a CPVC between 20 to 40% pyrrole. The formulations showed excellent adhesion to Aluminum 2024T3 including the sample comprised entirely of polypyrrole. SEM images provided visual evidence of the development of polypyrrole domains in the coatings as well. Coating formulations 40% PPy and 60% PPy showed surface resistances in the antistatic regime while higher polypyrrole content resulted in lower surface resistivities. Local C-AFM mapping displayed local electrically conductive regimes first observed at polypyrrole concentrations of 40%. Photo-DSC does not provide useful information in studying the curing rate of polypyrrole under UV-illumination, but measuring the electrical conductivity with respect to illumination time is an effective testing method in finding the optimum curing time to maximize the resulting composites electrical properties. Future work in the use of these coatings as possible

anti-corrosion paints as well as optimizing the physical properties of the final coatings is currently underway.

2.5. Acknowledgements

The authors would like to thank the Army Research Laboratories for providing the funding for this research under the grant numbers W911NF-09-2-0014, W911NF-10-2-0082, and W911NF-11-2-0027.

2.6. References

1. Zhang, P., Z. Yang, D. Wang, S. Kan, X. Chai, J. Liu and T. Li, Electrochemical deposition and photovoltaic properties of Nano-Fe_2O_3-incorporated polypyrrole films. *Synthetic Metals* 1997, 84 (1), 165-166.

2. Chen, M., Printed electrochemical devices using conducting polymers as active materials on flexible substrates. *Proceedings of the IEEE* 2005, 93 (7), 1339-1347.

3. Mabrook, M., C. Pearson and M. Petty, Inkjet-printed polypyrrole thin films for vapour sensing. *Sensors and Actuators B: Chemical* 2006, 115 (1), 547-551.

4. Jadhav, N., C. A. Vetter and V. J. Gelling, Characterization and Electrochemical Investigations of Polypyrrole/Aluminum Flake Composite Pigments on AA 2024-T3 Substrate. *ECS Transactions* 2012, 41 (15), 75-89.

5. Mano, V., M. Felisberti, T. Matencio and M. A. De Paoli, Thermal, mechanical and electrochemical behaviour of poly (vinyl chloride)/polypyrrole blends (PVC/PPy). *Polymer* 1996, 37 (23), 5165-5170.

6. Cassignol, C., M. Cavarero, A. Boudet and A. Ricard, Microstructure-conductivity relationship in conducting polypyrrole/epoxy composites. *Polymer* 1999, 40 (5), 1139-1151.

7. Aydinli, B., L. Toppare and T. Tincer, A conducting composite of polypyrrole with ultrahigh molecular weight polyethylene foam. *Journal of applied polymer science* 1999, 72 (14), 1843-1850.

8. Wang, Y., G. A. Sotzing and R. Weiss, Preparation of conductive polypyrrole/polyurethane composite foams by in situ polymerization of pyrrole. *Chemistry of Materials* 2008, 20 (7), 2574-2582.

9. Rabek, J., J. Lucki, M. Zuber, B. Qu and W. Shi, Polymerization of pyrrole by cationic photoinitiators. *Polymer* 1992, 33 (22), 4838-4844.

10. Rinaldi, A., M. Kunita, M. Santos, E. Radovanovic, A. Rubira and E. Girotto, Solid phase photopolymerization of pyrrole in poly (vinylchloride) matrix. *European polymer journal* 2005, 41 (11), 2711-2717.

11. Segawa, H., T. Shimidzu and K. Honda, A novel photo-sensitized polymerization of pyrrole. *J. Chem. Soc., Chem. Commun.* 1989, (2), 132-133.

12. Strandwitz, N. C., Y. Nonoguchi, S. W. Boettcher and G. D. Stucky, In situ photopolymerization of pyrrole in mesoporous TiO2. *Langmuir* 2010, 26 (8), 5319-5322.

13. De Barros, R., W. De Azevedo and F. De Aguiar, Photo-induced polymerization of polyaniline. *Materials characterization* 2003, 50 (2-3), 131-134.

14. Yagci, Y., F. Yilmaz, S. Kiralp and L. Toppare, Photoinduced polymerization of thiophene using iodonium salt. *Macromolecular Chemistry and Physics* 2005, 206 (12), 1178-1182.

15. Koleske, J. V., *Radiation curing of coatings* ASTM international.

16. Decker, C., New developments in UV radiation curing of protective coatings. *Surface Coatings International Part B: Coatings Transactions* 2005, 88 (1), 9-17.

17. Jafarzadeh, S., A. Adhikari, P. E. Sundall and J. Pan, Study of PANI-MeSA conducting polymer dispersed in UV-curing polyester acrylate on galvanized steel as corrosion protection coating. *Progress in Organic Coatings* 2011, 70 (2), 108-115.

18. Feng, X., H. Huang, Q. Ye, J. J. Zhu and W. Hou, Ag/polypyrrole core-shell nanostructures: Interface polymerization, characterization, and modification by gold nanoparticles. *The Journal of Physical Chemistry C* 2007, 111 (24), 8463-8468.

19. Guyard, L., P. Hapiot and P. Neta, Redox chemistry of bipyrroles: Further insights into the oxidative polymerization mechanism of pyrrole and oligopyrroles. *The Journal of Physical Chemistry B* 1997, 101 (29), 5698-5706.

20. Kalendová, A., D. Veselý, I. Sapurina and J. Stejskal, Anticorrosion efficiency of organic coatings depending on the pigment volume concentration of polyaniline phosphate. *Progress in Organic Coatings* 2008, 63 (2), 228-237.

21. Hodko, D., M. Gamboa-Aldeco and O. J. Murphy, Photopolymerized silver-containing conducting polymer films. Part II. Physico-chemical characterization and mechanism of photopolymerization process. *Journal of Solid State Electrochemistry* 2009, 13 (7), 1077-1089.

22. Kasisomayajula, S. V., X. Qi, C. Vetter, K. Croes, D. Pavlacky and V. J. Gelling, A structural and morphological comparative study between chemically synthesized and photopolymerized poly (pyrrole). *Journal of Coatings Technology and Research* 2010, 7 (2), 145-158.

23. Ferreira, C., S. Domenech and P. Lacaze, Synthesis and characterization of polypyrrole/TiO2 composites on mild steel. *Journal of applied electrochemistry* 2001, 31 (1), 49-56.

24. Wynne, K. J. and G. B. Street, Poly (pyrrol-2-ylium tosylate), electrochemical synthesis and physical and mechanical properties. *Macromolecules* 1985, 18 (12), 2361-2368.

25. Breimer, M. A., G. Yevgeny, S. Sy and O. A. Sadik, Incorporation of metal nanoparticles in photopolymerized organic conducting polymers: A mechanistic insight. *Nano Letters* 2001, 1 (6), 305-308.

26. Jakab, E., E. Mészáros and M. Omastová, Thermal decomposition of polypyrroles. *Journal of thermal analysis and calorimetry* 2007, 88 (2), 515-521.

27. Yang, X. and Y. Lu, Preparation of polypyrrole-coated silver nanoparticles by one-step UV-induced polymerization. *Materials Letters* 2005, 59 (19), 2484-2487.

28. Martins, C., Y. De Almeida, G. Do Nascimento and W. De Azevedo, Metal nanoparticles incorporation during the photopolymerization of polypyrrole. *Journal of materials science* 2006, 41 (22), 7413-7418.

29. Hodko, D., M. Gamboa-Aldeco and O. J. Murphy, Photopolymerized silver-containing conducting polymer films. Part I. An electronic conductivity and cyclic voltammetric investigation. *Journal of Solid State Electrochemistry* 2009, 13 (7), 1063-1075.

30. Dhawan, S., N. Singh and S. Venkatachalam, Shielding behaviour of conducting polymer-coated fabrics in X-band, W-band and radio frequency range. *Synthetic Metals* 2002, 129 (3), 261-267.

31. Adachi, A. and J. Yamauchi, Effect of UV irradiation on polypyrrole as studied by electron spin resonance. *Synthetic Metals* 1995, 73 (2), 101-105.

CHAPTER 3. SOLVENT FREE ELECTRICALLY CONDUCTIVE UV-CURABLE HYBRID NETWORKS

3.1. Abstract

Prior research yielded coatings based on hybrid networks of polypyrrole and UV-curable polyester acrylates. Photopolymerization of pyrrole was achieved through the use of the silver nitrate as a photooxidant. Solubility problems of silver salts were circumvented through the use of the solvent acetonitrile. These coatings showed promising properties in the area of ant-static technologies. Unfortunately, acetonitrile is known to be toxic due to the ability to be transformed into hydrogen cyanide in the body. In this study solvent free UV-curable hybrid networks were developed utilizing acrylonitrile as a reactive diluent to replace the acetonitrile. Formulations at various pyrrole concentrations were developed and cured on aluminum 2024T3 substrates. The liquid formulations were studied for their reactivity through the use of photo differential scanning calorimetry (P-DSC). Cured coatings were studied for their mechanical and physical propertied through standard coatings tests. Electrical properties were studied through the four point probe technique as well as conductive atomic force microscopy (C-AFM). Thermal properties were studied with thermal gravimetric analysis. The coatings were also studied for their corrosion inhibitive properties through electrochemical impedance spectroscopy (EIS) as well as ASTM B117 salt spray technique.

3.2. Introduction

Functionalized coatings utilizing electrically conductive polymers and traditional polymeric materials show promise in various areas of application. Polypyrrole is a popular choice as the conductive polymer in these functional coatings due to the facile synthesis methods employed, tailorable electrical properties by varying reaction parameters such as pH and dopant

concentration, and superior thermal and environmental stability. Polypyrrole does have limitations, most notably poor mechanical properties.

Polypyrrole can be produced through two methods: electrochemical and chemical oxidation of pyrrole monomer. Polypyrrole films can be produced through electropolymerization. This technique has produced uniform films that show excellent adhesion, superior electrical conductivity, as well as inhibiting corrosion.[1] Electropolymerization however is limited to the type of substrate that can be used as well as the geometry of the substrate.

Chemical oxidative polymerization of pyrrole through the use of oxidizing agents such as ammonium persulfate and ferric chloride can be used to produce large quantities of oxidized, electrically conductive polypyrrole.[2, 3] Polypyrrole synthesized with chemical oxidizing agents results in a black powder that is insoluble in solvents and thus uniform films cannot be formed.[4] Doping of polypyrroles with bulky large organosulfates such as di(2-ethylhexyl) sulfosuccinate, result in polypyrroles soluble in polar organic solvents, but this is deleterious to the overall electrical properties, and thus not widely used.[5]

Polypyrrole powder can however be blended with traditional organic coatings to make up for the lackluster mechanical properties and be able to make uniform well adhering films. Blending with traditional organic coating resins will retard the overall electrical properties, but blending ECPs at level greater than the percolation threshold will still demonstrate appreciable electrical conductivity.[6, 7] In applications such as corrosion protection of metal alloys, large quantities of polypyrrole might not be needed and as such can be incorporated at levels below the percolation threshold. Formulations below the CPVC of the ECP results in coatings with improved barrier properties thus protecting the substrate from electrolyte penetration for longer exposure times.

Using polypyrrole as a pigment can be problematic in the sense that dispersing pigments in organic coatings requires a large amount of energy to break up agglomerations to insure adequate dispersion.[8] In addition pigments tend to naturally settle over time resulting in the need to redisperse at a future time. Polymerizing pyrrole while organic coating resins cure upon application to the substrate would circumvent the problems associated with dispersion. This method however is difficult due to the different polymerization mechanisms between pyrrole and organic coating resins.

Prior research at NDSU has developed a technique to make hybrid networks of polypyrrole and UV-curable polyester acrylates. This technique used silver salts to oxidize pyrrole to polypyrrole upon exposure to UV light. Photopolymerization of conductive polymers is well documented and can be achieved through the use of photooxidative salts, with the most effective being silver and gold salts, although others have been used.[9-18] The hybrid networks of UV-curable acrylates and polypyrrole demonstrated good coating properties, including excellent adhesion to sandblasted Al-2024T3 substrates, which is typically problematic for UV-curable coatings. In addition the resulting hybrid networks with PPy content of 40% or greater had surface resistance and bulk conductivities in the range for anti-static technologies.

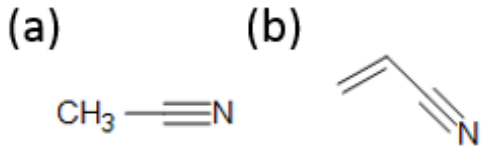

Figure 3.1: Chemical structures of (a) acetonitrile, and (b) acrylonitrile

These hybrid networks were synthesized in the presence of a significant amount of solvent. One of the major positives of UV-curable technology is the ability to develop VOC free coatings which are becoming a greater necessity due to increased regulation in VOC output. In addition to acetonitrile being a VOC, it is highly flammable and moderately toxic, due to its conversion in the body to hydrogen cyanide.[19] The goals of this research is to develop hybrid networks of UV-curable acrylate and polypyrrole, but in a formulation that is free of solvent, thus 0 VOC. Acrylonitrile has a similar structure to acetonitrile (see Figure 3.1) and can be used as a reactive diluent for free radical UV-curable formulations. In addition, silver nitrate is soluble in acrylonitrile, thus it can help solubilize the silver nitrate used in the formulations to oxidize pyrrole. Research has demonstrated the ability to synthesize composites of polyacrylonitrile and silver nitrate crystals that were then further used to make polyacrylonitrile-PPy composites.[20]

3.3. Experimental

3.3.1. Materials

All chemicals used in the study were used as received unless noted. Silver nitrate and acrylonitrile were purchased from Sigma Aldrich. Pyrrole was purchased from VWR and was distilled prior to use. EBECRYL® 436 was supplied by Cytec Industries and is a chlorinated polyester acrylate diluted with trimethylolpropane triacrylate. This UV-Curable blend was selected due to its excellent adhesion to metal. 2-Hydroxy-2-methyl-1-phenyl-propan-1-one (DAROCUR® 1173) is a Norrish type I photoinitiator supplied by BASF. Substrates used in this study were 3" x 6" aluminum 2024T3 panels purchased from Q-Panel. All panels were sandblasted with alumina grit and then degreased with hexanes prior to coating application. Coatings were also cast onto 3" x 6" glass panels purchased from a local hardware store.

3.3.2. Coating Formulations

For all formulations the coatings were prepared in a multi-step system. In the first vial silver nitrate was dissolved in pyrrole by slowly adding silver nitrate and mixed via magnetic stirrer. Half of the acrylonitrile was added to the pyrrole upon final addition of silver nitrate to help facilitate solubilization. In a second vial, the remaining acrylonitrile and EBECRYL 436 were added together. The vial containing the acrylate blend was then added drop wise to the pyrrole-silver nitrate solution. Lastly the DAROCUR 1173 was added and the formulation was left to mix via magnetic stirring for 5 minutes.

Coating formulations in this study were made at varying levels of pyrrole concentration in increments of 20%. In addition to studying the effect of pyrrole concentration, two different pyrrole:silver ratios were used in this study. The ratios used were 5 pyrrole : 1 silver molecule so that comparisons could be drawn between solvent free and the solvent borne hybrid networks previously developed, as well as a ratio of 8 pyrrole : 1 silver molecule to determine if lower levels of silver could be used to reduce the overall cost. For both studies, coatings containing 0% pyrrole were used as control coatings for these studies.

Coating formulations were cast onto aluminum 2024T3 and glass substrates via drawdowns. Drawdowns were conducted at a wet film thickness of 4 mils. Coated panels were then exposed to UV radiation via DYMAX Model 5000-EC UV-Light Curing Flood System equipped with a metal halide bulb with a spectral intensity of 174 mW/cm^2. Spectral intensity of the bulb was measured with a UV Power Puck made by EIT instruments. Coatings were cured in curing cycles of 60 seconds exposed to radiation followed by 60 seconds off to allow for adequate cooling. Coatings were cured until black and tack free.

3.3.3. Coating Characterization

Photo-Differential Scanning Calorimetry (P-DSC) was used to study how fast the formulations cured when exposure to UV-radiation through the use of a TA instruments Q-1000 differential scanning calorimeter equipped with a TA instruments Q-Series PCA photo-calorimeter with a spectral output of 50 mW/cm^2 under a nitrogen atmosphere.

Gloss of the final cured coating was studied using a BYK Gloss meter. König hardness was studied by a BYK König hardness tester. Cross hatch adhesion on aluminum 2024T3 substrates was performed following the ASTM D3359 method. All coatings tests were performed in triplicate to ensure reproducibility and to quantize the drift in these values.

Morphology of the hybrid networks was studied with scanning electron microscopy using a JEOL JSM-6300 scanning electron microscope equipped with a field emission electron gun with a back-scattering electron detector. In addition, elemental analysis was conducted through energy dispersive spectroscopy with a detector on the scanning electron microscope. Thermal stability of the cured coatings was studied through Thermal Gravimetric Analysis. TGA was performed on a TA instruments Q-500 thermogravimetric analyzer. TGA scans were conducted under an inert, N_2 atmosphere with a scan range from room temperature to 800°C at a scan rate of 20°C/minute.

Electrical properties were studied both at a macro and micro level. Macro electrical properties were studied through the use of a Four-Point Probe technique which consisted of a Keithley® 2100 digital multimeter connected to a Signatone® four point probe assembly. Local electrical properties were studied using a Veeco® 3100 atomic force microscope in contact mode with a platinum-iridium current sensing tip. Scans were conducted at an applied potential of 1V through the sample at scan rates of 1.51Hz and 256 samples points per line.

Coatings containing 40%, 20%, and control coatings were studied for their corrosion inhibitive nature. For these corrosion studies 3 samples of each formulation were studied via electrochemical impedance spectroscopy (EIS). For EIS studies, samples were exposed to 5% NaCl solution and EIS scans were taken at standard intervals. EIS was conducted in a three-electrode setup with a Ag/AgCl reference electrode, a platinum counter electrode, and the aluminum 2024T3 substrate acting as the working electrode. EIS scans were conducted in a frequency range of 100,000 to 0.01 Hz, at 10 points per decade, with a perturbation of 10 mv. In addition to EIS, coated panels were scribed and placed in a weathering chamber following ASTM B117 protocol. Scribed panels were taken out at regular intervals and pictures were taken to observe the progressive corrosion product buildup.

3.4. Results and Discussion

3.4.1. Liquid Coating Formulations and Characterization

Table 3.1 lists the formulations for the solvent free hybrid network coatings. In all of these formulations a slight yellowing was noticed with increased pyrrole concentration. This yellowing is due to the presence of low molecular weight pyrrole oligomers that develop when silver nitrate is dissolved in pyrrole. Oxidation of pyrrole to polypyrrole with silver salts is possible without exposure to UV-light as reported in literature, although the reaction proceeds very slowly, where full cure takes around 48 hours to occur.[11] For all coatings in this study, samples were exposed to 180 seconds of UV-light in 60 second increments. During curing of the coatings, coatings with the 5:1 pyrrole to silver ratio turned brown to black slightly faster than the samples with the 8:1 ratio, although both were fully cured at 180 seconds. This is due to a faster reaction rate due to the higher concentration of oxidizing agents in the formulations. Control coatings were tack free after about 60 seconds of UV exposure, but were still exposed to the whole 180 seconds to remain

consistent with the other formulations. In addition, the formulation 20%_PPy_5 had silver nitrate collapse out. This is due to the solubility of silver nitrate in acrylonitrile being slightly poorer than in acetonitrile as those formulations in the previous chapter had no visible miscibility problems.

Table 3.1: Formulations for solvent free UV-curable hybrid networks

Formulation	Ebecryl® 736 (g)	DAROCUR 1173 (g)	Acrylonitrile (g)	Pyrrole (g)	Silver Nitrate (g)
0%_PPy_Control	12.0	0.075	3.00	0.0	0.00
20%_PPy_5	9.6	0.06	2.4	3.00	1.52
40%_PPy_5	7.2	0.045	1.8	6.00	3.04
60%_PPy_5	4.8	0.03	1.20	9.00	4.56
80%_PPy_5	2.4	0.015	0.60	12.00	6.08
20%_PPy_8	9.6	0.06	2.4	3.00	0.95
40%_PPy_8	7.2	0.045	1.8	6.00	1.90
60%_PPy_8	4.8	0.03	1.20	9.00	2.85
80%_PPy_8	2.4	0.015	0.60	12.00	3.80

3.4.2. Physical Property Testing

Coatings were characterized for their respective properties and graphs of the properties are shown in Figure 3.2. From Figure 3.2a it is apparent the gloss value drops much more sharply for the formulations with a 5:1 ratio of pyrrole to silver nitrate. This drop after 20% pyrrole concentration was previously observed with the solvent borne coatings systems (see previous chapter) as is explained by the fact that electrically conductive polymers display a CPVC of around 35%. The formulation at 40% PPy but with a ratio of 8:1 still display high gloss values. This is attributed to the fact there is insufficient silver nitrate to oxidize pyrrole to polypyrrole thus limiting the amount of high molecular weight polypyrrole and a larger presence of pyrrole oligomers in the sample.

König hardness tests (Figure 3.2b) show that samples formulated with 5:1 are much harder than samples formulated with an 8:1 ratio. Due to sufficient silver nitrate in the coating

formulations, there is a lower presence of pyrrole oligomers thus less plasticizing of the UV-curable matrix occurs which results in a harder film.

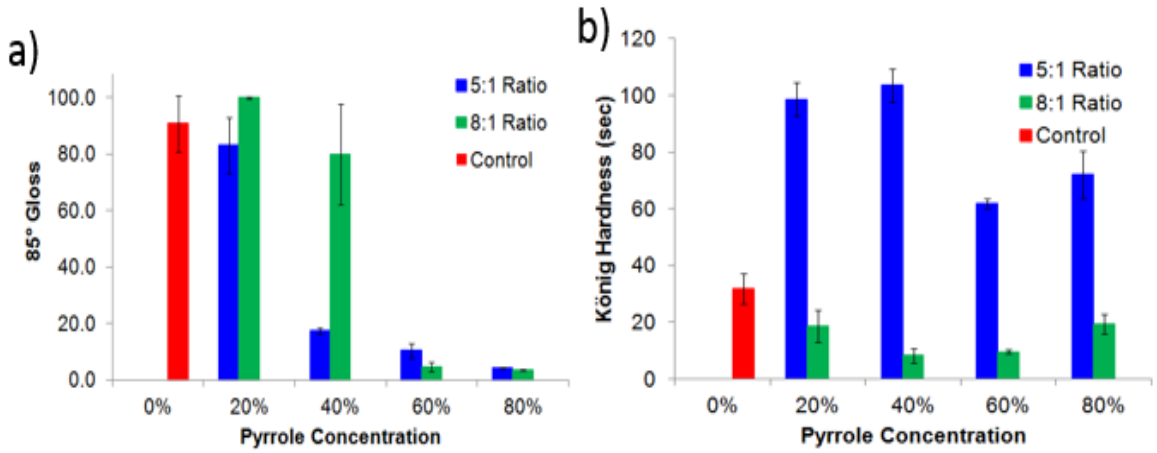

Figure 3.2: Plots for 85° Gloss (a) and König hardness (b) with respect to pyrrole concentration.

Table 3.2: Adhesion and solvent resistant results

Formulation	Cross Hatch Adhesion	MEK DR
0%_PPy_Control	0	40
20%_PPy_5	0	20
40%_PPy_5	0	0
60%_PPy_5	5	0
80%_PPy_5	5	0
20%_PPy_8	5	20
40%_PPy_8	5	0
60%_PPy_8	5	0
80%_PPy_8	5	0

Cross hatch adhesion and MEK double rub values are listed in Table 3.2. From the results it shows that all coatings have poor solvent resistance with just the control clear coat showing MEK double rub values of 40. This is attributed to the control coating containing 30% acrylonitrile

which would in effect lower the crosslink density of the final film compared to traditional reactive diluents such as hexanediol diacrylate (HDDA) or trimethylolpropane triacrylate which both have functionalities greater than 1.

3.4.3. Morphology Study of Coatings

SEM images for formulations of the control (Figure 3.3), 5:1 formulations (Figure 3.4), and 8:1 formulations (Figure 3.5) are shown below. Back scatter electron filter is used to distinguish the silver nanoparticles that exist within the hybrid networks. Silver nanoparticles exist predominantly in the polypyrrole regimes due to the reduction from Ag^{+} to Ag^{0} upon photooxidation of pyrrole to polypyrrole.[17] SEM photograph for the control coating displays no unique morphology and very little surface features. This correlates well with the gloss measurements.

As pyrrole content increases for both 5:1 and 8:1 ratio formulations, rougher surface characteristics develop. This rougher surface is due to the development of higher molecular weight polypyrrole which typically displays a rough-cauliflower morphology. In addition, hybrid networks made up of predominantly polypyrrole (60% and 80%) show distinguishable areas of high silver content where polypyrrole is located. Formulations with lower polypyrrole content show no localized areas of high silver nanoparticle content which means the polypyrrole is relatively evenly distributed throughout the cured coatings.

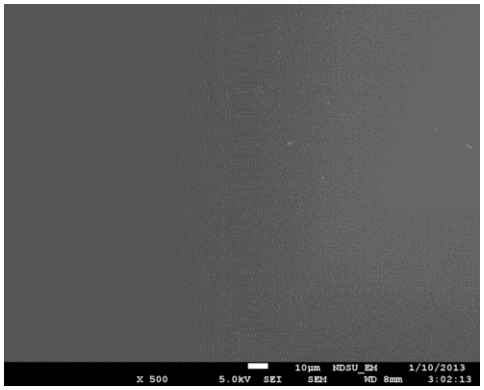

Figure 3.4: SEM micrograph for control clear coat

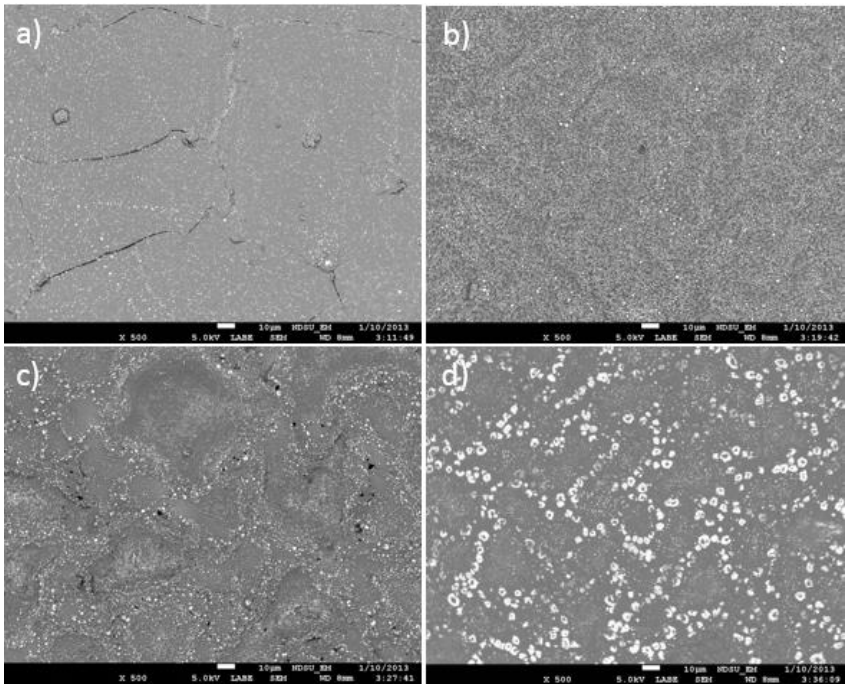

Figure 3.4: SEM images for 5:1 coating formulations for (a) 20%PPy, (b) 40%PPy, (c) 60% PPy, and (d) 80% PPy.

Formulations at 5:1 ratio showed cracks at 20% and 60% polypyrrole content. Cracking in UV-curable coatings is rather common due to the high volume shrinkage during the photopolymerization reaction.[21] With the reaction proceeding so quickly, the resulting coating does not have time to relax and thus microcracks develop and can proceed to cause macroscopic

coating failure. This effect is exacerbated by the fact that formulations for 5:1 at 20% PPy content had collapsed out silver nitrate which would provide areas for these cracks to propagate from during curing.

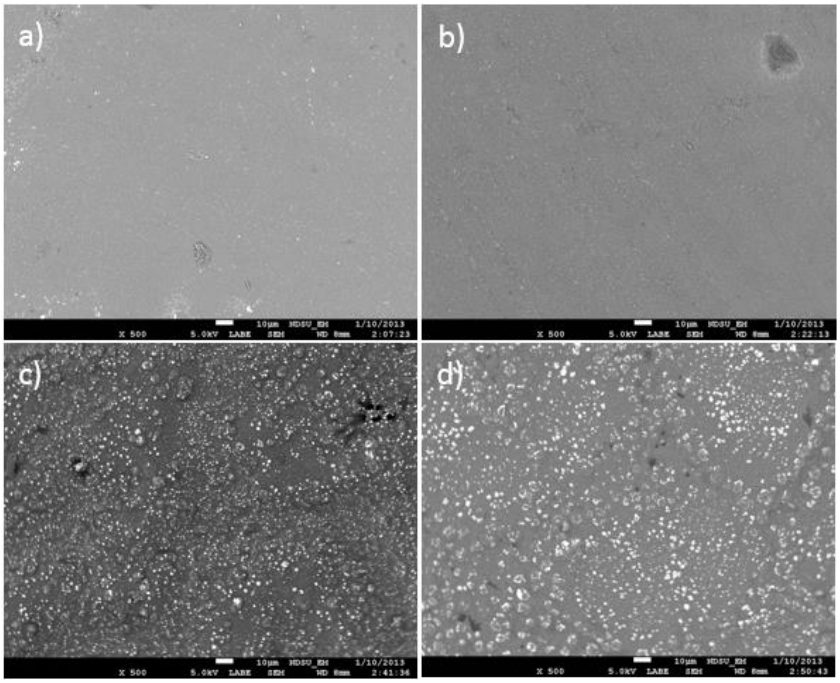

Figure 3.5: SEM images for 8:1 coating formulations for (a) 20%_PPy, (b) 40%_PPy, (c) 60%_ PPy, and (d) 80%_PPy.

The localized holes in 60% PPy formulations are also apparent in the SEM image for 60% PPy at 8:1 ratio. These localized defects seem to be on boundaries between areas with high silver content thus being at the boundary between the UV-curable acrylate regime and polypyrrole regimes possibly indicating poor interaction between these respective domains.

For formulations with an 8:1 ratio, SEM images for 20%_PPy_8 and 40%_PPy_8 showed very little silver on the surface as well as very little surface roughness. This lack of silver on the surface compared to the 5:1 counterparts is attributed to the fact that less silver is in the overall formulation and the lack of surface characteristics is attributed to the lower levels of conversion from pyrrole to high molecular weight polypyrrole.

Element analysis obtained via EDXA is presented in table 3.3. The nitrogen content for coatings is from the nitrogen atoms in each pyrrole ring, as well as the nitrogen in the nitrate anion that is doping the oxidized polypyrrole. For samples containing low amounts of polypyrrole (40%, and 20%), nitrogen was not detected. This is due to the peak being sandwiched between carbon and oxygen peaks and the detector just cannot separate the three. At higher PPy concentrations, the nitrogen peak is large enough to distinguish. The increase in silver content for both 5:1 and 8:1 is due to the higher silver concentrations for formulations at higher PPy levels. Samples at 5:1 ratio showed high levels of silver on the surface of the coatings compared to the 8:1 counterparts.

Table 3.3: Elemental analysis for UV-curable hybrid networks

Formulation	C	O	Cl	N	Ag
0%_PPy	79.52	15.09	5.39	---	---
20%_Ppy_8:1	79.59	14.92	4.87	---	0.62
40%_Ppy_8:1	76.56	17.84	4.74	---	0.86
60%_Ppy_8:1	66.55	21.06	2.54	5.64	4.22
80%_Ppy_8:1	62.55	19.98	1.35	8.95	7.16
20%_Ppy_5:1	74.27	18.24	5.38	---	2.10
40%_Ppy_5:1	63.34	21.45	4.58	5.42	5.21
60%_Ppy_5:1	61.86	22.74	3.97	6.15	5.28
80%_Ppy_5:1	63.01	23.36	1.57	3.13	8.63

3.4.4. Thermal Stability Experiments

Thermal gravimetric analysis is a useful technique in studying the thermal stability of various organic coatings. In Figures 3.6(a) and 3.6(b) TGA overlays for the 5:1 and 8:1 formulations are displayed. For the control coatings after 175°C only 3% weight loss was noticed. This 3% weight loss is attributed water uptake during formulation as well as unreacted acrylonitrile

that would exist in the cured formulations (the boiling point of acrylonitrile is 170°C). Water uptake is fairly minimal as only about 0.3% weight loss was observed after 100°C. This means for the control coatings which consisted of 30% acrylonitrile by weight, 2.7% was left unreacted in the final films. This unreacted acrylonitrile will effectively plasticize the final films which could be the cause for the soft control coatings as observed from the König hardness results.

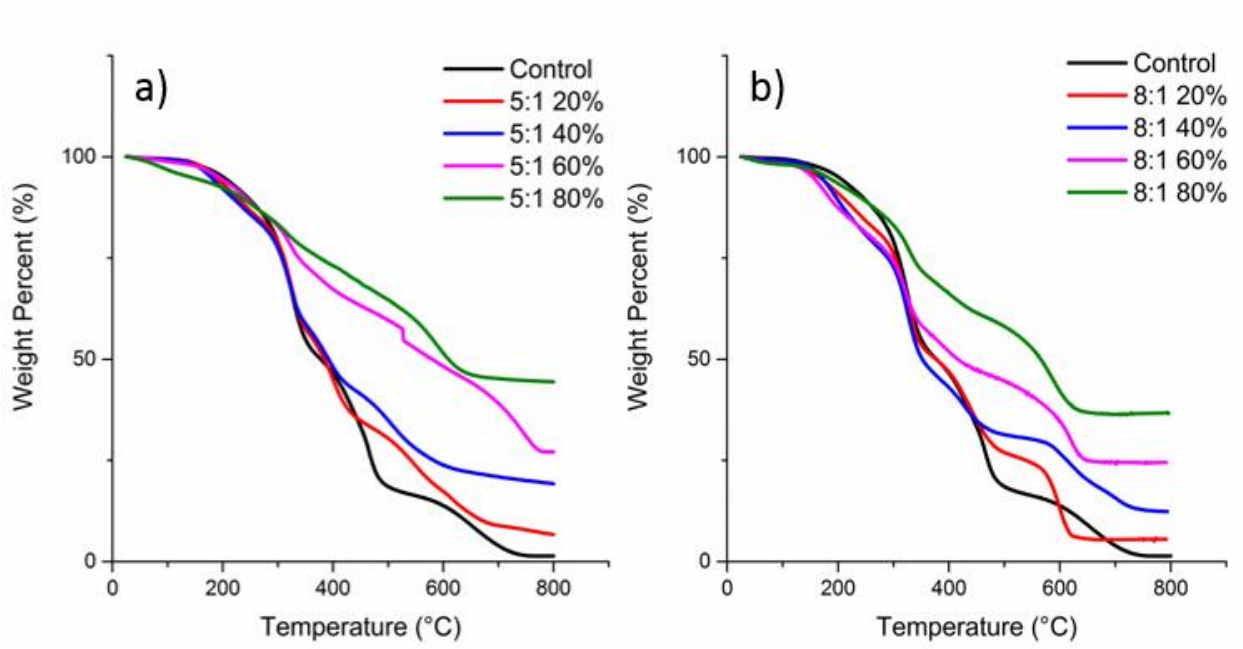

Figure 3.6: TGA graphs for (a) 5:1 ratio formulations and (b) 8:1 ratio formulations.

Prior research in the development of these hybrid networks with the aid of acetonitrile as a solvent showed control coatings consisting of the polyester acrylate and trimethylolpropane triacrylate displayed 3 major temperature degradation regimes. Polyacrylonitrile demonstrates its major thermal breakdown point between 300 and 400°C and thus overlaps with the first regime where degradation of the polyester acrylate occurs.[22]

Previous studies in photopolymerization of polypyrrole without UV-curable resins demonstrated two degradation regimes which correlate to the degradation of nitrate ions that dope the polypyrrole (between 150°C and 250°C) as well as the breakdown of the polypyrrole chains

between 350-500°C. As polypyrrole content increases in both the 5:1 and 8:1 formulation the polypyrrole chain breakdown regime becomes more apparent. There is a drastic increase in overall thermal stability for 60% and 80% PPy coatings at a ratio of 5:1. For almost all formulations at an 8:1 ratio there is noticeable amounts of thermal degradation between 100-300°C. Pyrrole monomer has a boiling point of 130°C thus the excessive degradation in this regime could be due to the volatilization of unreacted pyrrole monomers trapped in the UV-curable matrix. Even though phase separation occurred in the 5:1 formulation at 20% PPy, no noticeable levels of pyrrole monomer was left unreacted indicating that pyrrole was still successfully oxidized to polypyrrole

The char of all samples that contain PPy are a mixture of the PPy char, as well as silver nanoparticles that are in the coatings. Increasing PPy in the formulations results in an increase in the char of the samples. This increase is due to both the largest quantities of PPy that exist in the cured coatings as well as the increased amount of silver used in formulations with higher levels of PPy. Thermal studies of PPy doped with organic surfactants had approximately 35 weight% of char after 800°C. For samples containing 80% PPy the formulation with a 5:1 ratio had a char of 44.01%, while the 8:1 ratio coating had a char of 36.58%. This difference in char between the two samples is close to the difference in total silver (by weight %) between each formulation. These TGA results indicate that the coating formulations containing an 8:1 ratio are inferior to the coatings formulated at a 5:1 ratio due to the unreacted pyrrole monomers that exist for the 8:1 coatings.

3.4.5. Electrical Properties

Figure 3.7 displays results obtained from the four point probe experiments. For the experiment the maximum measurable value for surface resistance is 100 MΩ. Coating

formulations at a 5:1 ratio showed measurable surface resistance at pyrrole concentration of 40% or greater in the liquid formulations. This breakpoint coincides with the solvent borne hybrid networks previously developed and is attributed to surpassing the percolation threshold of polypyrrole. Comparing the solvent free formulations to the solvent borne predecessors coating resistance at 60% and 80% pyrrole loading displayed sheet resistances of 1 and 2 orders of magnitude greater respectively.

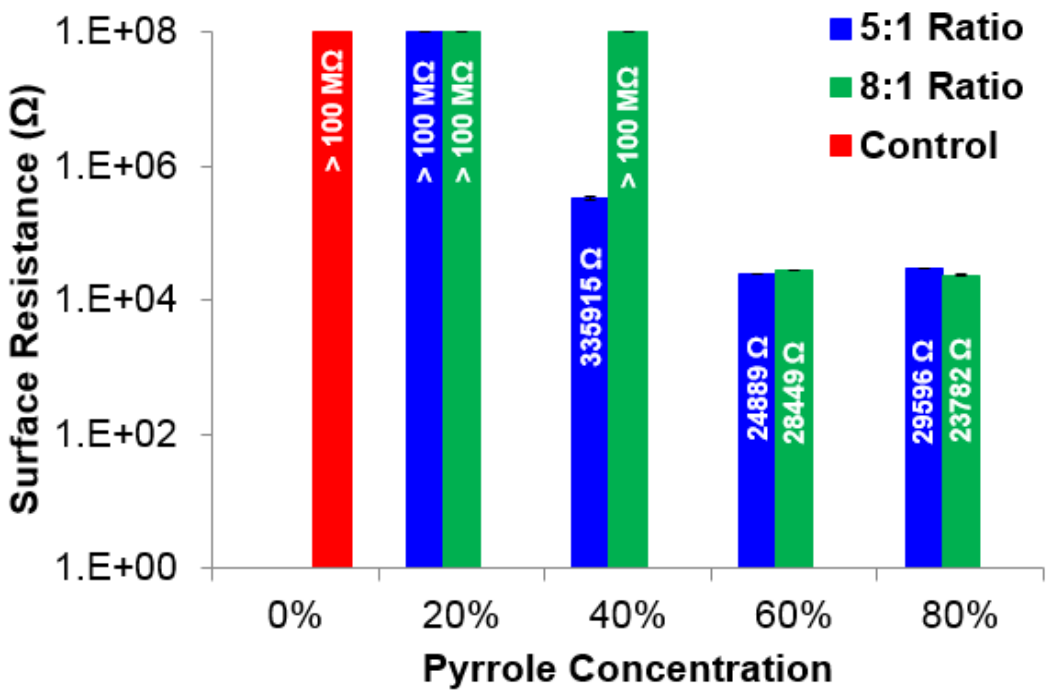

Figure 3.7: Surface resistance measurements for cured hybrid networks.

For anti-static purposes, a materials needs to have a sheet resistance on the order of 10^4-10^8 Ω to be effective at static charge dissipation.[23] For the 5:1 formulations a minimum 40% PPy content is needed while for the 8:1 ratio formulations a minimum content of PPy is 60%. The higher PPy concentration required for the 8:1 is attributed to the insufficient silver salt to polymerize high molecular weight PPY at sufficient quantities to achieve percolation. In addition,

previously discussed SEM results show PPy domains developing at the 40% pyrrole concentration for the 5:1 ratio coatings, while these domains do not appear until 60% pyrrole concentration for 8:1 films.

While four point probe measurements give macro level information for sheet resistance and electrical conductivity, CAFM gives valuable information of the domains that are electrically conductive at a local level.[24] Figure 3.8 are CAFM scans for all formulations. The formulations at a 5:1 ratio showed large levels of electrical conductivity for 40% and 80% pyrrole concentration, with small levels of conductivity observed at 20% and 60% pyrrole concentration. The difficulty of acquiring a proper scan at 60% pyrrole concentration was due to the large amount of surface roughness as measured by tapping mode AFM. These large topography changes make it difficult for the CAFM tip to remain in contact with the surface.

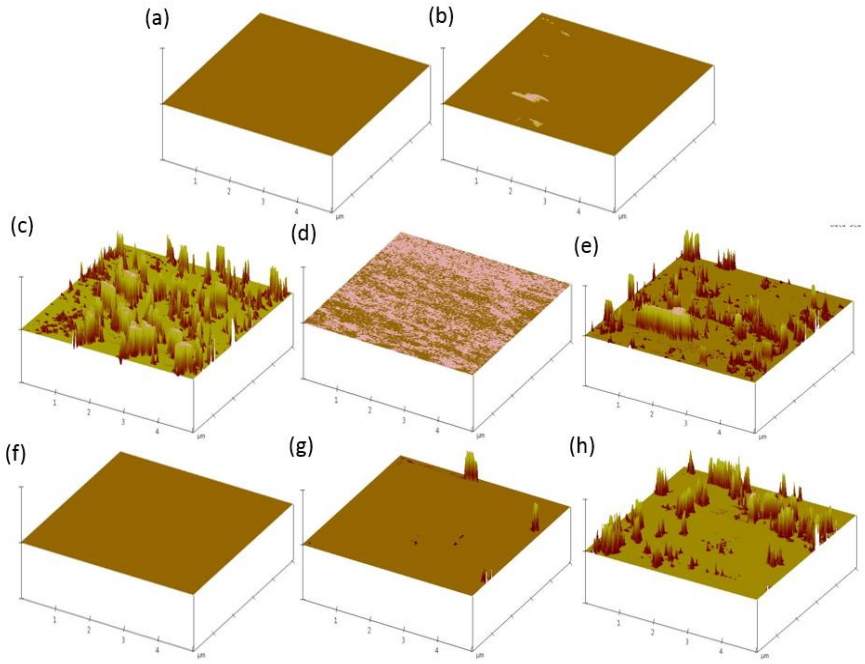

Figure 3.8: CAFM scan results for: (a) control, (b) 20%_PPy_5, (c) 40%_PPy_5, (d) 60%_PPy_5, (e) 80%_PPy_5, (f) 20%_PPy_8, (g) 60%_PPy_8, and (h) 80%_PPy_8. Z-Scale is 2μA. Scan area is 5μm x 5μm.

For the 8:1 formulation series scans at 40% PPy could not be acquired. These coatings were too soft for the tip to engage the surface thus measurements could not be obtained. Measurable conductivity was noted at 60% and 80% pyrrole concentration. The CAFM results correlate with the four point probe measurements. This means that formulations at a 5:1 ratio are superior for anti-static purposes as less polypyrrole content is needed in the final cured coatings. Formulations are 8:1 ratio are inferior due to not being able to sufficiently oxidize pyrrole to polypyrrole due to the lower concentration of oxidant in the formulation.

3.4.6. Corrosion Inhibition Studies

Prior research on solvent borne UV-curable hybrid networks focused predominantly on general coating characterization and the feasibility of implementation as an anti-static materials. Polypyrrole can also be used for corrosion protection of metal alloys due to its ability to scavenge oxygen thus hindering corrosion reactions from progressing when it exists in the reduced state, or by passivating the underlying metal alloy when it is in the oxidized form. Although traditional UV-curable coating systems which provide corrosion protection through acting as a barrier from electrolyte penetrating to the surface are inferior to traditional step growth organic coatings such as epoxy-amine and polyurethane chemistries, incorporating polypyrrole into the coatings could provide adequate active corrosion mitigation to make up for these pitfalls.

From the prior results it is apparent that 5:1 ratio formulations are superior in overall coating properties thus were used for corrosion protection studies. Accelerated weathering images are displayed in Figure 3.9 before and after 168 hours of exposure in ASTM B117 conditions. It is apparent that even after a short duration in accelerated weathering conditions, excessive corrosion is observed through the coating consisting of 20% PPy. This is attributed to collapse out of silver nitrate that is observed during formulation thus allowing a slightly more porous coating.

Control coatings also showed corrosion within the scribe, as well as some slight filiform corrosion underneath the coating. In addition, slight coating delamination was observed around the scribe indicating poor adhesion to the Al-2024T3 substrate.

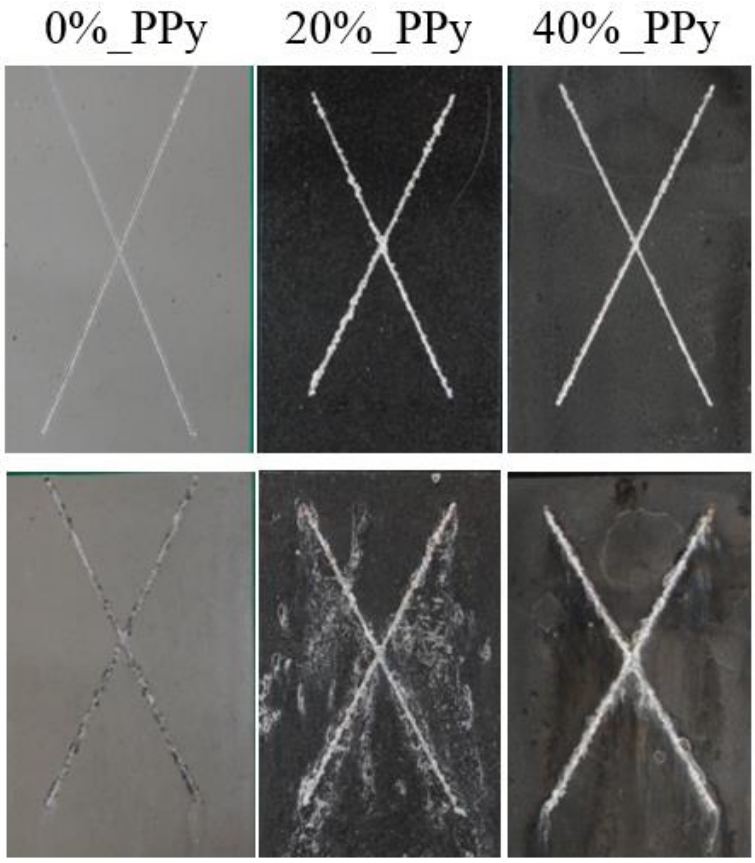

Figure 3.9: Optical photographs of ASTM B117 salt spray results. Top – prior to exposure, Bottom – after 168 hours exposure.

Coatings containing 40% PPy displayed large levels of corrosion in the scribe as well as coating discoloration away from the scribe. Black spots away from the scribes are believed to be areas of filiform corrosion beginning thus indicating coating failure. This failure in all coatings are indicative of two problems that exist in these formulation. The first problem with these coating formulations is the relatively soft nature of the UV-curable control coating as indicated by the König hardness tests. This is attributed to the lower crosslink density that is a result of formulating

with the monofunctional acrylonitrile as a reactive diluent. In addition to the soft UV-curable resin, the control coatings displayed poor adhesion to the metal substrate which is a common problem from the fast curing during UV-irradiation.

Secondly, the polypyrrole synthesized during photopolymerization utilized silver salts resulting in PPy containing silver metal nanoparticles. Unprotected Al-2024T3 demonstrates poor corrosion resistance properties due to the more noble elements such as copper that are present in this alloy.[25] Silver is a highly noble metal that could galvanically couple with the aluminum 2024T3 substrate resulting in galvanic corrosion of the aluminum in the Al-2024T3 alloy. From the accelerated weathering results it seems coatings containing PPy show poorer corrosion protection than the control coatings.

EIS gives valuable information that traditional accelerated weathering techniques do not supply. EIS is a useful tool in studying how quickly electrolytes can permeate a coating system, as well as allow determining when electrolyte reaches the substrate surface and corrosion reactions begin by circuit modelling the EIS results to fit an equivalent circuit. Below in figure 3.10 are the Bode modulus plots for up to 336 hours of immersion. The control coatings showed very high impedance upwards of 1 GΩ on initial immersion. As time progressed the control clear coat samples showed large drops in impedance on the order of 2 orders of magnitude. This drop in impedance is due to electrolyte permeation through the coating. After about 24 hours of immersion the impedance change only dropped about 1 order of magnitude up until 336 hours. It is apparent that after about 3 hours of immersion the slope in the low frequency impedance range flattens indicating a change from a purely capacity material to a material also showing a resistive portion indicating a measureable pore resistance (R_p). This means electrolyte has begun to pass through the clear coat samples only after 3 hours of immersion indicating poor barrier properties. After

about 168 hours of immersion a second time constant appears indicating a developed of an oxide layer underneath the coating.

Coatings consisting of 20% PPy showed very low impedance values at all frequencies. This low impedance is attributed to the porous coating that developed as observed by SEM. These results indicate that even after 1 hour very little protection is offered from electrolyte reaching the aluminum 2024 T3 surface and thus are ineffective at protecting the substrate. Coatings consisting of 40% PPy showed little to no change in the impedance after 48 hours. The overall impedance for these coatings in about 5 orders of magnitude lower than the control coatings as well as the low to mid frequencies displaying a resistive behavior, but this is attributed to the electrically conductive nature of polypyrrole. The AC signal used in EIS prefers the least resistive pathway when travelling through the coating and thus passes through the electrically conductive polypyrrole domains. This phenomena has been observed by others working with polypyrrole-composite pigments for the protection of Aluminum 2024T3 as well. [26]

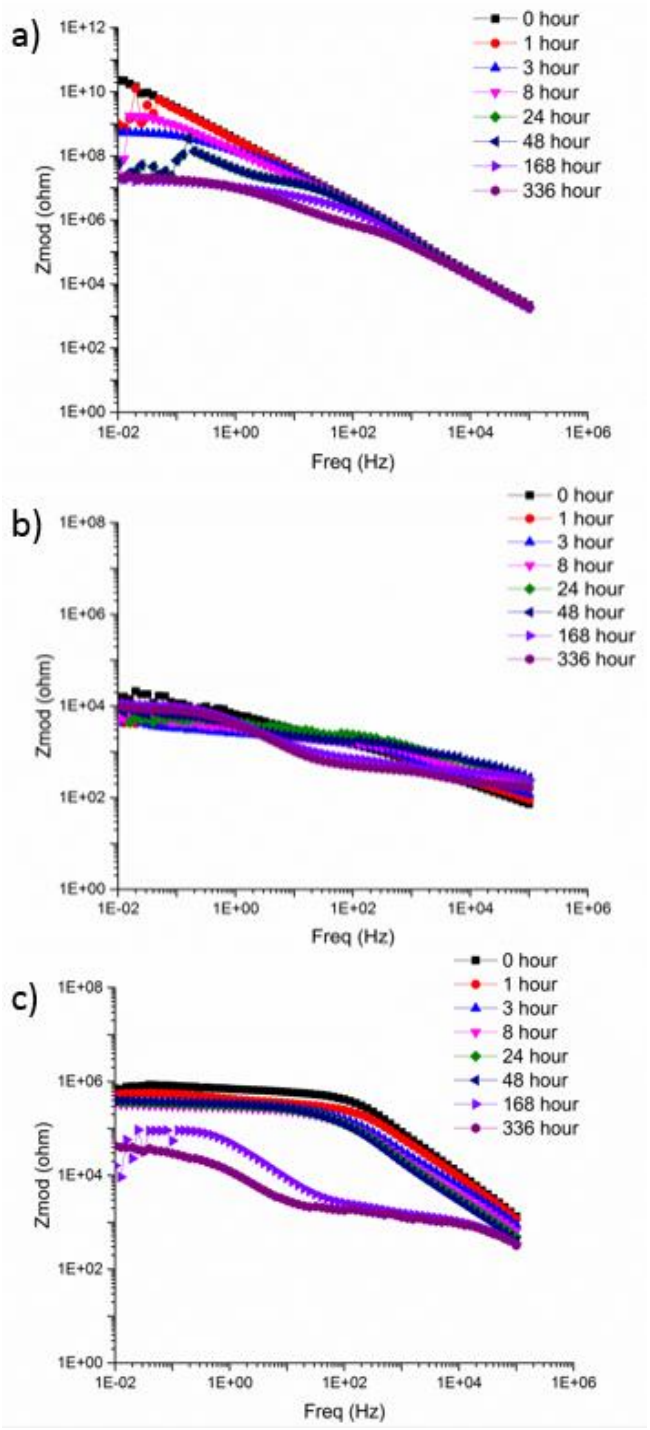

Figure 3.10: Bode modulus plots for control (a), 20% PPy (b), and 40% PPy (c) coatings.

After 48 hours however a drop in impedance on the order of 1 order of magnitude is observed as well as a development of a second time constant indicating corrosion at the aluminum 2024T3 surface has begun to occur.

Using software to model the EIS results as equivalent circuits gives valuable insight in how electrolyte permeates a coating system and also gives information on the progression of corrosion reaction after electrolyte reaches the substrate's surface. Below in Figure 3.11 is an example image demonstrating the accuracy of the modelling values compared to the actual data. The green line in the scans is the line obtained from the model values, while the red line is the actual values.

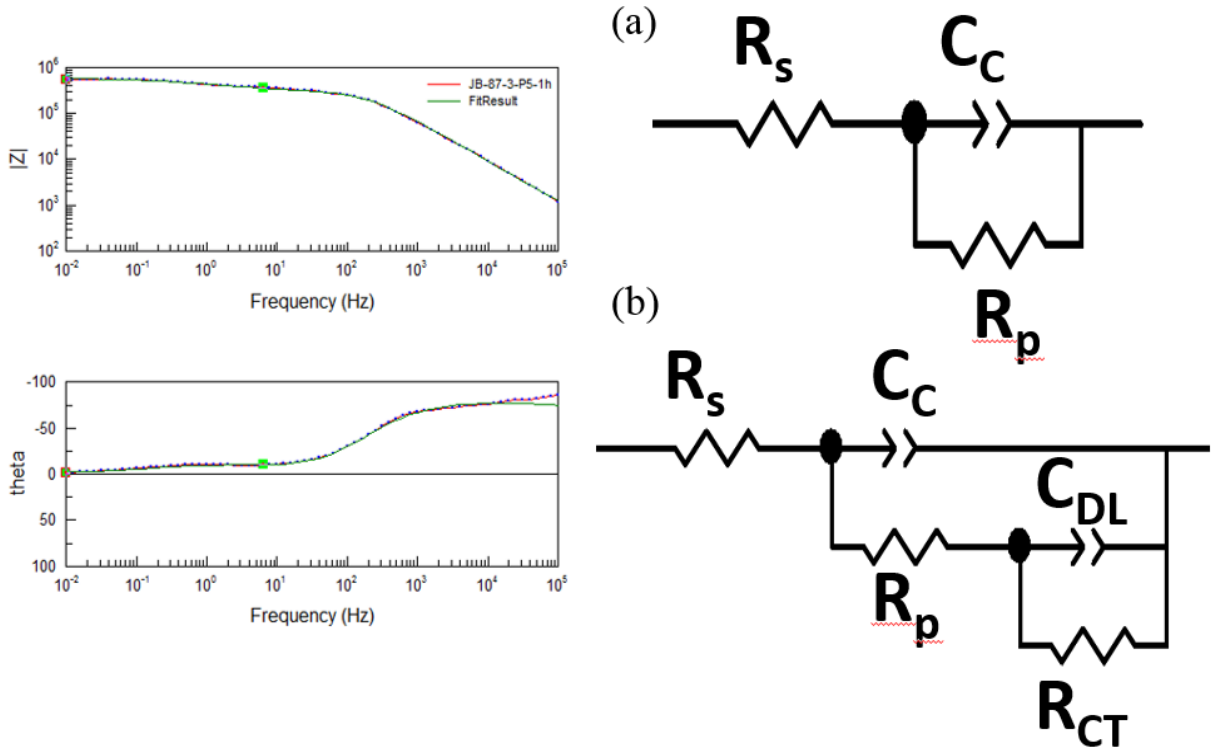

Figure 3.11: Example image for modelling results (left) and the common equivalent circuits used in the modelling of EIS results.

For modelling EIS results, there are two common equivalent circuits. The first equivalent circuit is (a) from Figure 3.11 and is referred to as a Randal's cell. This equivalent circuit models

an undamaged typical organic coating where R_s stands for the electrolyte resistance, C_c is the coating capacitance, and R_p is the pore resistance which described how difficult it is for electrolyte to permeate the coating. The second equivalent circuit listed as (b) in Figure 3.10 illustrates a failed coating in which electrolyte has permeated through the coating and reached the metal substrate. For this situation a second time constant consisting of a constant phase element and resistor in parallel are used to model the developing oxide layer from the corrosion reaction. C_{DL} symbolizes the double layer capacitance, which is the oxide layer developing from corrosion and R_{CT} is the charge transfer resistance, which is used to describe the resistance of electrolyte permeation of the oxide layer.

From the modelling results, monitoring the R_p with respect to time is displayed in Figure 3.12. Control coatings had a drop of 3 orders of magnitude in the pore resistance after only 8 hours of immersion. 40%_PPy coatings displayed no little to no change in the pore resistance even after 48 hours of immersion. Between 48 hours and 168 hours however, a sharp drop in pore resistance is noted indicating raping electrolyte permeation. Coatings containing 20%_PPy displayed the lowest R_p values and had little to no change from the beginning. This low of an R_p however indicates little to no barrier properties as electrolyte can easily permeate to the coating surface. In addition, after 168 hours of immersion a third time constant appeared indicating pitting corrosion of the aluminum 2024. This three time constant model has been used to describe pitting corrosion of aluminum 2024T3 substrates coated with sol-gel coatings.[27]

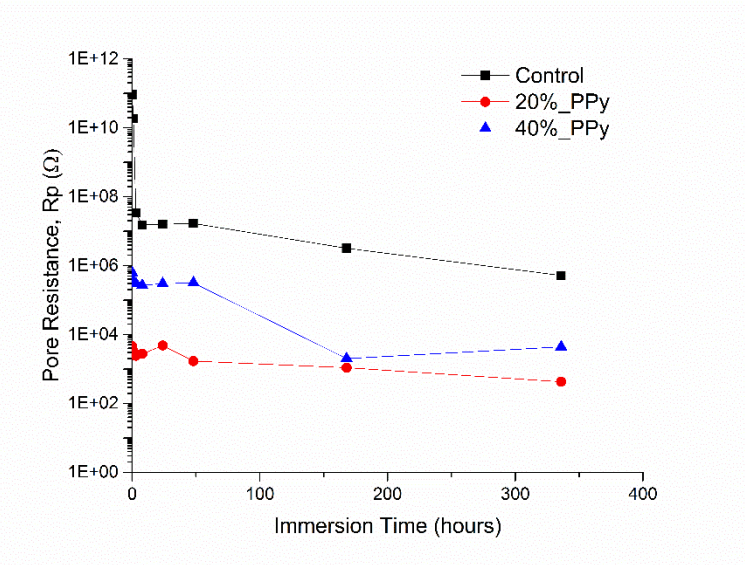

Figure 3.12: Effect of immersion time on the R_p for UV-curable hybrid networks.

From these results, it is concluded that all coating formulations offer poor long term protection of aluminum 2024T3 substrates. This is attributed to the poor adhesion of the UV-curable acrylate binder used, as well as the silver domains that develop in the photopolymerized polypyrrole leading to galvanic corrosion of the Al-2024T3 substrate. With this said, 40% PPy coatings showed very good corrosion inhibiting properties for short term electrolyte immersion, thus could find suitable areas of use where they will not be subjected to highly aggressive media.

3.5. Conclusions

Utilizing acrylonitrile as a reactive diluent for UV-curable acrylic coatings, solvent free hybrid networks of polyester acrylates and photopolymerized polypyrrole were developed. Formulations at two different pyrrole to silver nitrate ratios were used to study the effect on silver concentration on the resulting properties. Coatings containing a 5:1 ratio were significantly harder and demonstrated a lower percolation threshold of high molecular weight, oxidized polypyrrole

than the 8:1 ratio formulations. These results indicated that formulations at a 5:1 ratio were superior.

Coatings with a 5:1 ratio at 20% and 40% PPy were further studied for their corrosion inhibitive properties for Al-2024T3 substrates. Accelerated weathering results and EIS results indicate poor corrosion inhibiting properties. These poor protective properties are attributed to the poor adhesion offered by the polyester acrylate, as well as the silver nanoparticles that exist in the polypyrrole domains which can cause galvanic corrosion of the aluminum.

3.6. Acknowledgements

The authors of this paper would like to thank the Army Research Labs for providing funding the study these hybrid networks under the grant numbers W911NF-09-2-0014, W911NF-10-2-0082, and W911NF-11-2—0087.

3.7. References

1. Nguyen Thi Le, H., B. Garcia, C. Deslouis and Q. Le Xuan, Corrosion protection and conducting polymers: polypyrrole films on iron. *Electrochimica acta* 2001, 46 (26), 4259-4272.

2. Armes, S. P., Optimum reaction conditions for the polymerization of pyrrole by iron (III) chloride in aqueous solution. *Synthetic Metals* 1987, 20 (3), 365-371.

3. Shen, Y. and M. Wan, In situ doping polymerization of pyrrole with sulfonic acid as a dopant. *Synthetic Metals* 1998, 96 (2), 127-132.

4. Satoh, M., K. Kaneto and K. Yoshino, Dependences of electrical and mechanical properties of conducting polypyrrole films on conditions of electrochemical polymerization in an aqueous medium. *Synthetic Metals* 1986, 14 (4), 289-296.

5. Lee, J., D. Kim and C. Kim, Synthesis of soluble polypyrrole of the doped state in organic solvents. *Synthetic Metals* 1995, 74 (2), 103-106.

6. Cassignol, C., M. Cavarero, A. Boudet and A. Ricard, Microstructure-conductivity relationship in conducting polypyrrole/epoxy composites. *Polymer* 1999, 40 (5), 1139-1151.

7. Wang, Y., G. A. Sotzing and R. Weiss, Preparation of conductive polypyrrole/polyurethane composite foams by in situ polymerization of pyrrole. *Chemistry of Materials* 2008, 20 (7), 2574-2582.

8. Parfitt, G., Fundamental aspects of dispersion. *Dispersion of solids in liquids: with special reference to pigments. Elsevier, Amsterdam, cap* 1969, 3, 81-121.

9. Segawa, H., T. Shimidzu and K. Honda, A novel photo-sensitized polymerization of pyrrole. *J. Chem. Soc., Chem. Commun.* 1989, (2), 132-133.

10. Rabek, J., J. Lucki, M. Zuber, B. Qu and W. Shi, Polymerization of pyrrole by cationic photoinitiators. *Polymer* 1992, 33 (22), 4838-4844.

11. Breimer, M. A., G. Yevgeny, S. Sy and O. A. Sadik, Incorporation of metal nanoparticles in photopolymerized organic conducting polymers: A mechanistic insight. *Nano Letters* 2001, 1 (6), 305-308.

12. De Barros, R., W. De Azevedo and F. De Aguiar, Photo-induced polymerization of polyaniline. *Materials characterization* 2003, 50 (2-3), 131-134.

13. Yagci, Y., F. Yilmaz, S. Kiralp and L. Toppare, Photoinduced polymerization of thiophene using iodonium salt. *Macromolecular Chemistry and Physics* 2005, 206 (12), 1178-1182.

14. Martins, C., Y. De Almeida, G. Do Nascimento and W. De Azevedo, Metal nanoparticles incorporation during the photopolymerization of polypyrrole. *Journal of materials science* 2006, 41 (22), 7413-7418.

15. Hodko, D., M. Gamboa-Aldeco and O. J. Murphy, Photopolymerized silver-containing conducting polymer films. Part I. An electronic conductivity and cyclic voltammetric investigation. *Journal of Solid State Electrochemistry* 2009, 13 (7), 1063-1075.

16. Hodko, D., M. Gamboa-Aldeco and O. J. Murphy, Photopolymerized silver-containing conducting polymer films. Part II. Physico-chemical characterization and mechanism of photopolymerization process. *Journal of Solid State Electrochemistry* 2009, 13 (7), 1077-1089.

17. Kasisomayajula, S. V., X. Qi, C. Vetter, K. Croes, D. Pavlacky and V. J. Gelling, A structural and morphological comparative study between chemically synthesized and photopolymerized poly (pyrrole). *Journal of Coatings Technology and Research* 2010, 7 (2), 145-158.

18. Strandwitz, N. C., Y. Nonoguchi, S. W. Boettcher and G. D. Stucky, In situ photopolymerization of pyrrole in mesoporous TiO2. *Langmuir* 2010, 26 (8), 5319-5322.

19. Ahmed, A. E., J. P. Loh, B. Ghanayem and G. I. Hussein, Studies on the Mechanism of Acetonitrile Toxicity I: Whole Body Autoradiographic Distribution and Macromolecular Interaction of 2–14C-Acetonitrile in Mice*. *Pharmacology & toxicology* 1992, 70 (5), 322-330.

20. Chen, R., S. Zhao, G. Han and J. Dong, Fabrication of the silver/polypyrrole/polyacrylonitrile composite nanofibrous mats. *Materials Letters* 2008, 62 (24), 4031-4034.

21. Wicks Jr, Z. W., F. N. Jones, S. P. Pappas and D. A. Wicks, *Organic coatings: science and technology* John Wiley & Sons.

22. Cheng, L., Y. Zhang, T. Zhao and H. Wang In Free radical polymerization of acrylonitrile in green ionic liquids, Macromolecular Symposia, 'Ed.'^'Eds.' Wiley Online Library: 2004; pp 9-16.

23. Dhawan, S., N. Singh and S. Venkatachalam, Shielding behaviour of conducting polymer-coated fabrics in X-band, W-band and radio frequency range. *Synthetic Metals* 2002, 129 (3), 261-267.

24. Olbrich, A., B. Ebersberger and C. Boit, Conducting atomic force microscopy for nanoscale electrical characterization of thin SiO2. *Applied physics letters* 1998, 73 (21), 3114-3116.

25. Chen, G., M. Gao and R. Wei, Microconstituent-induced pitting corrosion in aluminum alloy 2024-T3. *Corrosion* 1996, 52 (1), 8-15.

26. Jadhav, N., C. A. Vetter and V. J. Gelling, Characterization and Electrochemical Investigations of Polypyrrole/Aluminum Flake Composite Pigments on AA 2024-T3 Substrate. *ECS Transactions* 2012, 41 (15), 75-89.

27. Zhu, D. and W. J. van Ooij, Corrosion protection of AA 2024-T3 by bis-[3-(triethoxysilyl) propyl] tetrasulfide in sodium chloride solution.: Part 2: mechanism for corrosion protection. *Corrosion Science* 2003, 45 (10), 2177-2197.

CHAPTER 4. DEVELOPMENT OF CROSSLINKABLE POLYPYRROLE PIGMENTS AND THEIR APPLICATIONS IN UV-CURABLE TECHNOLOGIES

4.1. Abstract

Crosslinkable polypyrrole (PPy) particles were synthesized through chemical oxidation of pyrrole in the presence of a variety of reactive surfactants, or "surfmers". These surfmer doped PPy pigments were characterized for morphological properties by scanning electron microscopy. The type of reactive surfactant present during the synthesis was shown to play a role in the resulting morphology and unique wire morphologies are even obtainable. Chemical and functional group analysis by x-ray analysis and Fourier transform infrared spectroscopy confirmed the presence of the reactive surfactants. Doping the PPy backbone with surfmers resulted in electrical conductivities and current densities similar to unfunctionalized PPy pigments as measured by four point probe technique and conductive atomic force microscopy (CAFM).

Crosslinkable PPy pigments were dispersed with a high shear mixer into a UV-curable resin system and cast onto aluminum 2024T3 and glass substrates. Evaluation of the cured coatings through tensile testing indicated the coatings containing surfmer doped PPy pigments showed improved mechanical properties compared to control coatings containing non-functionalized PPy pigments. Corrosion assessment of coatings through linear polarization, electrochemical impedance spectroscopy and accelerated weathering methods showed coatings containing the PPy pigments doped with the reactive surfactant BISOMER® SEM showed improved corrosion resistant properties.

4.2. Introduction

Due to increasingly stringent regulations controlling the amount of volatile organic compounds (VOCs) that are allowed in coating systems, the coating industry has been developing more environmentally friendly coatings.[1] These technologies focus on high-solids or solvent free systems and include technologies such as powder coatings and radiation curable resin systems. Radiation curable resins are an interesting class of coatings as they allow the use of low viscosity reactive diluents which enable solvent free formulations to be developed, but also exhibit fast cure times under UV-light with the appropriate photoinitiator.[2] In addition, the energy requirement for radiation curable resins is considerably less than tradition thermal cured epoxy and polyurethane systems.

Radiation curable coating systems, however, exhibit problems which make then unsuitable for certain applications. Due to the fast cure times, the final coating systems undergo high levels of volume shrinkage in a small amount of time. Without adequate time to relieve the stresses built up from the volume shrinkage, cured coatings are known to exhibit poor adhesion to substrates, and cracking of the final films.[3] This limits most radiation curable systems to porous substrates, such as wood, where better adhesion can be obtained.[4] Over the past few decades, radiation curable resins with improved adhesion to substrates, such as metal, have been developed utilizing ionic functional groups for greater interaction between the coating and the substrate.

Even with these improvements in the overall adhesion to metal substrates, radiation curable systems do not provide comparable corrosion protection to traditional epoxy-amine and urethane coating technologies. Barrier properties of radiation curable systems are inferior to traditional thermal cured system.[2] These inferior barrier properties are attributed to lower crosslink densities in radiation curable systems, which is required to maintain adequate adhesion during the rapid

volume loss upon exposure to UV light.[5] Incorporation of other materials, such as nanoclays, in coatings have been utilized to improve the overall barrier properties of the final cured system by providing a tortuous pathway that hinders electrolyte permeation through the coating.[6-10] Decker et al. developed radiation curable clay nanocomposites based on acrylated and epoxy resins that demonstrated comparable cure times to radiation curable clear coats. The clay nanocomposites also demonstrated improved resistance to moisture penetration.[7] Other reports indicated incorporation of nanoclays, such as montmorillonite, displayed improved adhesion to metal substrates as well.[8] Corrosion studies on radiation curable clay nanocomposites have been reported, improvement in the overall corrosion protection with the incorporation of nanoclays exfoliated with cationic surfactants was found.[11]

To further improve the overall mechanical properties, techniques to improve the interactions between the nanoclays and radiation curable resins have been implemented. A popular technique is to use reactive surfactants, or "surfmers" during the clay exfoliation process.[12-14] This technique allows covalent bonding between the radiation curable resin and the nanoclay that is ionically attracted to the cationic surfmer. The final coatings and composites demonstrated improved overall mechanical properties compared to their counterparts made with traditional organic surfactants.

These radiation curable clay nanocomposites coatings are suitable for clear coats as transparent coatings up to about 10% nanoclay loading can be achieved. For primer technologies, however, coatings containing an active form a corrosion protection are required outside of the barrier properties to boost performance. Electrically conductive polymers, ECPs, are an attractive option of active corrosion mitigation due to its easy of synthesis and implementation as a pigment, tailorable properties by modifying the dopant incorporated, and the environmentally friendly

nature of the compound. There is little research on the incorporation of ECP pigments into UV-curable resin systems currently available.[15] Jafarzadeh et al. incorporated polyaniline (PANI) at a 2.5 wt.% loading into a urethane acrylate resin system and coated onto steel substrates.[16] The OCP results demonstrated a passivating effect for the underlying galvanized steel substrates coated with coatings containing PANI compared to the control clear coats. Utilization of PANI and other ECPs as a corrosion protective pigment in traditional coating systems has also been reported.[17-21]

ECPs with the ability to incorporate anionic compounds as dopants offer an intriguing method to functionalize the final products. Synthesis of ECPs in the presence of anionic surfmers, should result in ECP pigments that are doped with these reactive surfactants. Figure 4.1 above shows an example of the polypyrrole structure with the surfmer doped into the backbone.

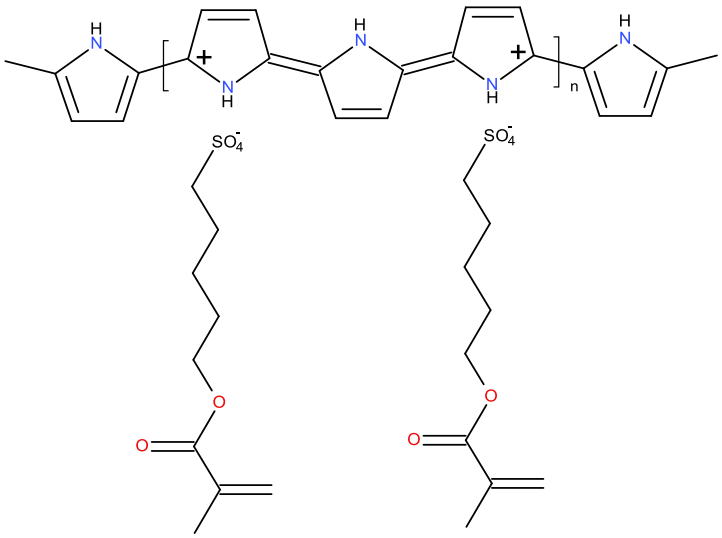

Figure 4.1: Structure of polypyrrole doped with sulphatoethyl methacrylate.

The final pigments could further be incorporated into a radiation curable resin resulting in a primer coating system with corrosion inhibiting pigments while improving the interactions between the pigments and binder resulting in decreased porosity of the final coating and improved

overall mechanical properties. The goal of this research is to develop a low solvent or solvent free coating system containing crosslinkable pigments based on ECPs. Additionally, the goal is also to determine if functionalizing ECP pigments with surfmers results in improved corrosion resistant properties.

4.3. Materials and Methods

4.3.1. Materials

For these studies, all materials were used as supplied except for pyrrole, which was distilled prior to use. Pyrrole and ferric nitrate was purchased from VWR. Pyrrole was vacuum distilled prior to use. Toluene was purchased from Sigma Aldrich. The surfmers Hitenol® BC10 and BC20 with are polyoxyethylene alkylphenyl ether ammonium sulfate salts were graciously provided by Montello Inc. Sodium 1-allyloxy-2-hydroxypropane sulfonate (COPS I), phosphate esters of PPG monomethacrylate (PAM 200), and phosphate esters of PPG monoacrylate (PAM 300) were supplied by Rhodia. BISOMER SEM, which is an aqueous solution of 25% ammonium sulphatoethyl methacrylate was provided by GEO Specialty Chemicals.

The coating system used in these studies consisted of the following: a polyurethane acrylate oligomer, EBECRYL® 8501 supplied by Cytec Industries; hexanediol diacrylate (HDDA) supplied by Sartomer; phosphate ester acrylate to improve adhesion, CD9053 also graciously supplied by Sartomer; and DISPERBYK 110 a dispersing agent supplied by BYK. The photoinitiator Irgacure® 819 and Irgacure® 184 were supplied by BASF.

4.3.2. Surfmer Doped PPy Pigment Synthesis

In a 400 mL Erlenmeyer flask, 200 mL of Milipore™ water was mixed with 6.7g of pyrrole to make a 0.5M pyrrole solution. To that, each surfmer was added at a molar ratio of 1 surfmer monomer to 5 pyrrole monomers. A ferric nitrate solution was added drop wise while undergoing

magnetic stirring. Ferric nitrate was added at a molar ratio of 2:1 with respect to pyrrole content. Upon final addition of the ferric nitrate solution, each reaction was mixed for 30 more minutes. PPy pigment was collected with vacuum filtration and washed with Millipore™ water until collected water was clear to ensure removal of pyrrole oligomers and excess salt or surfmers. All samples were dried at 40°C under vacuum to remove residual water.

4.3.3. Surfmer Doped PPy Pigment Characterization

To study the morphology of these crosslinkable PPy pigments, scanning electron microscopy (SEM) was conducted with a JEOL JSM-6300 scanning electron microscope equipped with a field emission gun. Elemental analysis was conducted during morphology studies with an energy dispersive spectroscopy (EDS) detector. Chemical structure analysis of the crosslinkable PPy pigments was carried out through Fourier transform infrared spectroscopy (FTIR) using a Thermo Scientific Nicolet 8700 infrared spectrometer.

The electrical properties of the PPy pigments were studied on a macro scale using a four point probe apparatus consisting of a Keithley 2100 multimeter connected to a Signatone® four point probe assembly. Micro level analysis of the electrical properties was accomplished with a Veeco® 3100 atomic force microscope operating in conductive atomic force microscopy (CAFM) mode. In this mode a potential of 1V is applied through the bottom of the sample and measured with an iridium-platinum cantilever rastering in contact mode on the pigment. For both of the techniques, samples were prepared by pressing pellets of virgin pigment and embedding the pellets in electrically conductive epoxy on a steel substrate. Thermal stability studies of the pigments were conducted with thermal gravimetric analysis (TGA). TGA was accomplished with a TA Instruments Q-500 Thermogravimetric Analyzer. Samples were heated from room temperature to 800°C at a rate of 20°C/minute.

4.3.4. Coating Preparation

Pigment grinds of crosslinkable PPy pigments were made by dispersing in a radiation curable resin system consisting of 42% EBECRYL 8501, 42% HDDA, and 6% CD9053. Grind formulations with 10% by weight loading of PPy pigments were made with a high shear Cowles disperser. Disperbyk 110 was added to the formulation prior to addition of pigment. Pigment was added slowly while under high shear mixing and mixed for an additional 30 minutes upon final addition of the PPy pigments.

From these grinds, final coating formulations were developed. To 40 grams of a pigment grind, a solution of Irgacure® 819 and Irgacure® 184 dissolved in toluene was added and mixed with magnetic stirring for 30 minutes. All coating formulations were applied to both sandblasted Al-2024T3 substrates and glass substrates at a wet film thickness of 4 mils. Both substrates were degreased with hexanes prior to application. Coatings were allowed 2 minutes to flash off the toluene present in the formulations. Coatings were cured with a DYMAX Model 5000-EC UV-Light Curing Flood System equipped with a metal halide bulb with a spectral intensity of 174 mW/cm^2. Samples were exposed to a total of 3 minutes of radiation in 1 minute cycles.

4.3.5. Coating Characterization

Mechanical properties of the coatings were studied with tensile testing with a TA Instruments Q-1000 Dynamic Mechanical Analyzer operating in stress strain mode. A ramping stress was applied on a cut rectangular strip of cured coating at room temperature and the resulting strain was measured. Corrosion protective assessment of Al-2024T3 substrates was studied through accelerated weathering studies utilizing ASTM B117 chambers and the advanced electrochemical experiments of linear polarization (LP) and electrochemical impedance spectroscopy (EIS). The electrolyte used in these experiments was 5% sodium chloride prepared

in 18 MΩ MilliQ water. LP experiments were performed with a three electrode technique utilizing platinum mesh as a counter electrode, a saturate calomel electrode as the reference electrode, and the Al-2024T3 substrate as the working electrode. The EIS data obtained was not adjusted for surface area prior to analyzing. The open circuit potential was measured for 300 seconds prior to LP scans and scans were performed in a range of -1V below to +1V above the OCP. EIS was performed with the three electrode technique as well, and EIS scans were taken at regular intervals, with triplicates of each to ensure reproducibility.

4.4. Results and Discussion

Table 4.1 lists the types of synthesized PPy pigments with incorporated surfmer. A variety of anionic surfmers were chosen to determine if different anions would preferentially dope at higher levels than others. This phenomenon has been observed with smaller inorganic anions such as chloride anions showing higher levels of doping from bulkier inorganic anions such as molybdate, tungstate, and vanadate.

Table 4.1: Corresponding chemical dopants for decorated PPy pigments

PPy Pigment	Surfactant Dopant (Trade Name)
PPy_NO_3	N/A
PPy_SDS	Dodecyl Sulfate
PPy_Hitenol10	Polyoxyethylene alkylphenyl ether sulfate (Hitenol BC-10)
PPy_Hitenol20	Polyoxyethylene alkylphenyl ether sulfate (Hitenol BC-20)
PPy_COPS1	1-Allyloxy-2-hydroxypropane-sulfonate (COPS 1)
PPy_PAM200	Monomethacrylate phosphate ester (PAM 200)
PPy_PAM300	Monoacrylate phosphate ester (PAM 300)
PPy_SEM	Sulphatoethyl methacrylate (BISOMER SEM)

4.4.1. Morphology and Elemental Analysis

During synthesis, the solution turned from a slight yellow color to a dark brown and finally a black solution while the ferric nitrate solution was added. This indicated that polymerization of PPy was occurring through chemical oxidation. Dried powders of each of the pigments, at the macro level looked the same to the naked eye and appeared as black powders. The morphology of each of the pigments was investigated with SEM to see the morphology of each individual pigment particle. Different morphologies of PPy have been exhibited by varying reaction conditions such as temperature, oxidizer concentration, as well as in the presence of various dopants. SEM images of the pigments are listed in Figure 4.2.

The control PPy pigments, without a surfmer/surfactant and doped with unreactive dodecyl sulfate exhibited the cauliflower morphology typically associated with PPy. This morphology was also visible for the pigments PPy_Hitenol10 and PPy_Hitenol20, but the individual clusters were at a much smaller scale. Comparing Figures 4.1a to 4.1d, the size of the clusters is about 2-3 times smaller for the PPy_Hitenol10 and PPy_Hitenol20 pigments compared to the controls. This size difference could be attributed to the ability of these polymeric surfactants to stabilize emulsions with smaller particle size thus resulting in smaller PPy pigment particles.

PPy_COPS1 and PPy_SEM resulted in particle morphologies similar to the control PPy_SDS. These two surfmers have a molecular weight much more similar to dodecyl sulfate thus might form the same size micelles in which the PPy pigments are synthesized. The most interesting morphologies that were observed were PPy_PAM200 and PPy_PAM300 respectively. Figures 4.1f and 4.11g both show a wire like morphology. Pigments with these higher aspect ratios have shown interesting properties in a variety of applications. Previously Jadhav et. al observed

that Al-flake pigments decorated with PPy displayed a wire morphology showed significant improvement in the corrosion protection properties compared to Al-flake decorated with PPy displaying the cauliflower like morphology.[22]

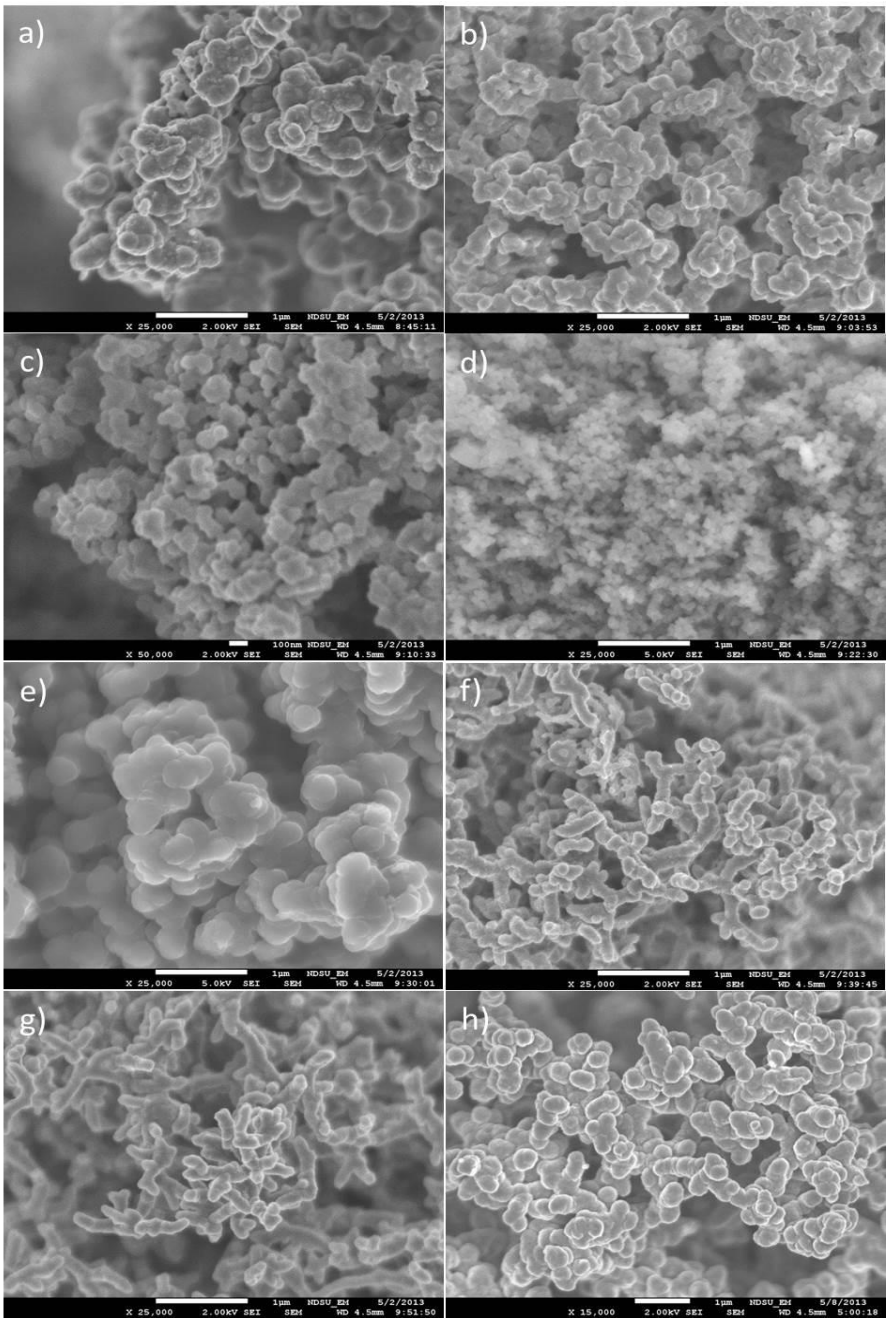

Figure 4.2: SEM images of PPy pigments (a-h): a – PPy_NO_3, b – PPy_SDS, c – PPy_Hitenol10, d – PPy_Hitenol20, e – PPy_COPS1, f – PPy_PAM200, g – PPy_PAM300, and h – PPy_BISOMERSEM

This wire like morphology was evident for both the acrylate phosphate ester and methacrylate phosphate ester indicating that this morphology is attributed to the phosphate ester surfactant. Surfactants have been shown to develop different sizes and shapes of micelles depending on the chemistry. It is theorized that these phosphate esters might form cylindrical shaped micelles from which wire like morphologies can grow during chemical oxidation.

EDS was used to study the relative levels of doping achieved by each of the surfmers. The results from EDS studies are presented in Table 4.2. From these results it is evident that when PPy is synthesized through chemical oxidation with ferric nitrate in the presence of anionic sufmers, these surfmers are incorporated into the PPy backbone. All PPy pigments that were synthesized in the presence of sulfonated surfactants (PPy_SDS, PPy_Hitenol10, PPy_Hitenol20, PPy_COPS1, and PPy_SEM showed significant levels of sulfur detected in the pigment. For the PPy pigments doped with phosphate surfmers (PPy_PAM 200 and PPy_PAM 300), phosphorus was detected indicating doping was also achieved.

Table 4.2: Elemental analysis of PPy pigments.

Sample	C	N	O	S	P
PPy_Nitrate	85.33	11.62	3.04	n/a	n/a
PPy_SDS	82.90	10.2	3.49	3.41	n/a
PPy_Hitenol10	82.48	13.12	3.63	0.76	n/a
PPy_Hitenol20	83.88	13.19	2.73	0.19	n/a
PPy_COPSI	80.94	14.79	3.77	0.50	n/a
PPy_PAM200	78.65	16.72	4.24	n/a	0.39
PPy_PAM300	86.38	7.01	6.26	n/a	0.35
PPy_BisomerSEM	87.67	8.82	2.50	1.01	n/a

EDS unfortunately does not indicate if the surfmers are present on outside of the pigments or if incorporated throughout the entire pigment as the penetration depth of EDS in an SEM is a few microns. Incorporation of these pigments into UV-curable coating and measuring the resulting

mechanical properties should provide evidence if these reactive sites are present on the outside of the pigments.

Fourier transform infrared spectroscopy is a useful tool studying the bond vibrations of organic molecules. Below in Figure 4.3 is the FTIR spectra for the synthesized PPy pigments. From the spectra, the peaks commonly associated with PPy can be observed. In addition, at approximately 1470 wavenumbers a small peak develops for all samples but PPy_NO_3.

Peaks in this regime belong to a –CH_2- bending vibration in alkyl chains. This this evidence of doping with the surfmers as they have long alkyl chains. In addition, the pigments PPy_PAM200 and PPy_PAM300 show an –OH bending vibration associated to the phosphate group on these acrylic phosphate esters.[23] It is possible that other distinguishable peaks that should be visible for the surfactants are covered up by the more prominent PPy peaks.

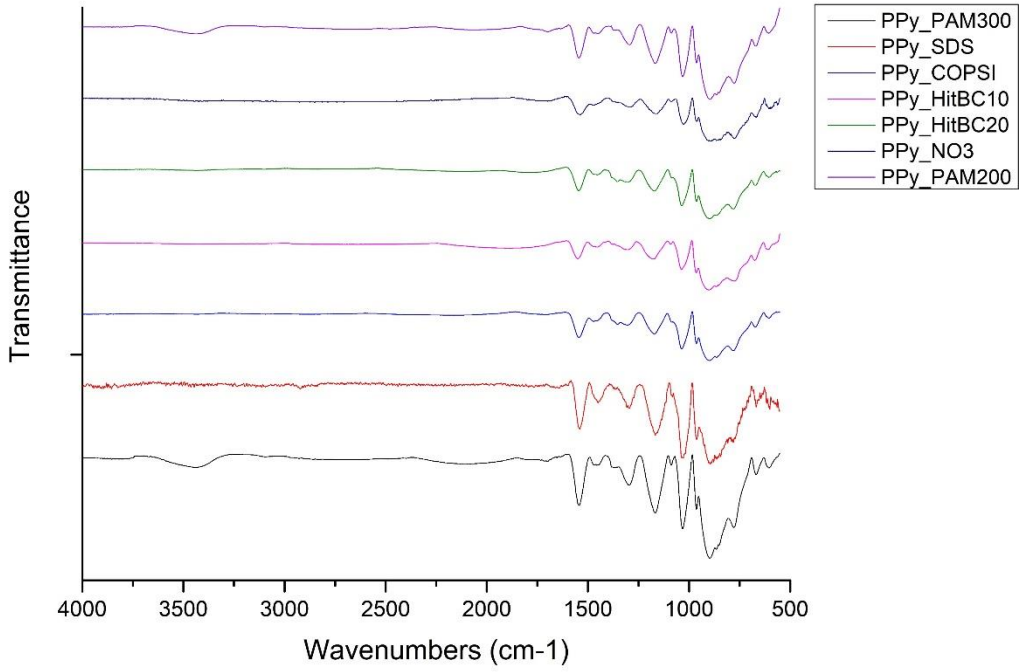

Figure 4.3: FTIR spectra for PPy pigments.

4.4.2. Thermal Stability of PPy Pigments

Incorporation of surfactants into ECPs in prior literature has indicated that a modification of the thermal stability of the resulting PPy powder can occur. This modification of the thermal stability is due to the breakdown of the surfactants in the temperature range of 250°C - 400°C.[24] TGA curves of the PPy pigments are presented in Figure 4.4. Until approximately 200°C, the PPy pigments doped with surfmers demonstrated no difference in thermal stability compared to control PPy pigment. For all samples containing a surfmer, no improvement or a slight loss in thermal stability is observed after 200°C.

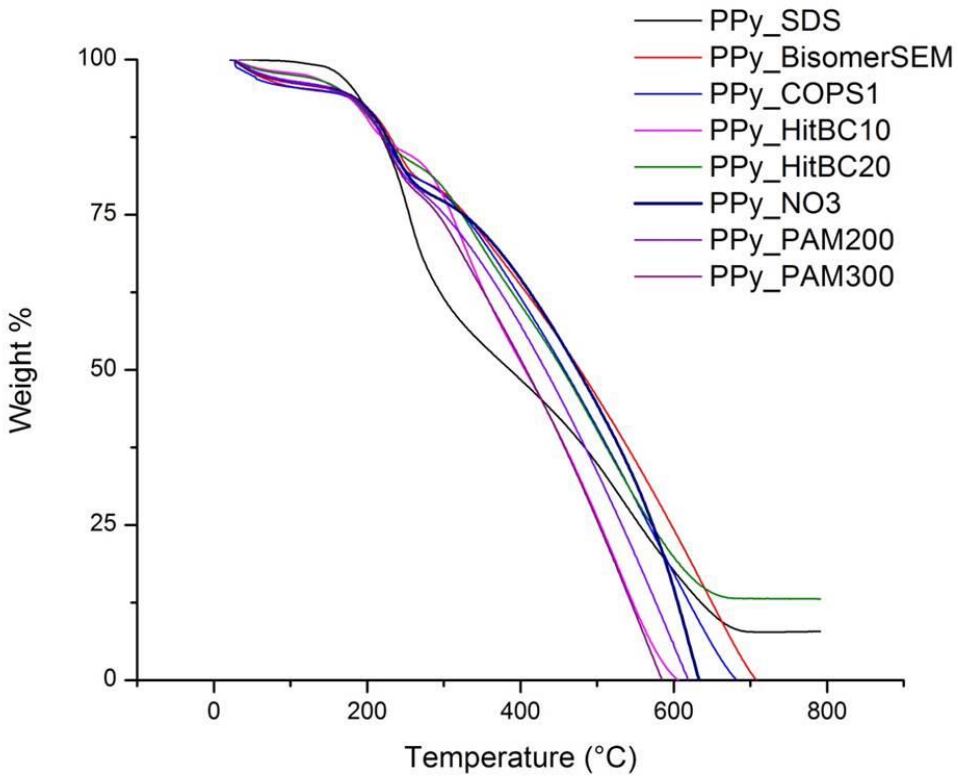

Figure 4.4: TGA curves for the PPy pigments.

Derivative weight loss curves for the TGA results are presented in Figure 4.5. Derivative weight loss curves are valuable in determining the onset of degradation at certain temperatures to determine what part of the material is thermally decomposing. For all samples containing a surfactant or surfmer a decomposition peak is observed between 250°C - 400°C. In comparison to the control PPy_NO_3 sample, no significant peak in the derivative weight loss curve is observed. These results, along with the EDS results, indicate that even after extensive washing and purification, the surfmers present during synthesis doped the PPy pigments.

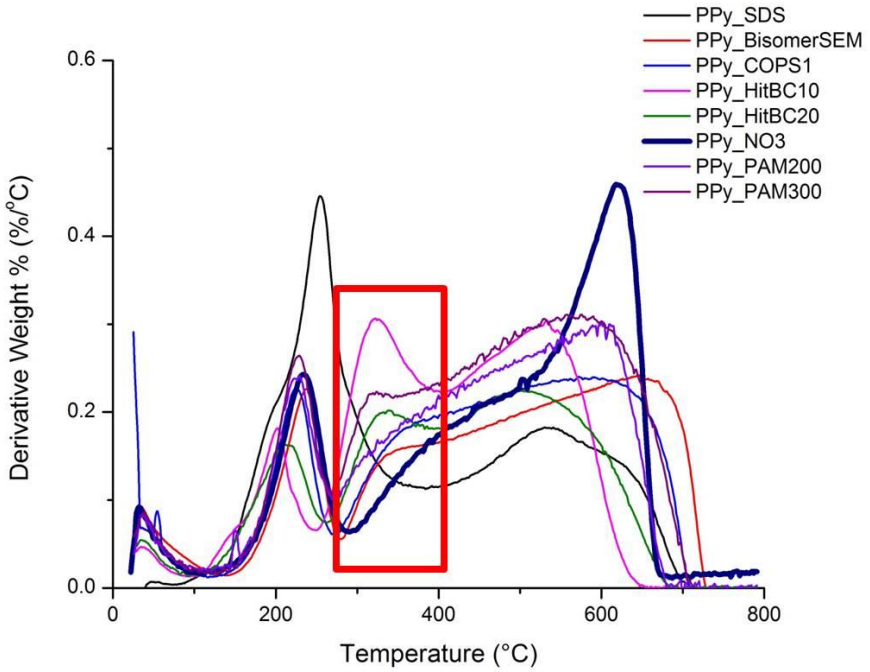

Figure 4.5: Derivative weight loss curves for all PPy pigments.

4.4.3. Electrical Properties of PPy Pigments

The concentration and type of dopant that is incorporated into PPy are two of the most important variables that affect the resulting electrical properties of PPy. Reports in the literature indicating orders of magnitude difference in the resulting electrical conductivity of PPy films and

powders can be obtained depending upon the type of dopant incorporated into the PPy backbone.[25] The electrical properties have also been observed to have a possible impact of the corrosion protective properties of a coating containing PPy, thus, it is important to ensure no substantial loss in electrical properties is observed when incorporating surfmers into the ECPs.

Figure 4.6 displays a chart comparing the surface resistances of a pressed pellet of each of the PPy pigments. From the data less than one order of magnitude of difference is observed for the PPy-surfmer pigments. PPy_HIT10 showed the largest difference in surface resistance while the other PPy-surfmer pigments showed little to no difference to the PPy_NO_3 control pigment. This indicates that incorporation of surfmers into the PPy backbone does not have a deleterious effect on the PPy electrical properties.

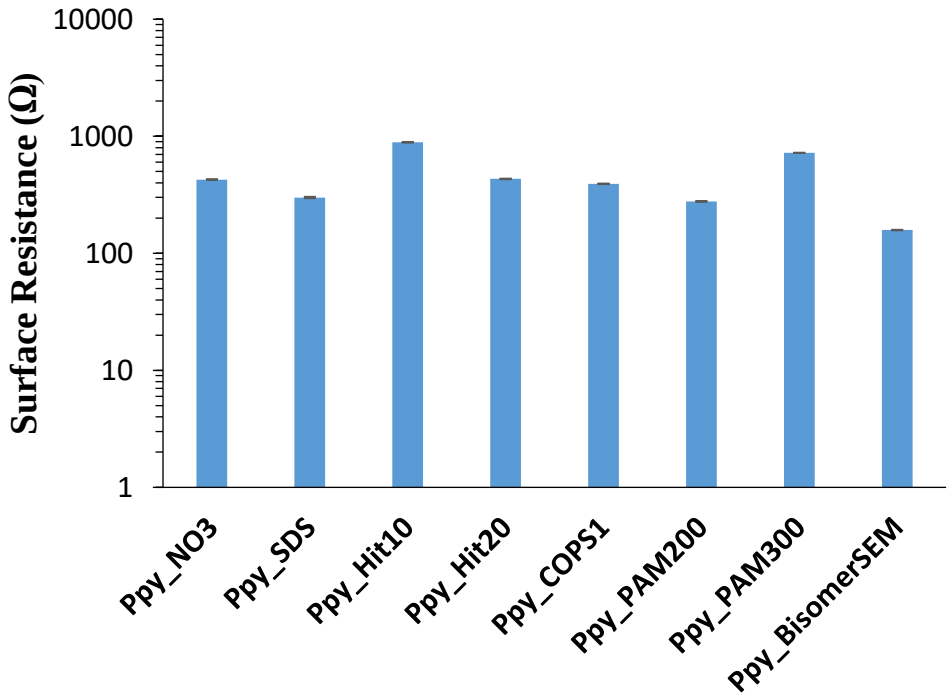

Figure 4.6: Surface resistance measurements for PPy pigments.

4.4.4. Coating Properties

Of the PPy pigments, four were chosen to be incorporated into the UV-curable matrix. These were PPy_Hitenol20, PPy_COPS1, PPy_PAM200, and PPy_BISOMERSEM. PPy_Hitenol20 was chosen over PPy_Hitenol10 due to the lower viscosity nature of the virgin Hitenol BC20, leading to believe the molecular weight was lower than its counterpart Hitenol BC10. PAM 200 was chosen over its counterpart PAM 300 due to the pigment demonstrating poorer electrical properties. In addition to coatings containing the surfmer doped PPy pigments, a set of coatings containing PPy_NO_3 was also produced and characterized.

Properties for the coatings are listed in Table 4.3. From these results it is evident that wide discrepancies exist for the König hardness for the cured coatings. This would indicate that coatings demonstrating the lowest König hardness values did not fully cure and would be slightly rubbery. Improper dispersion of pigment could lead to the photoinitiator package chosen to be inadequate in penetrating through resulting in coatings that are tack free, but not 100% cured.

Table 4.3: General coating properties

Sample	König Hardness (s)		85° Gloss (%)		X-hatch	Adhesion
	Avg	Std. Dev	Avg	Std. Dev	Avg	Std Dev
PPy_NO3	84.4	2.7	23.74	2.30	5b	n/a
PPy_PAM200	51.0	18.9	5.42	1.85	5b*	*
PPy_Hitenol20	48.8	2.0	45.04	3.82	5b*	*
PPy_COPS1	89.0	1.7	29.64	2.59	5b	n/a
PPy_BisomerSEM	122.4	5.9	40	2.69	5b	n/a

85-degree gloss values also vary greatly from sample to sample leading to the conclusion that some PPy pigments were more readily dispersed than others in the UV-curable matrix. In all

of these samples, however low gloss values were noted. All coatings, however, showed exceptional adhesion to metal which could result in these coatings proving to be useful in the protection of metal substrates. Coatings containing PPy_PAM200 and PPy_Hitenol20 have an "*" noted next to the cross hatch adhesion values, this is to indicate that small corners of only a few squares were lifted but was not enough to constitute a value of 4B as per the ASTM standard.

The goal of doping these PPy pigment particles with reactive surfmers was to crosslink into the UV-curable matrix improving the matrix-filler interaction thus improving the final mechanical properties. Tensile tests were conducted to elucidate the ultimate tensile strength of the cured coatings and compared to the control coatings. Below, in Figure 4.7 is a plot of the stress-strain curves for the tensile tests.

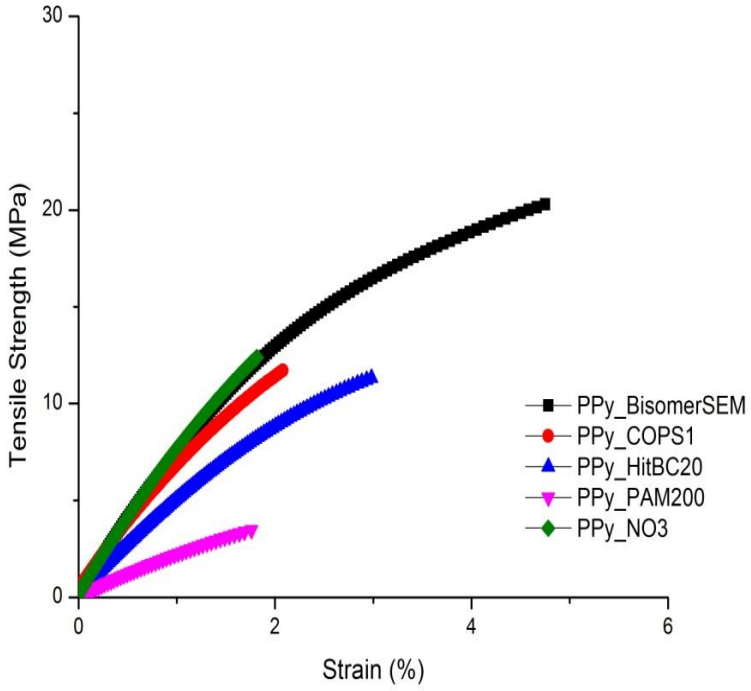

Figure 4.7: Stress-strain plots for coatings containing the PPy pigments.

From these results coating samples showed a rubber-like nature as they showed larger strain at breaks. However, only coatings containing PPy_BISOMERSEM and PPy_COPS1 showed average ultimate tensile strengths larger than the control coatings containing PPy_NO_3. In the case of PPy_COPS1, the standard deviation overlaps with the standard deviation of the ultimate tensile strength of PPy_NO_3 coatings which indicates no discernable difference can be made between the two. A graph depicting the ultimate tensile strengths of each coating is presented in Figure 4.8.

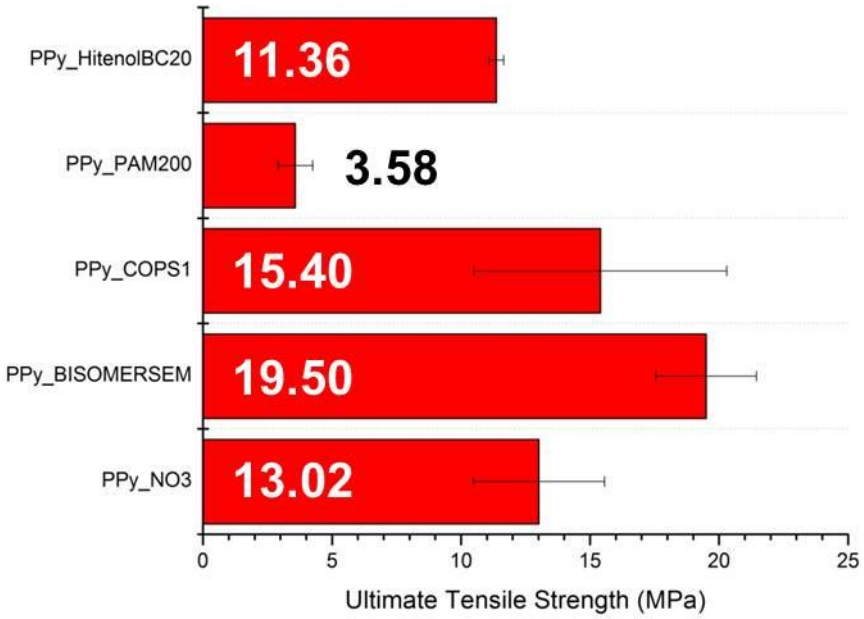

Figure 4.8: Ultimate tensile strength of the pigmented coatings.

4.4.5. Corrosion Protective Properties of the PPy Pigments

PPy and other ECPs have found a promising niche in the area of active corrosion protection for metal alloys.[26, 27] The ability to act as a corrosion inhibitor through a variety of mechanisms makes it an interesting replacement for traditional corrosion inhibitors such as hexavalent

chromates. To study the ability of these coatings to protect Al-2024T3 substrates, a combination of electrochemical techniques and traditional accelerated weathering techniques were utilized to give an in depth understanding of which pigments performed better than others, as well as to deterimine if surfmer doped PPy pigments were indeed superior to unmodified PPy pigments.

Linear polarization was utilized to determine if the PPy synthesized in the presence of surfmers offered any improvement in the level of passivation offered by PPy when in contact with Al-2024T3 substrates. Below in Figure 4.9 is a plot of the linear polarization scans for all coatings immersed in 5% NaCl solution. Coatings containing the pigments PPy_Hitenol20 and PPy_PAM200 showed corrosion potentials very similar to bare Al-2024T3 indicating little to no passivation of the underlying Al-2024T3 substrate. The other coatings however demonstrated passivation of the surface with more noble corrosion potentials with coatings containing PPy_COPS1 showing the highest level of passivation with a corrosion potential of 19mV.

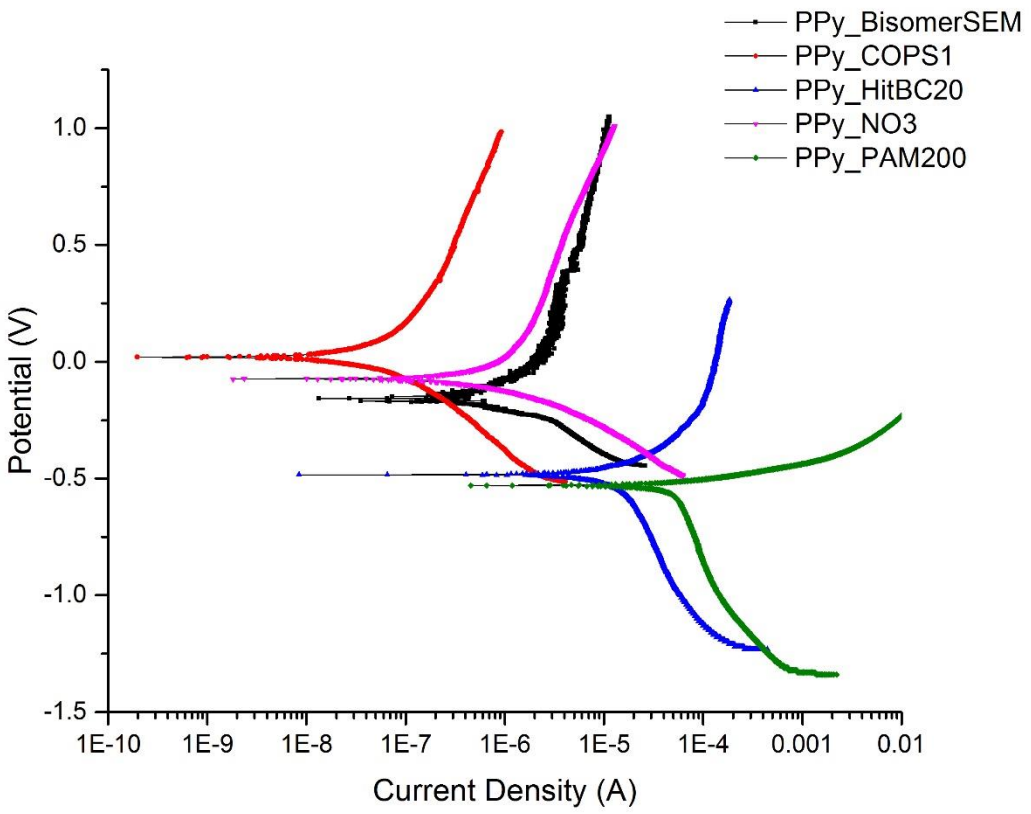

Figure 4.9: Linear polarization plots of each coating after 30-minute immersion in 5% NaCl solution.

EIS results for coatings containing the PPy pigments are shown on the following page in Figure 4.10. During initial measurements it was observed that a stable OCP could not be reached for coatings containing either PPy_PAM200 and PPy_HitBC20. This inability to hold a steady OCP is illustrated by the inductance in the impedance at low frequencies. A change in OCP can be due to rapid progression of electrolyte through a coating at reaching the surface of the substrate. This means poor corrosion protection through the barrier route. This may indicate poor protection was also evident with the lowest corrosion potentials measured by linear polarization. This poor barrier protection is further illustrated in accelerated weathering techniques discussed later.

The control coatings containing PPy_NO3, PPy_COPS1, and PPy_BisomerSEM showed a steady decline in low frequency impedance over the course of 672 hours indicating electrolyte permeation through the UV-curable coatings. After 168 hours, however, a second time constant is evident in the spectra indicating electrolyte has reached the substrate surface and corrosion of the Al-2024 has begun. Between 504 and 672 hours of immersion the low frequency impedance started to climb possibly due to the oxide layer growth on the Al-2024 surface. The results do not show a substantial difference between these three coatings ability to protect the surface of the coating.

Accelerated weathering of scribed panels allows for artificial weathering of panels at a faster rate resulting in quicker screening of coatings. In Figure 4.11 are the panels prior to immersion and after 168 hours of immersion. Even after only one week of exposure, a large amount of corrosion, even at locations away from the scribe, is evident for coatings containing PPy_NO_3, PPy_PAM200, and PPy_Hitenol20. This indicates poor barrier properties of the final coatings as well as little to no active protection being offered by the PPy pigments. The passivation observed in the linear polarization results for PPy_NO_3 thus must be short lived.

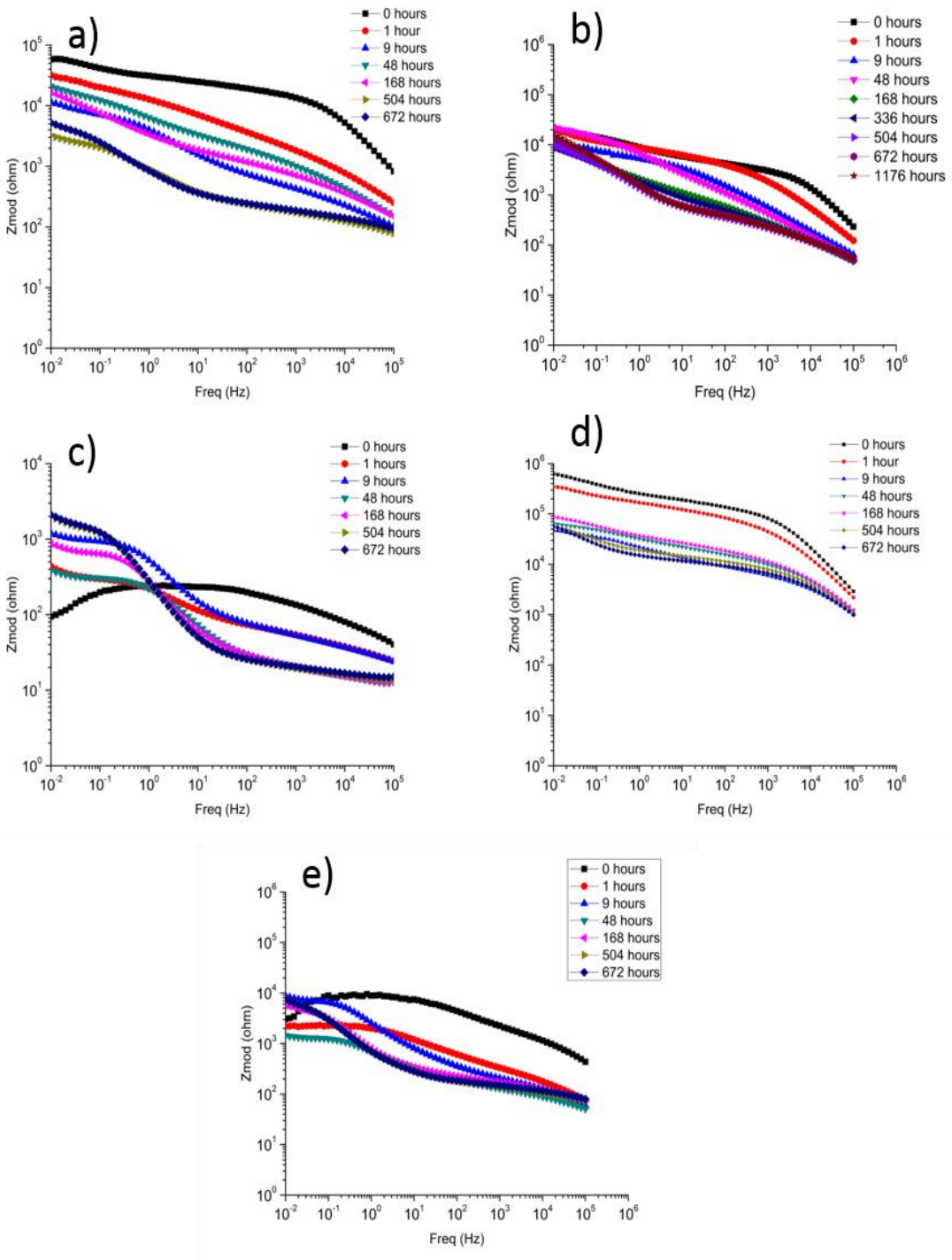

Figure 4.10: EIS spectra of coatings containing the PPy pigments: a) PPy_NO_3, b) PPy_BisomerSEM, c) PPy_PAM200, d) PPy_COPS1, and e) PPy_HitBC20

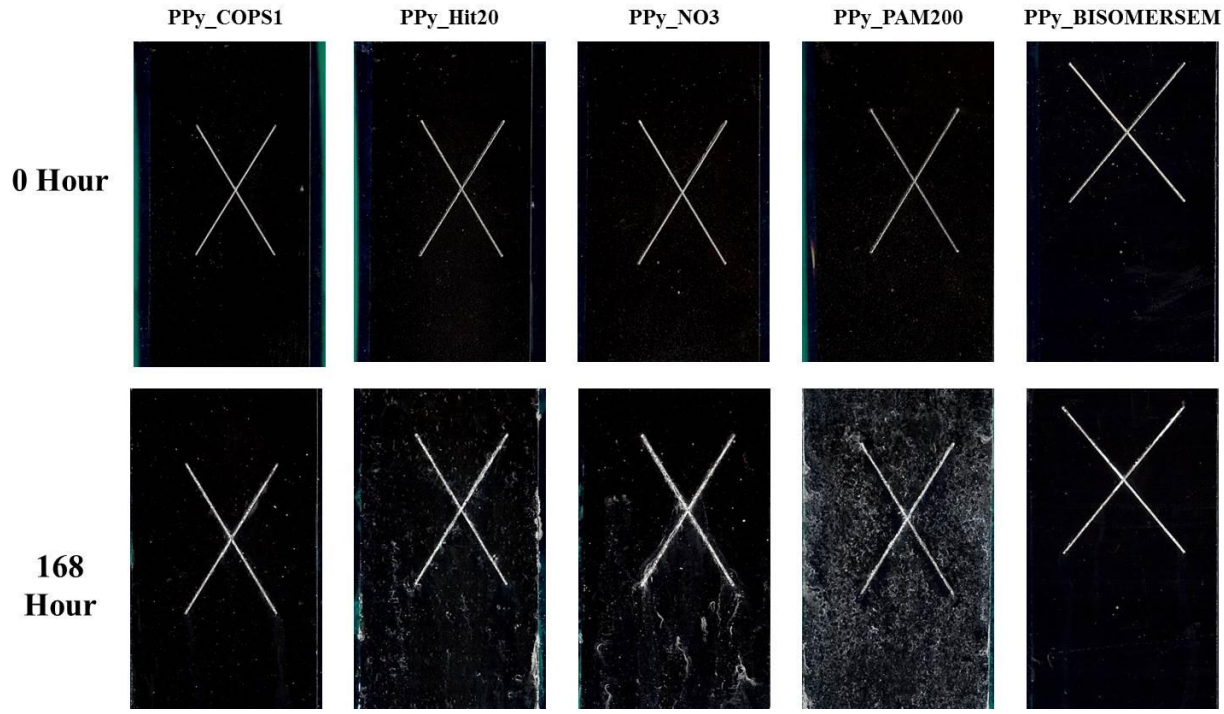

Figure 4.11: Panels before (top) and after (bottom) 168 hours of exposure to ASTM B117 environment.

Coatings containing PPy_COPS1 and PPy_BISOMERSEM show little to no corrosion in the scribe and no observable blisters throughout the bulk of the coating. These results indicate that the UV-curable matrix for this study does indeed demonstrate good barrier properties. The poor barrier properties observed in the failed coatings is thus attributed to poor dispersability of the PPy pigments, leading to a porous coating structure, allowing for rapid electrolyte penetration and, thus, resulting in coating delamination and quick failure of ASTMB117. Future work establishing degree of dispersion via Hegmann gauge analysis would help corroborate this idea.

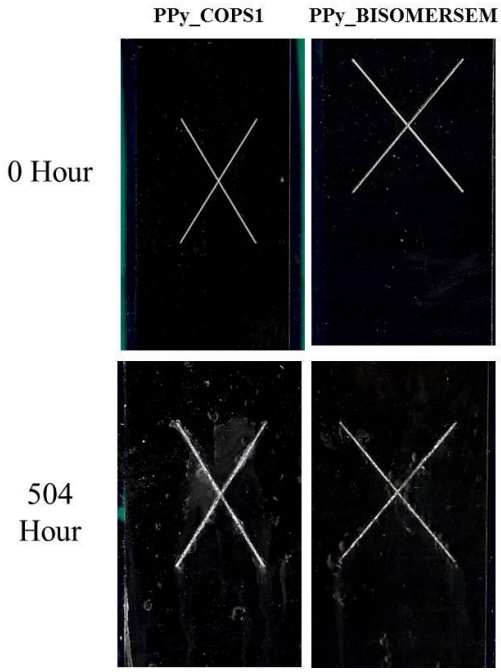

Figure 4.12: Coating formulations with the pigments PPy_COPS1 and PPy_BISOMERSEM prior to exposure (top) and after 504 hours of exposure to ASTM B117 (bottom).

The coating system containing the pigment PPy_COPS1 failed after 504 hours in ASTM B117. Small amounts of filiform corrosion were observed for the coatings containing PPy_BISOMERSEM along with small blisters around the scribe was observed, thus, exposure was continued to see if further damage would continue. After 1008 hours in ASTMB117, coatings made with the PPy_BISOMERSEM pigment began to show large blisters around the scribe and considerable filiform corrosion. These results indicate the pigment PPy_BISOMERSEM as the superior corrosion inhibiting pigment of the group through a combination of a passivation mechanism, as well as superior barrier properties due to crosslinking into the UV-curable matrix.

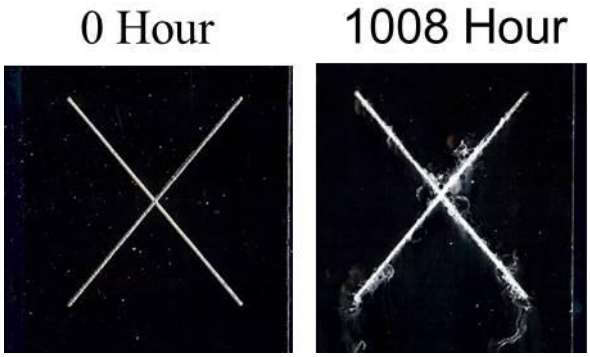

Figure 4.13: Images at 0 hour and 1008 hours of immersion in ASTM B117 for coatings containing PPy_BISOMERSEM pigment.

4.5. Conclusions

PPy pigments were successfully synthesized in the presence of reactive surfactants. The morphology of these pigments was found to change depending upon what surfmer was present during the reaction, and more novel morphologies including wires are possible. Chemical analysis through EDS and FTIR as well as thermal analysis confirmed that these surfmers were incorporated as dopants into the PPy backbone of these pigments. The electrical properties of these surfmers were found to be comparable to control PPy powder synthesized without surfmers were comparable.

The functionalized PPy pigments were dispersed into UV-curable resin and cast and cured on Al-2024T3 substrates. During mechanical testing only the coatings developed with PPy_BISOMERSEM showed a substantial improvement in the ultimate tensile strength compared to control coatings. Corrosion testing further proved that coatings with the PPy_BISOMERSEM pigment were superior to all other coating formulations. Future work on optimizing the synthesis of PPy_BISOMERSEM pigments will be completed to improve the properties of these pigments.

4.6. References

1. Jotischky, H., Coatings, regulations and the environment reviewed. *Surface Coatings International Part B: Coatings Transactions* 2001, 84 (1), 11-20.

2. Koleske, J. V., *Radiation curing of coatings* ASTM international, 2001.

3. Pappas, S. P., Radiation curing: science and technology.1992.

4. Bongiovanni, R., F. Montefusco, A. Priola, N. Macchioni, S. Lazzeri, L. Sozzi and B. Ameduri, High performance UV-cured coatings for wood protection. *Progress in Organic Coatings* 2002, 45 (4), 359-363.

5. Pappas, S. P., *Radiation curing: science and technology* Springer Science & Business Media.

6. Benfarhi, S., C. Decker, L. Keller and K. Zahouily, Synthesis of clay nanocomposite materials by light-induced crosslinking polymerization. *European polymer journal* 2004, 40 (3), 493-501.

7. Decker, C., L. Keller, K. Zahouily and S. Benfarhi, Synthesis of nanocomposite polymers by UV-radiation curing. *Polymer* 2005, 46 (17), 6640-6648.

8. Fogelström, L., P. Antoni, E. Malmström and A. Hult, UV-curable hyperbranched nanocomposite coatings. *Progress in Organic Coatings* 2006, 55 (3), 284-290.

9. Uhl, F. M., D. C. Webster, S. P. Davuluri and S.-C. Wong, UV curable epoxy acrylate–clay nanocomposites. *European polymer journal* 2006, 42 (10), 2596-2605.

10. Di Gianni, A., E. Amerio, O. Monticelli and R. Bongiovanni, Preparation of polymer/clay mineral nanocomposites via dispersion of silylated montmorillonite in a UV curable epoxy matrix. *Applied Clay Science* 2008, 42 (1), 116-124.

11. Malucelli, G., A. Di Gianni, F. Deflorian, M. Fedel and R. Bongiovanni, Preparation of ultraviolet-cured nanocomposite coatings for protecting against corrosion of metal substrates. *Corrosion Science* 2009, 51 (8), 1762-1771.

12. Morizur, J.-F. and L. J. Mathias, Synthesis of new acrylate-based cationic surfmers and their use in the synthesis of PMMA-clay nanocomposite via heterophase polymerization. *Polymer Preprints* 2007, 48 (1), 340.

13. Samakande, A., P. C. Hartmann, V. Cloete and R. D. Sanderson, Use of acrylic based surfmers for the preparation of exfoliated polystyrene–clay nanocomposites. *Polymer* 2007, 48 (6), 1490-1499.

14. Sangermano, M., N. Lak, G. Malucelli, A. Samakande and R. Sanderson, UV-curing and characterization of polymer–clay nanocoatings by dispersion of acrylate-funtionalized organoclays. *Progress in Organic Coatings* 2008, 61 (1), 89-94.

15. Sababi, M., J. Pan, P.-E. Augustsson, P.-E. Sundell and P. M. Claesson, Influence of polyaniline and ceria nanoparticle additives on corrosion protection of a UV-cure coating on carbon steel. *Corrosion Science* 2014, 84, 189-197.

16. Jafarzadeh, S., A. Adhikari, P. E. Sundall and J. Pan, Study of PANI-MeSA conducting polymer dispersed in UV-curing polyester acrylate on galvanized steel as corrosion protection coating. *Progress in Organic Coatings* 2010.

17. Sathiyanarayanan, S., S. Muthukrishnan, G. Venkatachari and D. Trivedi, Corrosion protection of steel by polyaniline (PANI) pigmented paint coating. *Progress in Organic Coatings* 2005, 53 (4), 297-301.

18. Saravanan, K., S. Sathiyanarayanan, S. Muralidharan, S. S. Azim and G. Venkatachari, Performance evaluation of polyaniline pigmented epoxy coating for corrosion protection of steel in concrete environment. *Progress in Organic Coatings* 2007, 59 (2), 160-167.

19. Sathiyanarayanan, S., S. S. Azim and G. Venkatachari, A new corrosion protection coating with polyaniline–TiO 2 composite for steel. *Electrochimica acta* 2007, 52 (5), 2068-2074.

20. Armelin, E., R. Pla, F. Liesa, X. Ramis, J. I. Iribarren and C. Alemán, Corrosion protection with polyaniline and polypyrrole as anticorrosive additives for epoxy paint. *Corrosion Science* 2008, 50 (3), 721-728.

21. Kalendová, A., D. Veselý and J. Stejskal, Organic coatings containing polyaniline and inorganic pigments as corrosion inhibitors. *Progress in Organic Coatings* 2008, 62 (1), 105-116.

22. Jadhav, N., C. A. Vetter and V. J. Gelling, The effect of polymer morphology on the performance of a corrosion inhibiting polypyrrole/aluminum flake composite pigment. *Electrochimica acta* 2013, 102, 28-43.

23. Stuart, B., *Infrared spectroscopy* Wiley Online Library.

24. Omastova, M., M. Trchova, J. Kovářová and J. Stejskal, Synthesis and structural study of polypyrroles prepared in the presence of surfactants. *Synthetic Metals* 2003, 138 (3), 447-455.

25. Stejskal, J., M. Omastová, S. Fedorova, J. Prokeš and M. Trchová, Polyaniline and polypyrrole prepared in the presence of surfactants: a comparative conductivity study. *Polymer* 2003, 44 (5), 1353-1358.

26. Sitaram, S. P., J. O. Stoffer and T. J. O'Keefe, Application of conducting polymers in corrosion protection. *Journal of Coatings Technology* 1997, 69 (866), 65-69.

27. Zarras, P., N. Anderson, C. Webber, D. Irvin, J. Irvin, A. Guenthner and J. Stenger-Smith, Progress in using conductive polymers as corrosion-inhibiting coatings. *Radiation Physics and Chemistry* 2003, 68 (3), 387-394.

CHAPTER 5. EFFECT OF PH DURING SYNTHESIS OF CROSSLINKABLE POLYPYRROLE PIGMENTS AND THE FINAL PROPERTIES

5.1. Abstract

Crosslinkable polypyrrole (PPy) pigments were synthesized as outlined in chapter 4. From these results it was indicated that the surfmer, Bisomer SEM provided the most beneficial modifications to both physical and corrosion inhibiting properties. Ladders varying both the ferric nitrate and the Bisomer SEM concentration in the reaction were conducted to find the optimal level of each of these materials to synthesize the final product. Chemical analysis was conducted with Fourier Transform Infrared Spectroscopy (FTIR). Thermal gravimetric analysis was conducted to study the thermal stability and ensure proper doping with Bisomer SEM. Electrical properties of the PPy pigments were studied via localized and bulk methods. From these experiments there was no significant difference in the resulting properties of the PPy pigments. These pigments were then dispersed into a UV-curable matrix and cast onto Al-2024T3 substrates and cured via ultraviolet light.

Cured coatings were studied for their corrosion protection nature via accelerated weathering in ASTM B117 conditions as well as electrochemical techniques such as Linear Polarization and Electrochemical Impedance Spectroscopy. The accelerated weathering results show an improvement on the protective nature of the coating containing PPy_BisomerSEM pigments compared to control clear coats. Linear polarization results show a passivation of the Al-2024T3 surface when coated with the PPy coatings indicating an active protection mechanism being offered by the pigments.

5.2. Introduction

Metals are one of the most important class of materials ever used by human societies. Metals such as iron, copper, tin, and aluminum have been used for millenia, allowing humans to develop technology in every area imaginable including architecture, military, travel, and electronics. Of these, one of the most fundamentally important properties of metals currently is the ability to conduct electricity. Without this property, life as we know it would not exist.

Over the past century, polymeric materials have slowly supplanted metals in many areas of applications as polymer mechanical properties have been improved. A prime example of polymeric composite replacing metal is the new Boeing 787 Dreamliner, where over 50% of the structural components have been replaced with advanced polymeric composites. Polymeric materials have the ability to solve a lot of drawbacks that metals bring including the density of these metals compared to traditional organic compounds is much greater (7.87 g/cm^3 for iron and 2.70 g/cm^3 for aluminum) and the susceptibility to oxidation leading to byproducts with inferior properties. If materials could be developed from organic compounds with much lower densities, the result would be light-weight, corrosion resistant products which could revolutionize multiple industries.

Electrically conductive polymers (ECPs) were first discovered in 1970s by Shirakawa et al. and demonstrated the ability of light-weight polymers (polyacetylene) to conduct electricity similarly to metals.[1] Since then there has been many more polymeric structures that show the ability conduct electricity. This inherent property of these polymers is attributed to the long range conjugation, as well as the presence of ionic dopants elevating these conductive polymers into an oxidized or electrically conductive state.[2] The most heavily studied of these polymers are polypyrrole (PPy), polythiophene (PTh), and polyaniline (PAni). These are the most studied due

to their inertness to the earth's atmosphere, as well as good heat stability. Since their discovery conductive polymers have been used to supplant metals in many areas including photovoltaics, super capacitors, battery technology, organic light emitting diodes (OLEDs), corrosion inhibition, and anti-static technologies.[3-6]

ECPs show great promise in replacing traditional materials in the areas of corrosion protection.[7, 8] Corrosion of infrastructure in the United States is expected to cost the US economy over 1 trillion dollars in 2016.[9] That is an estimated 6.2% of the GDP effectively is used to maintain the current buildings, roads, and bridges that we have today. Due to this, there is a great demand to develop new methods to combat the corrosion of metals but at the same time provide this in an environmentally friendly manner.

A common method to protect steel substrates is galvanizing.[10] During this treatment a thin layer of zinc metal is deposited onto the surface of steel to act as a sacrificial layer. An inherent problem with galvanizing is lack of adhesion of organic coatings to the zinc layer leading to blistering and early coating delamination which cuts the life expectancy of the metal drastically. Other methods to improve adhesion to the galvanizing layer have been developed (galvanneal) but these can be costly and, thus, often not used. Other methods to protect bare steel is to deposit zinc-rich primers onto the steel surface.[11]

Zinc-rich primers are epoxy coatings filled over the critical pigment volume concentration (CPVC) with zinc dust. These coatings act as sacrificial barriers much like how galvanizing does, but the topcoat has increased adhesion due to the higher surface area to volume ratio that occurs in Zn-rich coatings being above the CPVC. Zinc-rich coatings are very popular but the downside is the density of these coatings is very high, thus, the cost to transport is a major drawback.[12] Zinc dust also is highly explosive, thus, these coatings can be very dangerous to develop. In addition

to these issues, zinc-rich powder primers also show poor electrostatic deposition due to the fact zinc-rich primer does not charge well. This results in very thin films and poorer corrosion protection.

Protection of aluminum alloys is just as critical as aluminum alloys are used in many cutting edge areas where lighter-weight structural materials are needed. Aerospace alloys such as Al-2024T3 are especially troublesome for corrosion as they contain large percentages of copper which galvanically corrodes the surrounding aluminum leading to catastrophic failure.[13] Chrome based pigments and chrome pretreatments have shown great success in the corrosion protection of aluminum and, thus, rose to popularity.[14] A study in the 1990s showed that hexavalent chromium compounds show very strong carcinogenic properties thus the use in the past few decades has been heavily restricted.[15] With this information, other avenues to protect aluminum have been developed and ECPs show great promise from academic studies to protect aluminum alloys.[16-19, 8] The goal of this study to further optimize the reaction of PPy with Bisomer SEM to hopefully further improve the benefits previously observed.

5.3. Materials and Methods

5.3.1. Materials

All materials used in these experiments were used as supplied unless stated otherwise. For the synthesis of the reactive polypyrrole pigments three materials were needed. Pyrrole, nitric acid, and ferric nitrate were purchased from VWR. The pyrrole was distilled under vacuum to purify the monomer before use. BISOMER SEM was supplied as a 25% active solution in water containing ammonium sulphatoethyl methacrylate, this sample was supplied by GEO Specialty Chemicals.

The coating system these pigments were dispersed into consisted of a polyurethane acrylate oligomer, EBECRYL® 8501 supplied by Cytec Industries; hexanediol diacrylate (HDDA) and phosphate ester acrylate to improve adhesion, CD9053, also supplied by Sartomer; and DISPERBYK 110 a dispersing agent graciously supplied by BYK. The photoinitiator Irgacure® 819 and Irgacure® 184 were supplied by BASF.

5.3.2. Surfmer Doped PPy Synthesis

Nitric acid solutions of various pH were first made by diluting concentrated nitric acid with Millipore 18MΩ water to obtain the desired pH. The pH of these solutions was measured with a pH probe to ensure the solution was properly made. Solutions of pH = 1, 2, 3, 4, and 5 were all developed

In a 400 mL Erlenmeyer flask 200 mL solution of nitric acid at a range of pH (1-5) were added. To that 6.7g of pyrrole monomer was added dropwise under magnetic stirring to form a 0.5M pyrrole solution. BISOMER SEM solution was added to obtain a ratio 1 BISOMER SEM to 5 pyrrole units. This solution was mixed for 30 minutes to ensure full dissolution of the pyrrole monomer.

A 100 mL ferric nitrate solution was then added dropwise to the pyrrole-BISOMER SEM solution. Upon addition of the ferric nitrate solution the clear solution turned brown to black rapidly indicating the polymerization of pyrrole to polypyrrole was taking place. After all of the ferric nitrate was added, the final black solution was allowed to mix for 30 more minutes before the black powder was collected through vacuum filtration. The black filtrate was washed with both water and acetone until the decanted water and acetone was clear indicating any residual BISOMER SEM, iron salts, and pyrrole oligomers were removed from the final products. The black cakes were dried at 40°C under vacuum until no moisture was present.

5.3.3. Characterization of Crosslinkable PPy Pigments

The crosslinkable PPy pigments chemical structure was studied with Fourier Transform Infrared Spectroscopy using a Thermo Scientific Nicolet 8700 infrared spectrometer. Electrical properties of the reactive pigments were studied at a macro scale using a four-point probe technique. This technique used a Keithley 2100 multimeter connected to a Signatone® four-point probe assembly. Micro level analysis of the electrical properties was conducted using a Veeco® 3100 atomic force microscope operating in conductive atomic force microscopy (CAFM) mode. In this mode, a 1V potential is applied to the bottom of the sample. Current is measured through an iridium-platinum cantilever rastering in contact mode with a pellet pressed of the pigment. In both of these experiments, the pellets of the powder were embedded in electrically conductive epoxy and glued to a steel 1 inch by 1inch square.

Thermal stability of these pigments was also studied with a Thermogravimetric Analyzer (TGA). For these studies small samples of the pigments were heated from room temperature to 800°C at a rate of 20°C/min. Weight loss as a function of temperature was analyzed to determine where thermal decomposition occurs.

5.3.4. Coating Preparation

The reactive pigments synthesized at various pHs were dispersed with a high shear disperser into the UV-Coating formulation. The UV-coating formulation consisted of a mixture of 42% EBECRYL 8501, 42% HDDA, and 6% CD9053 all by weight percentage. Pigment was dispersed to reach a PVC of 10% based on total solids. Small amounts of Disperbyk 110 was added to lower the viscosity during addition. After pigment was added, the grind was allowed to mix for 30 more minutes to ensure the reactive pigments effectively dispersed into the coating system.

40 grams of each pigment dispersion were blended with a toluene solution containing the photo initiator package consisting of Irgacure® 819 and Irgacure® 184. This mixture was mixed via magnetic stirring for 30 minutes to ensure homogeneity. Drawdowns were performed with a drawdown bar on sandblasted Al-2024T3 substrates that were degreased with hexanes. All drawdowns were allowed 2 minutes to flash off any toluene present in the formulation prior to curing in the UV cabinet. The coatings were cured in a DYMAX Model 5000-EC UV-Light Curing Flood System equipped with a metal halide bulb with a spectral intensity of 174 mW/cm^2. All drawdowns were exposed to 3 minutes of UV-radiation in 1 minute on/off intervals.

5.3.5. Coating Characterization

Corrosion protective assessment of Al-2024T3 substrates was studied through accelerated weathering studies utilizing ASTM B117 chambers and the advanced electrochemical experiments of linear polarization (LP) and electrochemical impedance spectroscopy (EIS). The electrolyte used in these experiments was 5% sodium chloride. LP experiments were performed with a three electrode technique utilizing platinum mesh as a counter electrode, a saturate calomel electrode as the reference electrode, and the Al-2024T3 substrate as the working electrode. Open circuit potential was measured for 300 seconds prior to LP scans after which the scans were performed in a range of 1V below to 1V above the OCP. The LP scans were taken at various immersion intervals to help determine the amount of time these pigments might protect the Al-2024T3 substrate underneath. EIS was performed with the three electrode technique as well, and EIS scans were taken at regular intervals. EIS results were modeled with Z-View software to elucidate vital information regarding the circuit models which pertain to the coating systems.

5.4. Results and Discussion

5.4.1. Structural Analysis of PPy Pigments

FTIR curves for each of the PPy_BisomerSEM samples are presented in Figure 5.1. Each polypyrrole pigment displays the prominent peaks of PPy. The common absorption bands for PPy are listed in table 5.1.[20] The peaks for Bisomer SEM are much more difficult to detect as they are mostly overlapped by the more prominent PPy peaks.

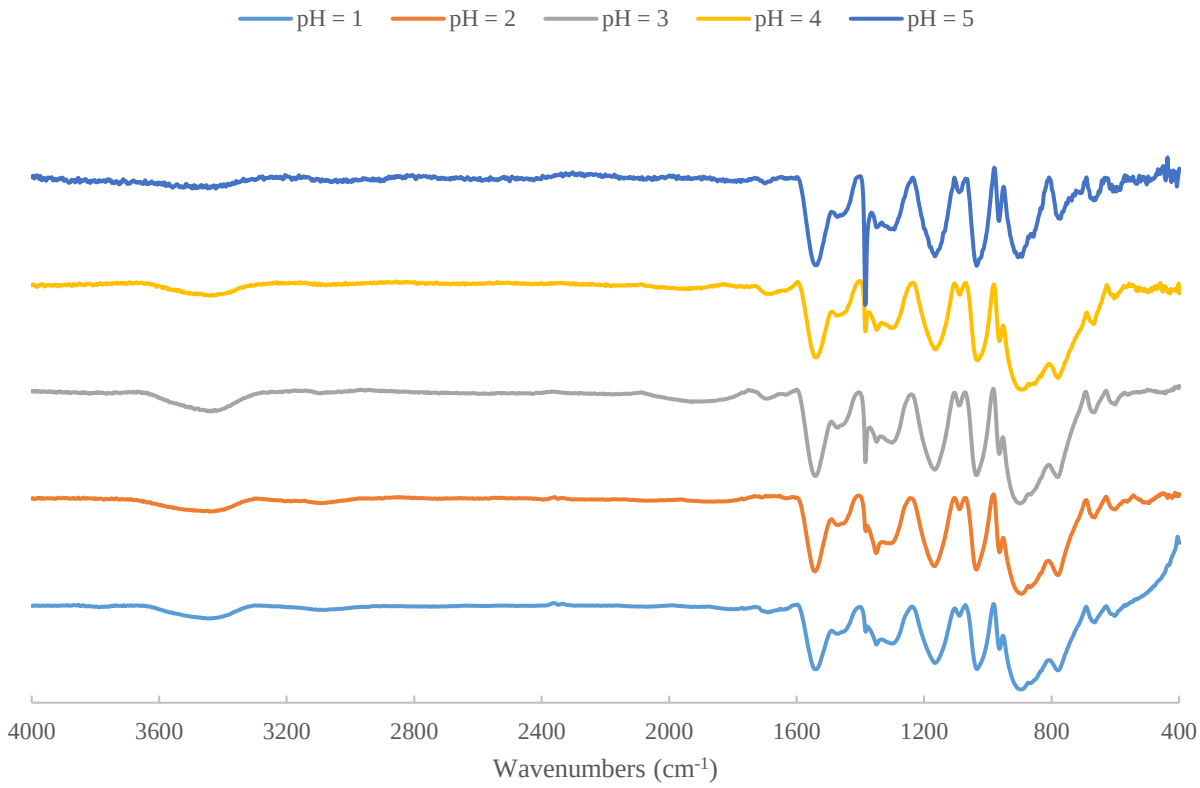

Figure 5.1: FTIR spectra for the different PPy_Bisomer SEM pigments (from top to bottom: pH = 1, pH = 2, pH = 3, pH = 4, pH = 5).

There is, however, one peak not associated with PPy that is evident in all samples located around 1089 wavenumbers (cm^{-1}). This is a peak associated with the C-O vibration in BISOMER SEM. This confirms the doping of the surfmer in the PPy backbone. With the surfmer doping the

PPy polymer chain, it is believed that the pigments have crosslinked into the final coating making a more impermeable coating that can also inhibit corrosion. Previous work in this area showed that with proper doping of reactive surfmers, the final coating physical properties were improved compared to traditionally doped polypyrrole.

Table 5.1: FTIR peaks associated with PPy

Peak Type	Wavenumbers (cm^{-1})
OH stretching	3633-3295
C=O Stretch	1687
C-C Stretch (Pyrrole ring)	1535
C-N Stretch Vibration	1468
C-H and C-N In-plane Deformation	1230-1395
Pyrrole Ring Breathing Vibration	1162
C-H and N-H In-Plane deformation	1033
C-C Out of Plane Ring Deformation	962
C-H Out of Plane deformation	890
C-H Out of Plane Ring Deformation	777

5.4.2. Electrical Properties of PPy Pigments

Pellets of each PPy_BisomerSEM pigment were made by pressing the pigment powder with a very high force forming a small puck of the pigment. These pucks were attached to 1 inch x 1 inch steel substrate with electrically conductive epoxy resin. The bulk electrical properties are presented in Figure 5.3. Pigments synthesized in solutions with a pH lower than 5 showed must lower surface resistances than the pigment synthesized at a pH of 5. These findings correlate with previous pH studies trying to optimize the electrical properties of PPy.[21] In these studies, however the bulk surface resistance shows an exponential decrease in terms of surface resistance with lower pH conditions during synthesis.

For some samples there was a wide disparity in the standard deviation. This is attributed to the poor packing nature of the pigments as the pucks were prone to crumbling. Without effective

packing of the pigment particles bulk surface measurements with a four-point probe can give widely varying results within each pigment sample.

The same pucks of compressed PPy pigments were also studied with C-AFM. This technique allows for the study of localized conductivity for materials. This technique is extremely useful when high deviations in bulk resistance are measured to determine the local conductivity. The results are depicted in Figure 5.4. The current densities for all samples except PPy_BisomerPH2 showed comparable density with maximum currents around 0.5 µA. The max current measured appeared to decrease with increasing pH which is expected as the electrical properties of polypyrrole being affected by reaction conditions including pH is well documented in the literature.[22, 23] The only outlier to this is the CAFM scans for PPy_BisomerPH2.

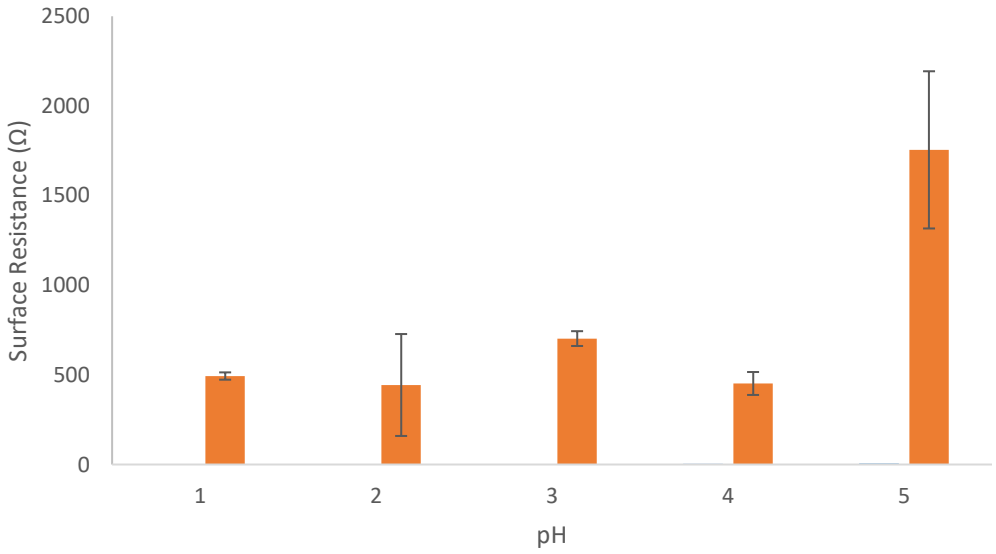

Figure 5.3: Bulk surface resistance results for the PPy_BisomerSEM pigments.

It was observed that during the synthesis of PPy_BisomerPH2 pigment that the pigment began to destabilize and flocculate, resulting in polypyrrole pigment settling at the bottom and a rapid increase in viscosity was also evident. This could have caused a problem with making highly

conductive PPy powder as it was not allowed to grow to as high of a molecular weight as the other pigment samples.[24] This could be due to a possible collapse of the surfmer at this particular pH but nothing has been found in literature suggesting such a phenomenon. It is noted that common polymer dispersions are in a pH range of 6-8 but the fact that the PPy did not crash at a pH of 1 but did crash at a pH of 2 is intriguing.

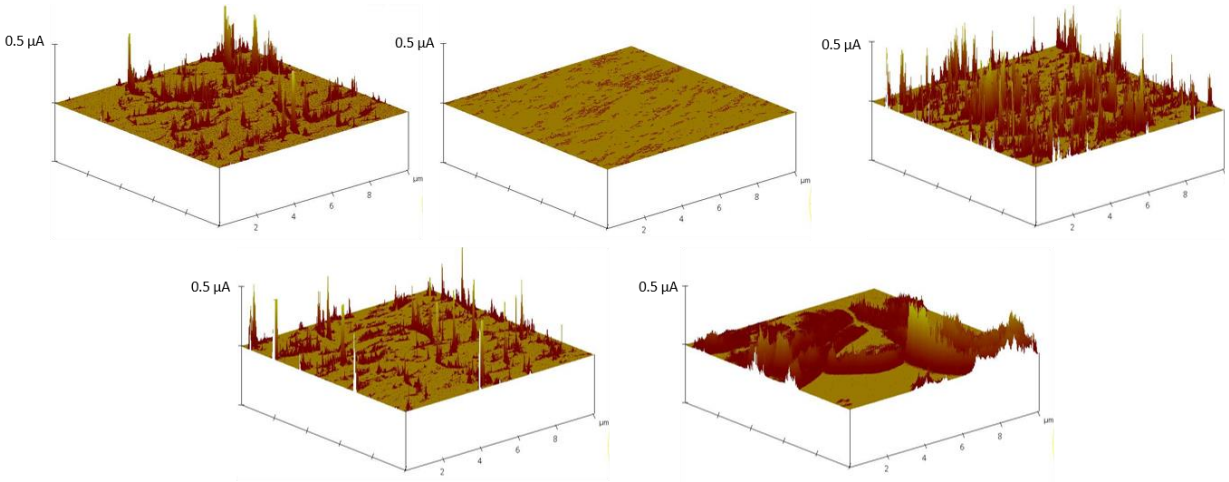

Figure 5.4: C-AFM current images for the PPy_Bisomer pigments. Top row from left to right: PPy_BisomerpH1, PPy_BisomerpH2, PPy_BisomerpH3. Bottom row from left to right: PPy_BisomerpH4, PPy_BisomerpH5. Scan area is 5µm x 5µm.

5.4.3. Thermal Properties of PPy Pigments

PPy_Bisomer pigments were also subjected to ramping temperatures in a TGA to determine the thermal stability of the pigments. Pure PPy is thermally stable up to approximately 200°C.[20, 25] Adding organic surfactants has shown to decrease the thermal stability of PPy as the inclusion of bulky surfactants results in the increase of distance between the chains thus decreasing the thermal stability.[20] Previous work with surfmer doped polypyrrole showed a small change in the thermal stability in the temperature range of 250-400°C.[26] Degradation in this region was shown to be due to the thermal breakdown of the surfactants.

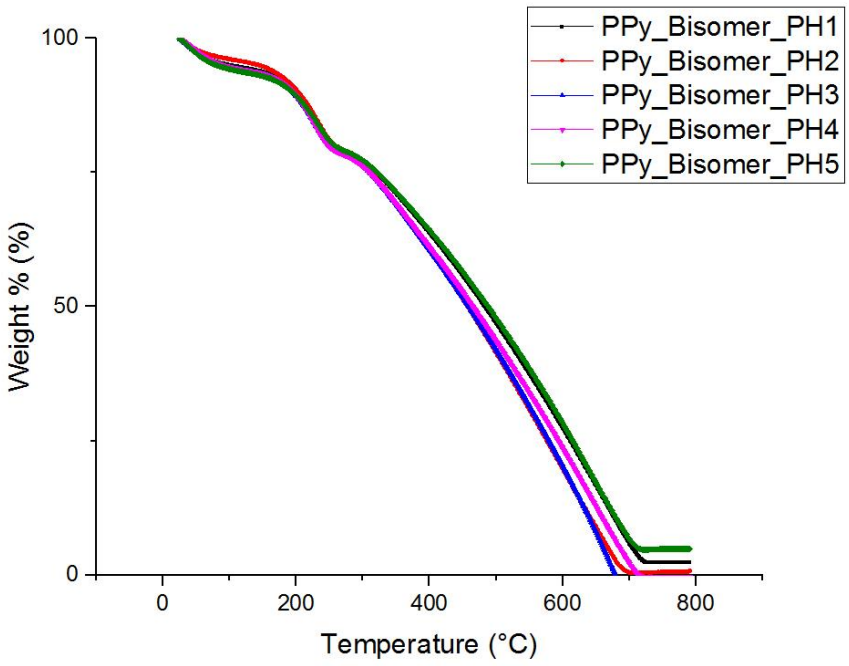

Figure 5.5: TGA curves for the PPy pigments synthesized at various pHs.

TGA curves for each of the PPy pigments synthesized at different pHs are presented in Figure 5.5. From these results there is not a significant difference on the final thermal properties with respect to pH during the reaction. Utilizing curves of the derivative of weight loss with respect to temperature helps identify where thermal degradation occurs. These curves are shown in Figure 5.6. Literature shows that polypyrrole was three major degradation zones. The first degradation zone occurs from room temperature to 100°C. This weight loss is due to the evaporation of water absorbed onto the polypyrrole surface. For all samples of PPy_Bisomer the weight loss is approximately 5-6 weight%. The second region is from 150-250°C. This region is the breakdown of lower molecular weight PPy. The last region of degradation occurs above 400°C. This region is where large scale breakdown in the polypyrrole backbone occurs and the polymer chain fully breaks down.

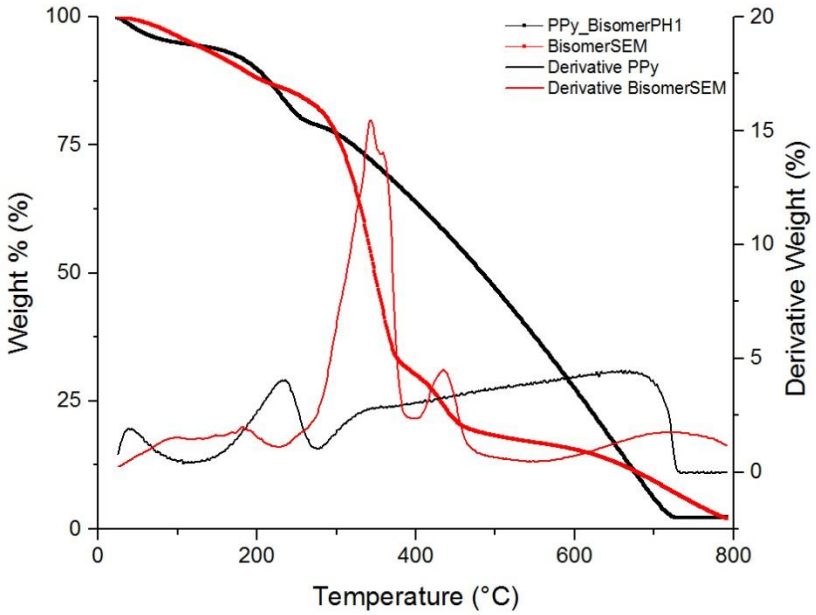

Figure 5.6: Weight loss and derivative weight loss curves for PPy_BisomerPH1 and Bisomer SEM.

TGA also is useful in determining if surfactant was incorporated into the polypyrrole and was shown to be successful in previous studies with various surfmers.[26] Figure 5.6 also shows the thermal stability of Bisomer SEM. The major thermal breakdown point for Bisomer SEM is different from the degradation regions. This degradation occurs from 250-400°C and can be observed in the PPy_BisomerPH1 sample. Analysis of the derivative weight loss curves of the other PPy_Bisomer pigments also show this drop indicating incorporation of Bisomer SEM into the polypyrrole pigments during synthesis.

5.4.4. Assessment of the Corrosion Protection Properties of PPy_BisomerSEM Pigments

Previous work showed that of all of the PPy pigments doped with surfmers, the PPy pigments doped with BisomerSEM showed the best corrosion protection of Al-2024T3.[26] Coatings with each of the PPy_Bisomer pigments synthesized at various pHs were cured onto Al-

2024T3 substrates and subjected to salt spray with a scribe. In addition, a control set of clear coats without pigment were submitted in accelerated weathering. Salt spray results are shown in Figure 5.7. The top set of pictures (a-f) are for all coatings at 0 hours, right before being exposed to ASTM B117 conditions. The second set (g-l) are for the panels after 744 hours of exposure.

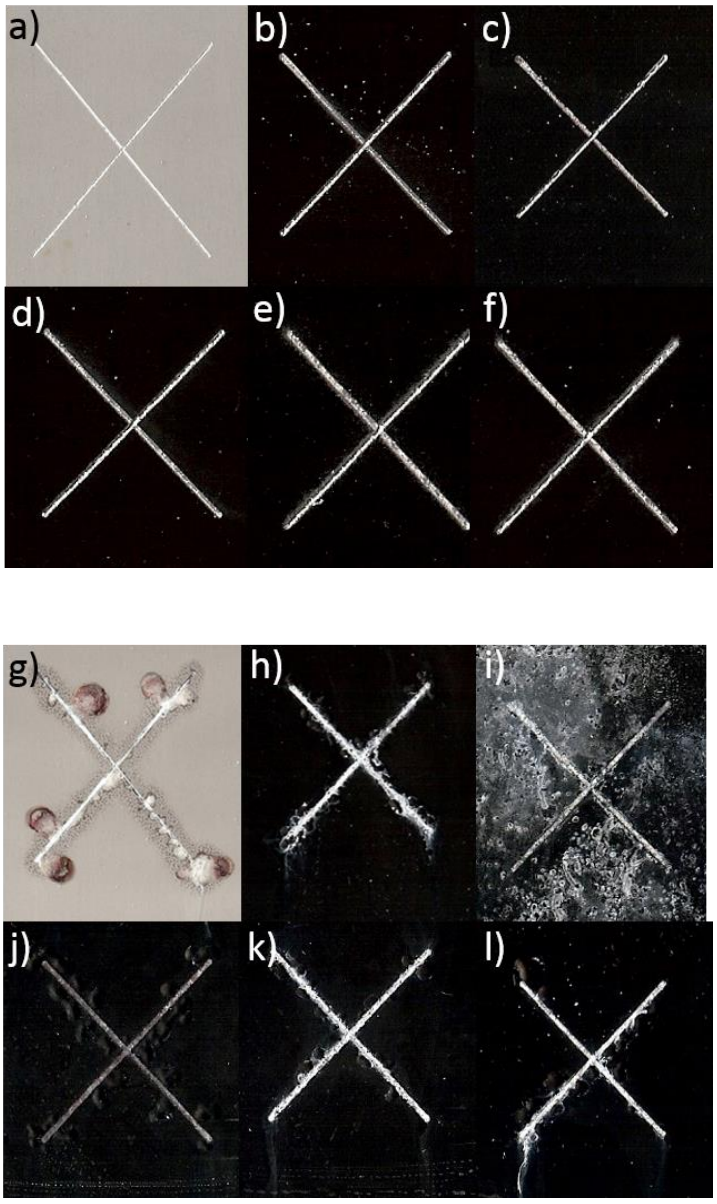

Figure 5.7: Top: Salt spray images at zero hours (a-f) for Clearcoat, PPy_pH1, PPy_pH2, PPy_pH3, PPy_pH4, and PPy_pH5. Bottom: Salt spray images at 744 hours (g-l) for Clearcoat, PPy_pH1, PPy_pH2, PPy_pH3, PPy_pH4, and PPy_pH5.

Aluminum 2024T3 has poor corrosion performance, which arises from the copper inclusions in the alloy. These inclusions cause galvanic corrosion to occur at the interface leading to rapid degradation of the alloy. On the clear coating after 744 hours it is evident of very large blisters forming and a large amount of microblisters all around the scribe (tiny black/red dots). ECPs have shown to passivate the metal surface and anodically protect the substrate.[16, 18, 27, 28] For all coatings containing the PPy pigments except the pigments synthesized at a pH of 2, the size of blisters is smaller. This is indicative of a protective nature of these PPy pigments on the Al-2024T3 surface. Inclusions of ECPs as pigments in these concentrations have also shown to provide a protective nature.

The effect of pH during synthesis of these PPy pigments does not seem to have any effect on the corrosion protective properties outside of the poor performance when synthesized at a pH of 2. This could be related to the lower levels of localized electrical conductivity as noted by CAFM results. Also with the instability during synthesis BISOMER SEM might not have been incorporated at a high enough level to adequately crosslink the pigments into the UV-curable network to help improve the barrier properties away from the scribe. The poor barrier protection of the coatings with PPy_BisomerPH2 is visually evident with corrosion penetrating the coating at great distances away from the scribe. From these results a primer doped with these crosslinkable PPy pigments could provide an active corrosion protection mechanism compared to coatings without these crosslinkable pigments.

5.4.5. Electrochemical Investigations of PPy_Bisomer Doped Coatings

Linear polarization offers a valuable method in determining the electroactive nature of a substrate and its susceptibility to corrosion. Coatings containing ECPs have shown to shift the corrosion potential to a more positive value indicating a passivating effect.[6] Over time however,

this passivating effect diminishes as the ECPs lose their protective nature. Linear polarization results for all coatings containing PPy pigments synthesized at various pHs are shown in Figure 5.8. Coatings containing PPy_BisomerPH3 through PPy_BisomerPH5 showed the strongest passivation effect with corrosion potential between 0 and -0.10V.

Coatings doped with PPy_BisomerPH2 show poor corrosion protection as a passivation region indicating development of aluminum oxide on the surface is evident on the linear polarization scan. This is attributed to the porosity evident in the final cured film. PPy's ability to passivate the substrates surface and inhibit corrosion is not strong enough to protect the Al-2024T3 surface due to the poor barrier protection of the final coating with this pigment. While PPy pigments synthesized at other pHs showed adequate protection for small coating defects, defects much larger (brought on by poor barrier properties) cannot be sufficiently protected.

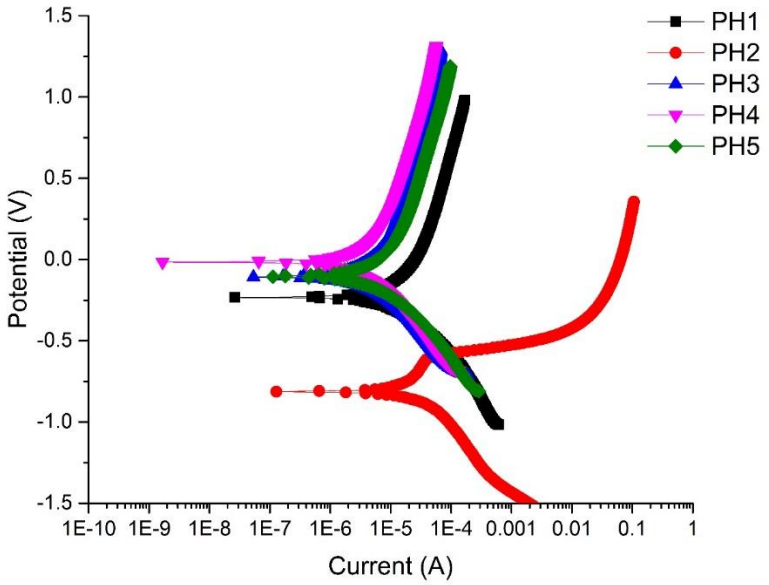

Figure 5.8: Linear polarization scans for containing surfmer doped polypyrroles synthesized at various pHs.

Coatings containing the PPy pigments synthesized at the other pHs have the corrosion potential steadily drop until comparable to the corrosion potential of PPy_BisomerPH2 coatings, however the corrosion current for all of these coatings is 1-2 orders of magnitude even with the same corrosion potential. These results mean that even after prolonged exposure to electrolytes the coatings are still offering exceptional protective properties of the surface. The passivation region observed on the PPy_BisomerPH2 linear polarization scan that is attributed to the buildup of an aluminum oxide surface first begins to appear around 336 hours of electrolyte immersion for the coatings doped with the other PPy pigments.

Electrochemical impedance spectroscopy can be used to analyze the protective properties of organic coatings on metal alloys. Impedance plots of the various coatings containing PPy_Bisomer pigments synthesized at various pHs are shown in Figure 5.9. Impedance is a direct measure of how difficult it is to pass a current from one electrode (counter) to the other electrode (substrate, aka working). For non-conductive coatings, a high impedance is desired as this indicates it acts as an excellent barrier to electrolyte penetration.

However, these conductive PPY doped coatings function on an entirely different protection mechanism and their impedance is markedly lower than traditional clear coats. For reference a traditional clear coat with excellent barrier properties would have an impedance value upwards of 1 gigaohm. For all impedance spectra the coatings containing PPy pigments synthesized at all pHs but 2 showed impedance values between 10,000-50,000 ohms. This drop in initial impedance is due to the conductive nature of PPy. It should be mentioned that while impedance is the measure of resistance for AC current it is not a direct measurement of the coatings surface resistance.

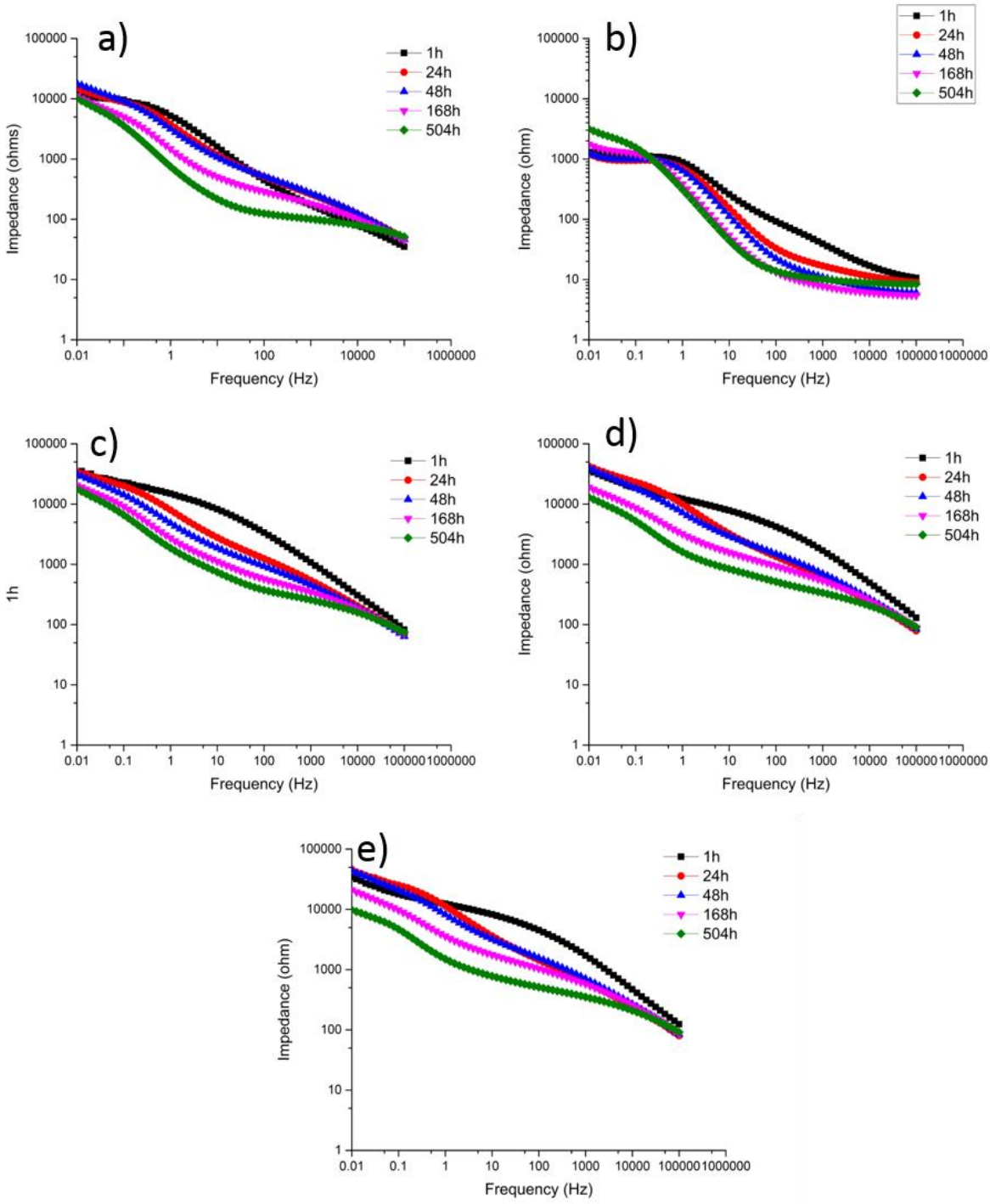

Figure 5.9: Impedance spectra plots for coatings containing: PPy_BisomerPH1 (a), PPy_BisomerPH2 (b), PPy_BisomerPH3 (c), PPy_BisomerPH4 (d), and PPy_BisomerPH5 (e).

Utilizing circuit modeling software, the impedance spectra obtained can be effectively translated into equivalent circuits to model the flow of electrons in the corrosion process. Figure 5.10 shows the two common circuit models that display how electrons flow in an EIS test when measuring a piece of metal coated with an organic coating. The "Randle's cell", depicted as the left circuit model in Figure 5.10 models the organic coating as a constant phasing element (CPE), also known as a leaky capacitor due to its not fully resistive properties. Rp is defined as the pore resistance of the coating, which is directly related to the ability for electrolytes to penetrate the coating to form an electrically conductive network. For ECP's however, the Rp starts at typically lower values due to the less resistive nature of ECP's versus traditional polymeric materials.

As electrolytes penetrate an organic coating and reach the metal substrate, corrosion begins resulting in an oxide layer forming on the metal surface. Aluminum oxide being resistive in nature, can also be modeled in the same way as an organic coating. This second circuit model has another CPE, which is defined as the double layer capacitance. Rct is defined as the charge transfer resistance and this is defined as the ability of electrolyte to permeate the aluminum oxide layer.

Previous research into PPy doped coatings showed that even at low impedance levels as measured by EIS the coatings still show superior corrosion protection compared to control coatings, due to its active corrosion protection mechanisms.[6] Coatings doped with PPy_BisomerPH2 show initial spectra very similar to bare Al-2024T3 indicating no barrier protection to electrolyte penetration. The impedance spectra quickly shift to a two time-constant model indicating rapid corrosion even under 24 hours of electrolyte immersion. Furthermore, there is a slight increase in impedance (< 1 decade) as exposure increases indicating a build up of aluminum oxide. This is indicative of electrolyte penetrating the coating to the metal surface resulting in the development of an aluminum oxide layer which means corrosion has begun.[29]

For the remaining PPy doped coatings the impedance spectra shift is observed to occur at later immersion times. However, for all of these coatings there is no rise in impedance after the two time-constant model develops and in the impedance continues to decrease indicating that even though the coating becomes less capacitive, protection of the Al-2024T3 still occurs and the aluminum oxide layer does not grow. This second time constant begins to appear around 168h of immersion in the electrolyte for coatings containing PPy_BisomerPH1, PPy_BisomerPH3, PPy_BisomerPH4, and PPy_BisomerPH5.

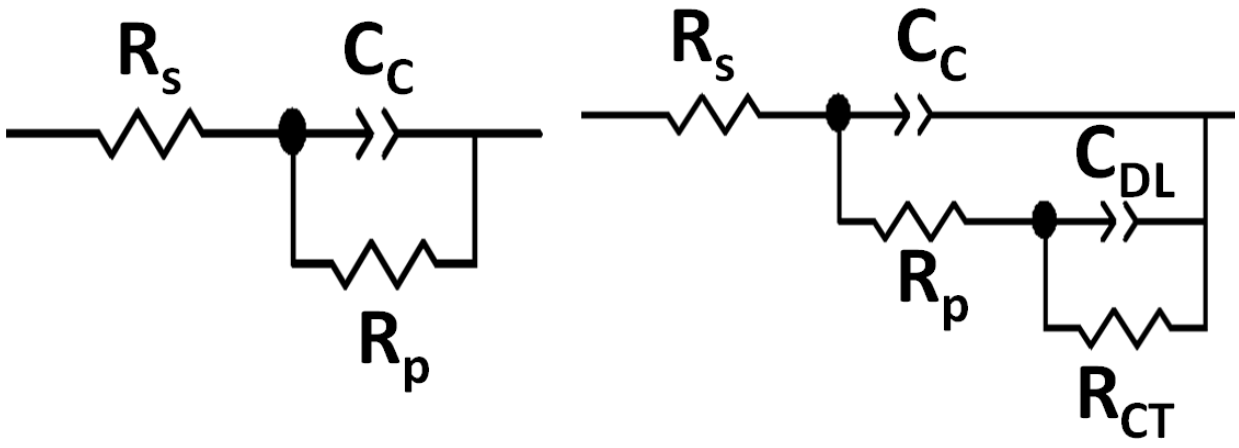

Figure 5.10: Equivalent circuit models used to model the EIS results of the coatings

Figure 5.11 is a plot of the Rp with respect to immersion time. It is evident that after initial immersion a drop of impedance is observed due to electrolyte permeation into the organic coating. The Rp for coatings containing PPy stabilizes after the drop indicating an equilibrium has been reached.

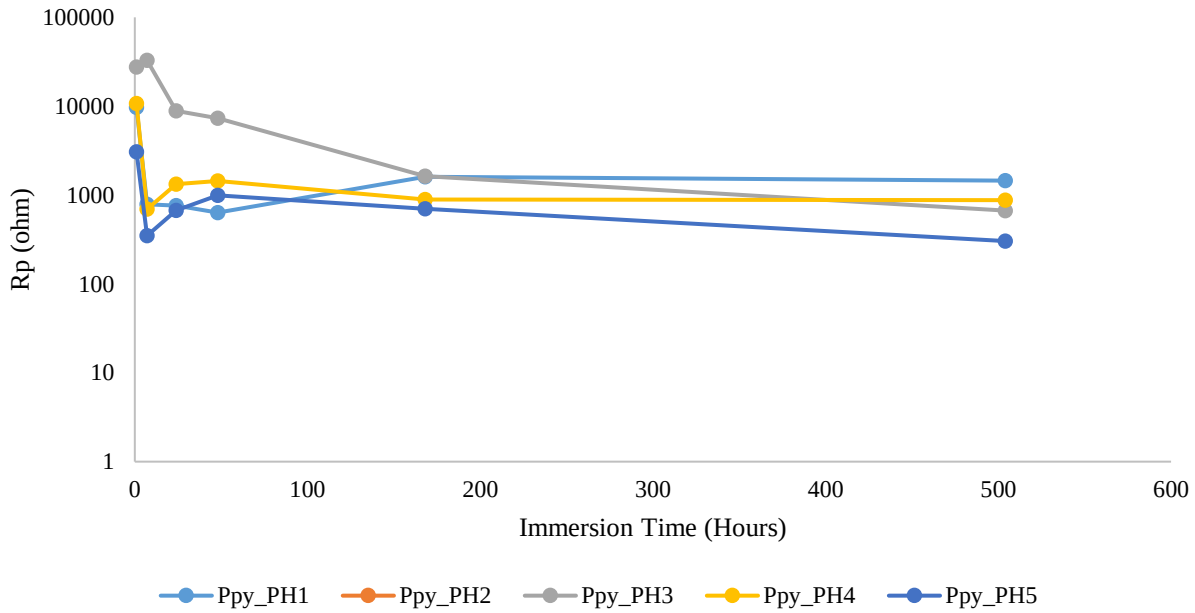

Figure 5.11: Effect of immersion time on the Rp of coatings containing crosslinkable polypyrrole pigments.

5.5. Conclusions

PPy pigments doped with Bisomer SEM were synthesized at various pHs. The final electrical properties were similar although an increase in bulk electrical conductivity was noted with PPy synthesized at lower pHs. It was observed during these reactions that a pH of 2 the resulting dispersion crashes and results in a very sponge like PPy pigment. Thermal properties of all PPy synthesized were comparable and no effect of pH was observed.

Coatings containing these reactive PPy pigments were cast onto Al-2024T3 substrates and cured under UV-light. Accelerated weathering tests showed an improvement in the corrosion protection of Al-2024T3 compared to clear coats without PPy pigments. Coatings containing PPy_BisomerPH2 were very porous and showed extremely poor protective properties. Linear polarization results for the coatings containing PPy pigments besides PPy_BisomerPH2 showed a passivation effect of the Al-2024T3 substrate indicating an active protection mechanism.

5.6. References

1. H. Shirakawa, S. I., Infrared Spectra of Poly(acetylene). *Polymer Journal* 1971, 2 (2), 231-244.

2. Chen, X., J. Devaux, J. Issi and D. Billaud, The stability of polypyrrole electrical conductivity. *European polymer journal* 1994, 30 (7), 809-811.

3. Zhang, P., Z. Yang, D. Wang, S. Kan, X. Chai, J. Liu and T. Li, Electrochemical deposition and photovoltaic properties of Nano-Fe< sub> 2</sub> O< sub> 3</sub>-incorporated polypyrrole films. *Synthetic Metals* 1997, 84 (1), 165-166.

4. Chen, M., Printed electrochemical devices using conducting polymers as active materials on flexible substrates. *Proceedings of the IEEE* 2005, 93 (7), 1339-1347.

5. Mabrook, M., C. Pearson and M. Petty, Inkjet-printed polypyrrole thin films for vapour sensing. *Sensors and Actuators B: Chemical* 2006, 115 (1), 547-551.

6. Jadhav, N., C. A. Vetter and V. J. Gelling, Characterization and Electrochemical Investigations of Polypyrrole/Aluminum Flake Composite Pigments on AA 2024-T3 Substrate. *ECS Transactions* 2012, 41 (15), 75-89.

7. Kalendová, A., D. Veselý and J. Stejskal, Organic coatings containing polyaniline and inorganic pigments as corrosion inhibitors. *Progress in Organic Coatings* 2008, 62 (1), 105-116.

8. Jadhav, N., C. A. Vetter and V. J. Gelling, The effect of polymer morphology on the performance of a corrosion inhibiting polypyrrole/aluminum flake composite pigment. *Electrochimica acta* 2013, 102, 28-43.

9. Koch, G. H., M. P. Brongers, N. G. Thompson, Y. P. Virmani and J. H. Payer (2002). Corrosion cost and preventive strategies in the United States.

10. Maeda, S., Surface chemistry of galvanized steel sheets relevant to adhesion performance. *Progress in Organic Coatings* 1996, 28 (4), 227-238.

11. Knudsen, O. Ø., U. Steinsmo and M. Bjordal, Zinc-rich primers—Test performance and electrochemical properties. *Progress in Organic Coatings* 2005, 54 (3), 224-229.

12. Sørensen, P. A., S. Kiil, K. Dam-Johansen and C. Weinell, Anticorrosive coatings: a review. *Journal of Coatings Technology and Research* 2009, 6 (2), 135-176.

13. Wu, T. and J. Wu, Effect of sulfate ions on corrosion inhibition of AA 7075 aluminum alloy in sodium chloride solutions. *Corrosion* 1995, 51 (3), 185-190.

14. Kendig, M. and R. Buchheit, Corrosion inhibition of aluminum and aluminum alloys by soluble chromates, chromate coatings, and chromate-free coatings. *Corrosion* 2003, 59 (5), 379-400.

15. Costa, M., Toxicity and carcinogenicity of Cr (VI) in animal models and humans. *Critical reviews in toxicology* 1997, 27 (5), 431-442.

16. Gelling, V. J., M. M. Wiest, D. E. Tallman, G. P. Bierwagen and G. G. Wallace, Electroactive-conducting polymers for corrosion control: 4. Studies of poly (3-octyl pyrrole) and poly (3-octadecyl pyrrole) on aluminum 2024-T3 alloy. *Progress in Organic Coatings* 2001, 43 (1), 149-157.

17. Akundy, G. S., R. Rajagopalan and J. O. Iroh, Electrochemical deposition of polyaniline–polypyrrole composite coatings on aluminum. *Journal of applied polymer science* 2002, 83 (9), 1970-1977.

18. He, J., D. E. Tallman and G. P. Bierwagen, Conjugated polymers for corrosion control: scanning vibrating electrode studies of polypyrrole-aluminum alloy interactions. *Journal of the electrochemical society* 2004, 151 (12), B644-B651.

19. Tallman, D. E., K. L. Levine, C. Siripirom, V. G. Gelling, G. P. Bierwagen and S. G. Croll, Nanocomposite of polypyrrole and alumina nanoparticles as a coating filler for the corrosion protection of aluminium alloy 2024-T3. *Applied Surface Science* 2008, 254 (17), 5452-5459.

20. Omastova, M., M. Trchova, J. Kovářová and J. Stejskal, Synthesis and structural study of polypyrroles prepared in the presence of surfactants. *Synthetic Metals* 2003, 138 (3), 447-455.

21. Kupila, E. and J. Kankare, Electropolymerization of pyrrole: effects of pH and anions on the conductivity and growth kinetics of polypyrrole. *Synthetic Metals* 1993, 55 (2-3), 1402-1405.

22. Wencheng, S. and J. O. Iroh, Effects of electrochemical process parameters on the synthesis and properties of polypyrrole coatings on steel. *Synthetic Metals* 1998, 95 (3), 159-167.

23. Carquigny, S., O. Segut, B. Lakard, F. Lallemand and P. Fievet, Effect of electrolyte solvent on the morphology of polypyrrole films: application to the use of polypyrrole in pH sensors. *Synthetic Metals* 2008, 158 (11), 453-461.

24. Street, G., S. Lindsey, A. Nazzal and K. Wynne, The structure and mechanical properties of polypyrrole. *Molecular Crystals and Liquid Crystals* 1985, 118 (1), 137-148.

25. Stejskal, J., M. Omastová, S. Fedorova, J. Prokeš and M. Trchová, Polyaniline and polypyrrole prepared in the presence of surfactants: a comparative conductivity study. *Polymer* 2003, 44 (5), 1353-1358.

26. Byrom, J. R. (2016). Development of Crosslinkable Polypyrrole Pigments and Their Applications in UV-Curable Technologies. *Polymers and Coatings*, North Dakota State University.

27. Armelin, E., R. Pla, F. Liesa, X. Ramis, J. I. Iribarren and C. Alemán, Corrosion protection with polyaniline and polypyrrole as anticorrosive additives for epoxy paint. *Corrosion Science* 2008, 50 (3), 721-728.

28. Adamczyk, L. and P. J. Kulesza, Fabrication of composite coatings of 4-(pyrrole-1-yl) benzoate-modified poly-3, 4-ethylenedioxythiophene with phosphomolybdate and their application in corrosion protection. *Electrochimica acta* 2011, 56 (10), 3649-3655.

29. Gelling, V. (2011). Lecture 12 - EIS: 2.

CHAPTER 6. ALUMINUM FLAKE-POLYPYRROLE COMPOSITE PIGMENTS DOPED WITH ORGANIC CORROSION INHIBITORS FOR PROTECTION OF ALUMINUM 2024T3

6.1. Abstract

Aluminum flake-Polypyrrole (Al-PPy) pigments were synthesized utilizing chemical oxidation with ammonium persulfate in an aqueous solution. These composite pigments were doped with five different organic corrosion inhibitors namely 4,5-dihydroxynaphthalene-2,7-disulfonate; anthraquinone-2-sulfonate; 4-hydroxybenzenesulfonate; 1,2-dihydroxybenzene-3,5-disulfonate; and hydroquinonesulfonate. The final products were characterized for their morphology and elemental composition through scanning electron microscopy (SEM) and energy dispersive spectroscopy respectively. Electrical properties of the pigments were studied with conductive atomic force microscopy (C-AFM). The pigments were then incorporated into a waterborne epoxy-amine coating and studied for their corrosion protection on Aluminum 2024-T3 through accelerated weathering and advanced electrochemical techniques such as electrochemical impedance spectroscopy (EIS), linear polarization (LP), scanning vibrating electrode technique (SVET), and galvanic coupling experiments. It was determined that the type of organic corrosion inhibitor has a dramatic impact on overall corrosion protection for long term exposure. EIS results indicated smaller changes in the pore resistance for the coatings containing Al-PPy compared to coatings pigmented with unmodified aluminum flake. Galvanic coupling experiments indicated galvanic coupling does take place with some of the pigments within 24 hours for some pigments but the induction time for others is longer. All coatings containing Al-PPy composite pigments demonstrated better corrosion resistance than the control coatings.

6.2. Introduction

The prevention of corrosion is a top priority in infrastructure development. It is currently estimated that for the United States alone 1.2 trillion dollars per year in either replacing materials that have corroded beyond their usability, or protecting them by various means including cathodic protection or by applying a protective coating to limit the substrates exposure to aggressive media.[1]

Structural aluminum alloys, such as Aluminum 2024T3 (Al-2024T3) are widely used in aerospace applications due to their excellent strength to weight ratio and good fatigue resistance.[2] Unfortunately, the corrosion resistance is quite poor due to the copper inclusions which results in galvanic corrosion.[3] In order to combat this poor corrosion performance, a variety of surface treatments and primers containing corrosion inhibiting pigments have been developed. Currently in aerospace applications a primer or surface treatment made from hexavalent chromates is used to protect Al-2024T3. Hexavalent chromate surface treatments are extremely effective at protecting Al-2024T3 as they have been demonstrated to show a "self-healing" effect.[4] In addition to this observable self-healing phenomenon, the oxide formed is inert, stable, and acts as a superb barrier to electrolyte ingress. Lastly, hexavalent chromium shows excellent adhesion to the naturally occurring aluminum oxide layer.

Unfortunately, hexavalent chromates have been known to be carcinogenic and thus regulation of their usage began in 1982.[5] Since then, the regulations have been severely tightened to the point now that hexavalent chromates only acceptable use is in the protection of aerospace structures. With increasing stringent regulation, novel replacements for hexavalent chromates have been developed. Trivalent chromate conversion coatings were one of the popular alternatives. Trivalent chromium conversion coatings are chemically inert films that can effectively protect the underlying substrate. Trivalent chromates also do not display the

carcinogenic effects that studies on hexavalent chromates demonstrated. Even with this reduced toxicity there is concern that trivalent chromates could become oxidized to the hexavalent stage in the environment thus the usage has been limited.

Sol-gel coatings have shown a great deal of promise in possibly replacing hexavalent chromate conversion coatings.[6-9] Sol-gel coatings are derived from zirconium and silane agents. Boegel™ has been developed by Boeing to replace the currently used chromate conversion coatings and have shown great promise in field trials due to the ability to adhere to not only bare metal, but metal oxides as well. In addition, the Boegel™ contains reactive functional groups that cross-link into common epoxy-amine primer systems to improve the adhesion between the sol-gel and primer coatings. Sol-gel coatings however are extremely thin (50-200 nm) and do not provide adequate corrosion protection if used alone.

Corrosion inhibiting primers are coatings systems highly pigmented with corrosion inhibiting pigments to provide active protection of the underlying substrate. Alternatives to traditional corrosion inhibiting pigments such as zinc chromates have been developed and have been commercialized. A popular alternative was the development of Mg-rich primers by Bierwagen.[10] The primers function as a sacrificial barrier by applying an organic coating containing magnesium particles. The coatings are formulated above CPVC to ensure adequate contact between the magnesium particles to achieve protection. Unfortunately once Mg particles are used and converted to the subsequent oxides, service lifetime becomes an issue.

A more novel idea is the use of electrically conductive polymers (ECPs) for protecting metal substrates. Since the discovery in 1970s by Shirakawa et al., numerous applications have been suggested for the applicability of these novel polymeric compounds including photovoltaics, supercapacitors, printable electronics, OLEDs, and corrosion protection.[11-14] ECPs are currently

heavily investigated and have shown great promise in the field of corrosion protection as an environmentally friendly replacement for currently utilized technology. The most widely studied conductive polymers are polypyrrole (PPy), polyaniline (PAni), and polythiophene (PTh). Review articles on approaches to using ECPs for corrosion protection are readily available.[15-17]

ECPs can be utilized as either intact films or by dispersing into organic paints as a pigment. Intact coatings of ECPs are synthesized electrochemically by anodic oxidation. Electropolymerized films of PPy and polyaniline onto steel have both shown the ability to provide improved corrosion protection over typical barrier coatings.[18-19] This improved corrosion protection was the result of a passivated iron oxide layer that forms during the electropolymerization process.

Electropolymerization however has its drawbacks mainly due to the required current to coat larger structures, active metals, and problems associated with electropolymerizing uniform films on abstract geometries. Chemical oxidation with oxidizing agents such as ferric chloride and ammonium persulfate offer an industrially scalable method to produce large quantities of ECPs effectively. In addition, these synthesis processes are performed in aqueous solution thus limiting the VOCs of the entire process. Unfortunately, ECPs are insoluble in common polar and nonpolar solvents thus uniform films cannot be made with ECPs alone.

Organic coatings pigmented with ECPs have also shown the ability to protect substrates.[20-21] SEM and XPS experiments with coatings containing PAni pigments demonstrated a passivation effect of the steel substrate much like was has been seen with pure PAni films.[22] Coatings containing PPy pigments have showed improvement for the corrosion protection for various substrates including steel, aluminum, and magnesium alloys.[21-23-24] Acrylic coatings pigmented

with up to 20 parts by weight PPy showed improved corrosion protection of magnesium alloys after 1000 hours of accelerated weathering.[24]

To further improve the ability to provide corrosion protection, more advanced pigments incorporating ECPs have been developed.[25-27] One method was developing composite pigments of nanoclays and PPy.[28] Nanoclays are a fascinating material as they provide superior barrier protection due to the platelet like morphology. This morphology when dispersed into an organic coating results in a tortuous pathway for outside media such as electrolyte and oxygen to pass through to reach the surface of the substrate. Epoxy nanocomposites containing these PPy-clay platelets demonstrated improved corrosion protection compared to epoxy nanocomposites containing just clay platelets and just PPy respectively. By combining these two materials the advantages of both were taken advantage of to provide a coating with superior barrier protection as well as active protection provided by the PPy.

Recently, our group has developed novel aluminum flake-PPy (Al-PPy) composite pigments for the protection of Al-2024T3.[29] Previous results showed deposition of PPy onto aluminum flake through chemical oxidation with ammonium persulfate. These pigments demonstrated the ability of the polypyrrole to galvanically couple with the underlying aluminum flake to activate it to provide sacrificial protection.[30] The composite pigments can be doped with corrosion inhibiting oxoanions such as phosphate and nitrate and show significant improvement in the corrosion protection of Al-2024 compared to unmodified aluminum flake.[31] Experiments with the scanning vibrating electrode technique (SVET) showed the ability to protect defects in a coating up to 2 mm in diameter even after 48 hours of immersion in DHS.[32]

In this study Al-PPy composite pigments were doped with organic corrosion inhibitors and incorporated into a waterborne epoxy-amine coating system. The coatings were subjected to

accelerated weathering and electrochemical methods to evaluate the corrosion resistant performance of the primers. Galvanic coupling experiments and SVET experiments show insight into the ability of these pigments to galvanically protect the underlying substrate. All Al-PPy composite pigments based coatings were compared to control coatings in which unmodified aluminum flake were dispersed.

6.3. Materials and Methods

6.3.1. Materials

All materials were used as received unless noted. Pyrrole monomer and ammonium persulfate was purchased from Alfa Aesar. Pyrrole monomer was distilled prior to use. The aluminum flake was graciously supplied by ECKHART America under the trade name STAPA Aloxal PM 2010. The organic corrosion inhibitors 4,5-dihydroxynaphthalene-2,7-disulfonic acid disodium salt, sodium anthraquinone-2-sulfonate, 4-hydroxybenzenesulfonic acid, 1,2-dihydroxybenzene-3,5-disulfonic acid disodium salt monohydrate, and hydroquinonesulfonic acid potassium salt were purchased from Sigma Aldrich. The coating system consisted of a two-part water reducible epoxy. Beckopox VEP 2381W/55WA is the epoxy resin and the amine crosslinker Beckopox EH625W/80WA were graciously supplied by Cytec Industries. The Al-2024T3 substrates were purchased from Q-Panel.

6.3.2. Composite Pigment Synthesis

Composite pigments of aluminum and PPy were synthesized through the chemical oxidation of pyrrole in the presence of aluminum flake. In an Erlenmeyer flask 1000 mL of a 0.2M pyrrole solution in 18 MΩ Milipore™ water was added followed by 30 grams of aluminum flake. The organic corrosion inhibitors were then added at a molar ratio of 1 pyrrole molecule to 2 corrosion inhibitor molecule. Lastly a solution of 1M ammonium persulfate was added slowly to

the dispersion. The reaction was allowed to proceed for 24 hours at room temperature. The aluminum flake-PPy pigment was collected through vacuum filtration and washed with Milipore™ water to remove byproducts of the reaction. The final product was dried at 60°C overnight. The composite pigments were then ground using a mortar and pestle then passed through a sieve with pore diameters of 106 microns.

6.3.3. Pigment Characterization

Morphology studies of the composite pigments were conducted with a JEOL JSM-6300 scanning electron microscope (SEM) equipped with a field emission gun. Elemental analysis of the composite pigment was performed in conjunction with the morphology studies utilizing energy dispersive spectroscopy (EDS). Pellets of each composite pigment were made and glued onto steel substrate with conductive epoxy for electrical properties characterization. Electrical properties were studied by conductive atomic force microscopy (C-AFM) with a Veeco Dimension 3100 atomic force microscope operating in contact mode with a platinum-iridium current sensing probe. Scans were conducted in 5 micron by 5 micron scan areas while applying a 50 mV potential bias through the bottom of the sample.

6.3.4. Corrosion Inhibition Studies

To assess the corrosion inhibition capabilities of these aluminum flake-PPy pigments, coatings loaded at a PVC level of 20 were developed. The stochiometric ratio of epoxy resin to amine crosslinker was kept at 1:1. The viscosity for the formulated paints was adjusted with Millipore water. Pigments were dispersed in the liquid coating resin by hand mixing with a spatula. The coatings were applied at a wet film thickness of 8 mils (approximately 200 microns) and cured at room temperature for one week to ensure complete crosslinking. The resulting cured coatings had a dry film thickness of about 80-100 microns. Prior to coating application the Al-2024T3

substrates were sandblasted to improve adhesion and degreased with hexanes to remove contaminants from the surface. For these studies control coatings containing unmodified aluminum flake pigment were also formulated.

Accelerated weathering tests were conducted with panels scribed to simulate artificial defects. Accelerated weathering studies were conducted in accordance with ASTM G85-A5, popularly known as Prohesion test. In this accelerated weathering technique, panels are exposed to 1 hour wet cycles at ambient temperature with the electrolyte consisting of a mixture of 0.35% ammonium sulfate and 0.05% sodium chloride which is known as dilute Harrison's solution (DHS) followed by 1 hour at 35°C dry cycle. Panels were removed at regular intervals and optical photographs taken to observe the coatings performance with respect to weathering time.

Electrochemical Impedance Spectroscopy (EIS) studies were conducted using a conventional 3-electrode cell on fresh coatings. The cell consists of a glass cylinder cell clamped onto a coated substrate and sealed with a rubber O-ring. In this cell, platinum mesh acts as the counter electrode, a saturated calomel electrode is the reference electrode, and the substrate acts as the working electrode. A dilute Harrison's solution was used as the electrolyte. EIS studies were run at the open circuit potential over a frequency range of 100,000 Hz to 0.01 Hz with 10 data points per decade. The potential perturbation was kept at 10 mV. EIS spectra were taken at regular intervals to monitor the ingress of electrolyte and monitor changes that occur as corrosion begins. Three replicates for each coating formulated were taken to ensure reproducibility. Circuit modeling of the EIS spectra was accomplished using Z-View software.

Galvanic coupling measurements were conducted with the two bath cell as shown in Yan et al.[30] In this setup, a 1 cm^2 circle of coating sample and 1 cm^2 bare Al-2024T3 is exposed to DHS. Each of these samples is connected via a salt bridge made from a rubber tube filled with

agar and soaked in 1M potassium chloride solution. In this setup the substrate of the coated sample acts as the working electrode and the bare Al-2024T3 sample acts as the counter electrode. A saturated calomel electrode is inserted into the bath where the coated substrate is located. The bath containing the coated substrate was deoxygenated by bubbling N_2 to simulate deaerated conditions while the bath containing the uncoated aluminum 2024-T3 panel had air bubbled simulating aerated conditions on the surface of the substrate. The cell was hooked up to a Gamry PC-4 potentiostat and run in zero resistance ohmmeter mode. The mixed potential and galvanic current was measured over a 24 hour period.

Scanning Vibrating Electrode Technique (SVET) from Applicable Electronics Inc. was employed to study the ability of the coating to protect substrate with a simulated defect. Scans were conducted in 0.5% sodium chloride solution. In all coating samples a 5 mm by 5 mm was taped off as the scanning area. In this scanning area an artificial circular defect was made by slowly eroding the coating area with a drill bit until the substrate surface was visible. SVET scans were conducted with an electrode consisting Pt-black tip on a Pt-Ir electrode purchased from Microprobe Inc. SVET scans were performed every hour for 48 hours for all coating samples to monitor corrosion current density that can develop as well as see if any cathodic protection is afforded by these Al-PPy composite pigments.

6.4. Results and Discussion

Table 6.1 lists the particular dopants were assigned to respective composite pigment. During pigment synthesis, it was observed that depending on the type of dopant included there was a slight change in the color of the suspension as the reaction progressed. This color changes from a dark grayish green color to brownish grey. This color change can be attributed to the

organic corrosion inhibitor that doped the PPy backbone deposited on the aluminum flake. During the chemical oxidation of pyrrole the dispersion also displayed these various colors.

Table 6.1: List of dopants contained in the composite pigments studied

Composite	Dopant
Composite 1	4,5-dihydroxynaphthalene-2,7-disulfonic acid disodium salt
Composite 2	Sodium anthraquinone-2-sulfonate
Composite 3	4-hydroxybenzenesulfonic acid
Composite 4	1,2-dihydroxybenzene-3,5-disulfonic acid disodium salt monohydrate
Composite 5	Hydroquinonesulfonic acid potassium salt
Composite 6	As received aluminum flake (without a dopant)

6.4.1. Morphology and Elemental Analysis

Scanning electron micrographs of the composite pigments are displayed in Figure 6.1. Comparing the SEM micrographs of the composite pigments to the as-received aluminum flake, deposition of PPy was achieved for all composite pigments. It is evident that deposition of PPy onto aluminum flake varied depending on the organic corrosion inhibitor included in the pigment synthesis. The composite doped with 4-hydroxybenzenesulfonic acid (Figure 6.1c) demonstrated the lowest level of deposition of PPy while differences in deposition in the other samples were not noticeable.

Previous reports of aluminum flake-PPy pigments demonstrated that the corrosion inhibiting performance depended on both the level of deposition of PPy and the morphology. Previous reports by Jadhav et al. also displayed the ability to include long range wire morphologies could be obtained that showed improved corrosion inhibiting capabilities which was attributed to the long range connectivity of the PPy which would allow more effective transport of electrons.

In these SEM micrographs small wires were only apparent on composites containing the dopant anthraquinone-2-sulfonate (Figure 6.1b).

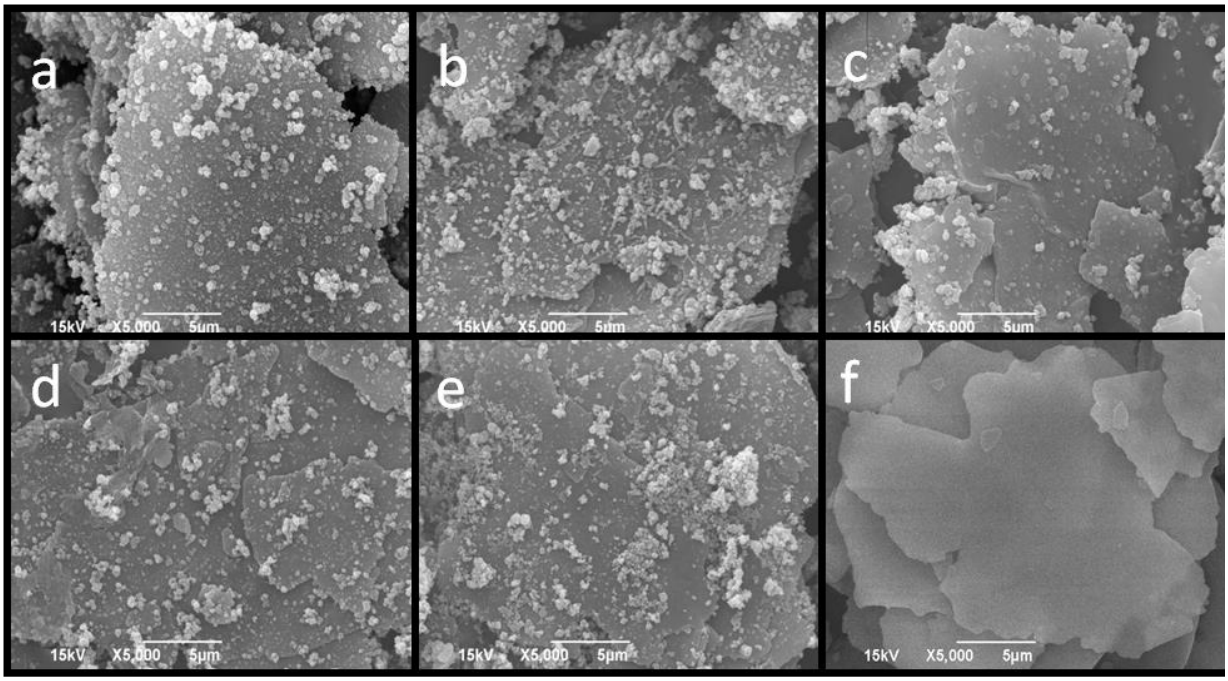

Figure 6.1: SEM micrographs of – (a) composite 1, (b) composite 2, (c) composite 3, (d) composite 4, (e) composite 5, and (f) composite 6.

To ensure the doping of PPy was achieved by the organic corrosion inhibitors elemental analysis of the composite pigments was conducted and the results are listed in Table 6.2. The carbon content that was observed on the bare aluminum flake is due to it being supplied with 1-methoxy-2-propanol treatment. For all composite pigments levels of nitrogen are detected. The high error associated with the nitrogen content is due to the peak being directly between carbon and oxygen in the EDS spectrum. The oxygen content is high for all composite pigments and as received aluminum flake. This is due to the natural aluminum oxide layer that forms when aluminum is subjected to the environment. The composite pigments synthesized all showed varying levels of sulfur content, which is attributed to the organic corrosion inhibitors as they all contain sulfonate groups.

Table 6.2: Elemental composition of Al-flake/PPy composites

Formulation	C		N		O		Al		S	
	Avg	Error	Avg	Error	Avg	Error	Avg	Error	Avg	Error
Composite 1	53.02	3.95	6.42	6.74	25.45	1.83	14.14	0.24	0.97	0.14
Composite 2	57.25	5.66	7.69	7.00	11.76	2.05	23.11	0.35	0.20	0.16
Composite 3	59.36	3.15	7.42	7.42	25.33	1.89	7.11	0.17	0.78	0.13
Composite 4	56.69	4.60	9.11	8.07	19.17	2.21	14.54	0.27	0.49	0.16
Composite 5	55.22	4.96	5.73	7.20	18.74	1.92	19.31	0.30	1.00	0.17
Composite 6	33.36	5.69	n/a	n/a	19.68	1.35	46.96	0.47	n/a	n/a

The differences in quantities of sulfur detected could be attributed to both the bulky nature of some of the organic corrosion inhibitors, as well as the weight percent of sulfur for each organic corrosion inhibitor. Composite 2 which is doped with anthraquinone-2-sulfonate showed the lowest level of sulfur content which could be attributed to the bulky nature of the anthraquinone group, resulting in ineffective doping into the PPy backbone. Composites 1 and 5 showed the highest level of sulfur present. Composite 1 incorporates 4,5-dihydroxynaphthalene-2,7-disulfonate which contains 2 sulfonate groups which might improve the chances of effective doping. Composite 5 is doped with hydroquinone sulfonate, a relatively small molecule dopant which should be more easily incorporated into the PPy backbone.

6.4.2. Electrical Properties

C-AFM scans are included in Figure 6.2. It is evident that in the deflection scans, the morphology of the PPy deposited onto the aluminum flake compared to the plain aluminum flake scan for composite 6. In addition to the morphology difference, all aluminum flake-PPy composite pigments showed observable levels of electrical conductivity while the plain aluminum flake displayed none. This is attributed to the fact that a native oxide layer exists on aluminum, which is inherently resistive and does not allow small potentials to pass through it. The conductive nature

of PPy on aluminum flakes surface will allow greater electrical connectivity between composite pigment particles.

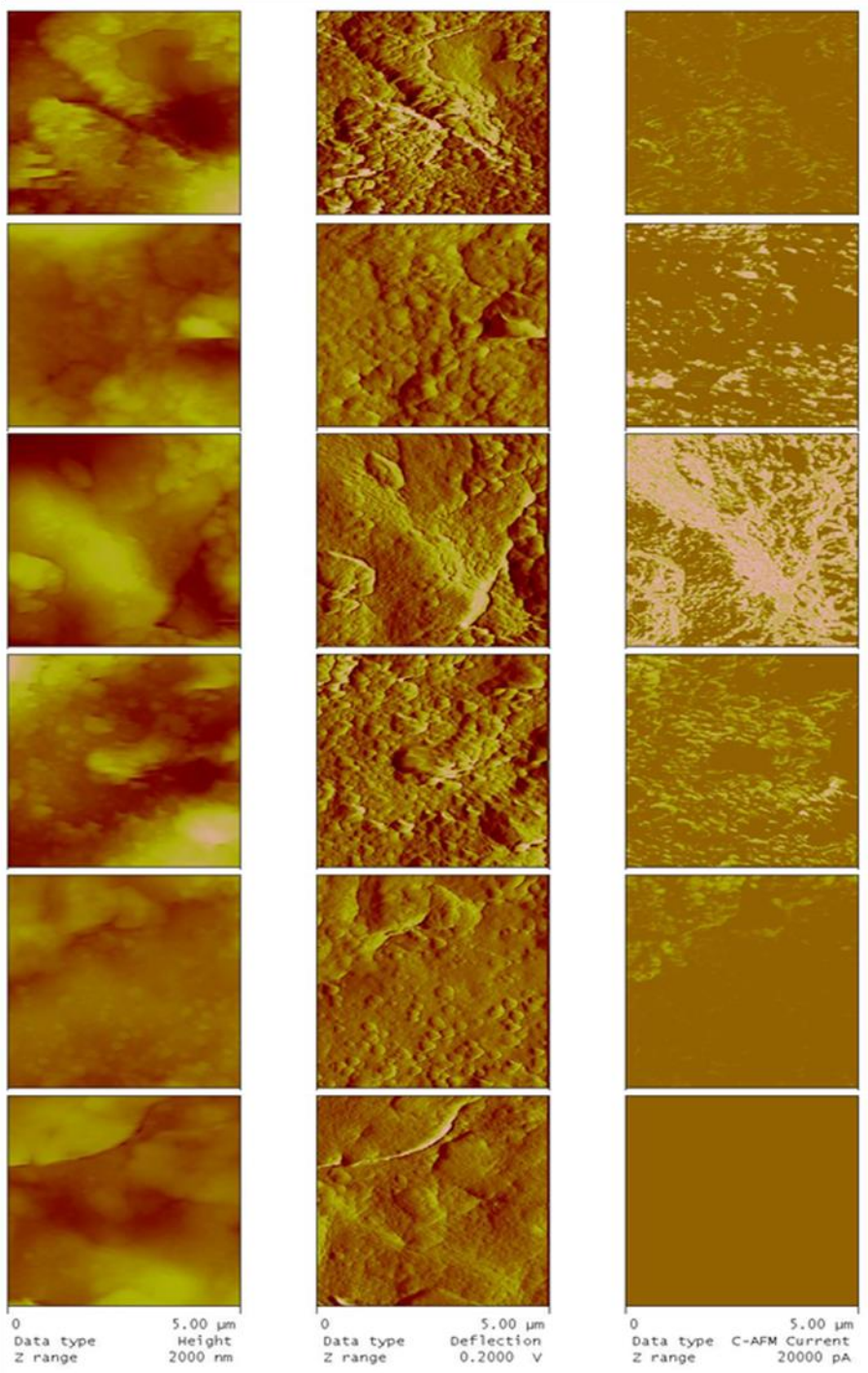

Figure 6.2: CAFM scans of height (left), deflection (middle), and current (right) images for composites 1 through 6 from top to bottom

6.4.3. Accelerated Weathering/Prohesion Studies

Accelerated weathering test methods are often used to simulate how a coating will protect a substrate in an aggressive environment without having to study samples for very long terms in outdoor environments. ASTM G85-A5, the Prohesion test, is a popular choice due to the aggressive nature that can deteriorate protective coatings fast to allow quicker determination of the best coating. In Figure 6.3, Prohesion results for scribed samples are displayed initially and after 672 hours of cyclic testing.

Coating formulation with composite 3 showed the least amount of corrosion inhibition as large blisters encompass most of the scribe and upon removal from the testing chamber some coating delaminated. This poor coating performance may be attributed to the fact this composite pigment showed the lowest level of PPy deposition of all of the composite pigments. Coating formulations containing the composite pigment doped with anthraquinone-2-sulfonate showed small blisters all along the scribe after 672 hours in Prohesion.

Coating formulations with PPy doped with 4,5-dihydroxynaphthalene-2,7-disulfonate, 1,2-dihydroxybenzene-3,5-disulfonate, and hydroquinonesulfonate displayed little to no blisters and only some corrosion product in the scribe even after 672 hours of exposure. Control coatings, which contained as received aluminum flake showed extensive corrosion product within the scribe. These control coatings also showed a loss of the reflective nature of the aluminum flakes indicating the aluminum flakes in the coating also corroded to form a thick aluminum oxide barrier.

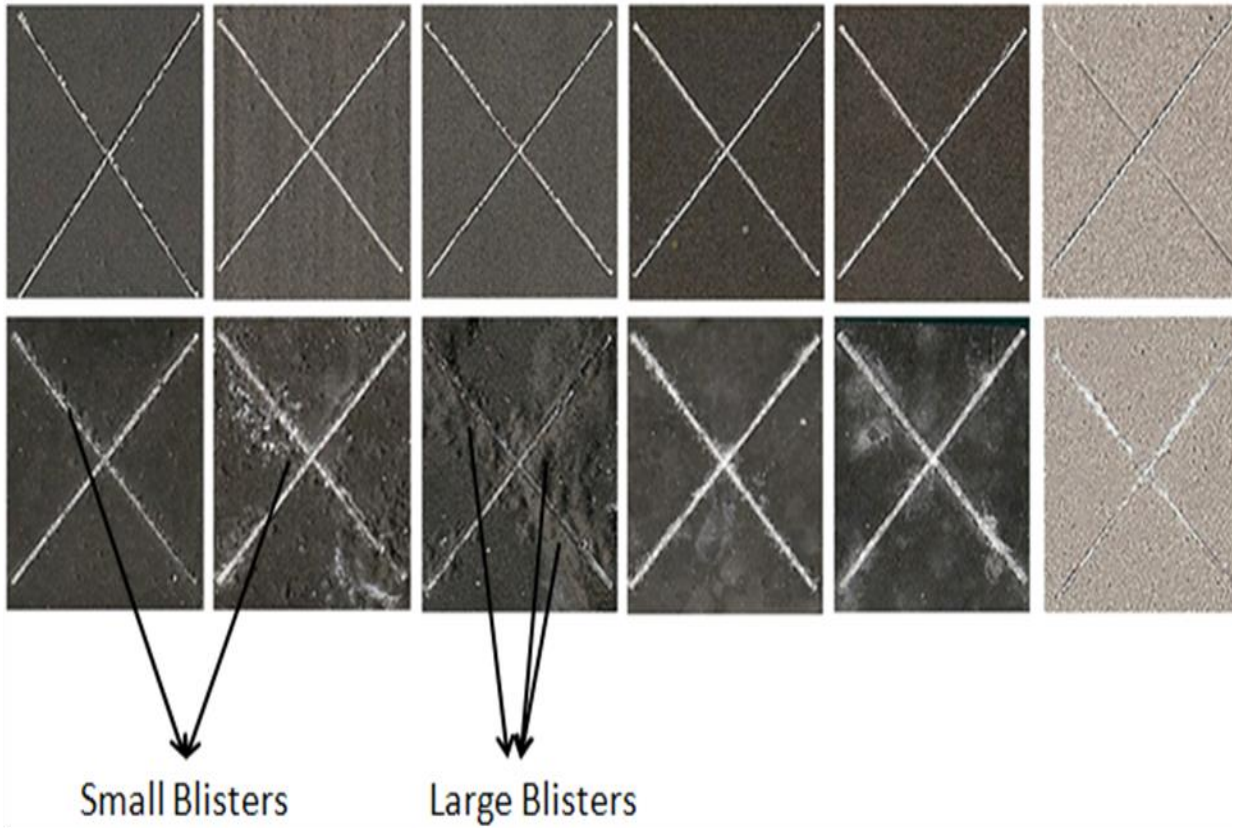

Figure 6.3: Prohesion results for coating formulations. Top row – 0h of exposure. Bottom row – 672 hours exposure. From left to right (composites 1 through 6).

6.4.4. Linear Polarization

Polarization scans for each coating are displayed in Figure 6.3. From this figure it is observed that a shift to more anodic corrosion potentials occurs when Al-PPy composite pigments are introduced into the system with respect to the control coatings containing only as received aluminum flake. This shift to more noble corrosion potentials indicates a passivation effect occurring, which is attributed to the inclusion of the conductive PPy clusters on the Al-flake pigment. This phenomena has been observed also by Gelling et al. when a solution of poly-3-octylpyrrole was cast onto Al-2024T3 panels.[33]

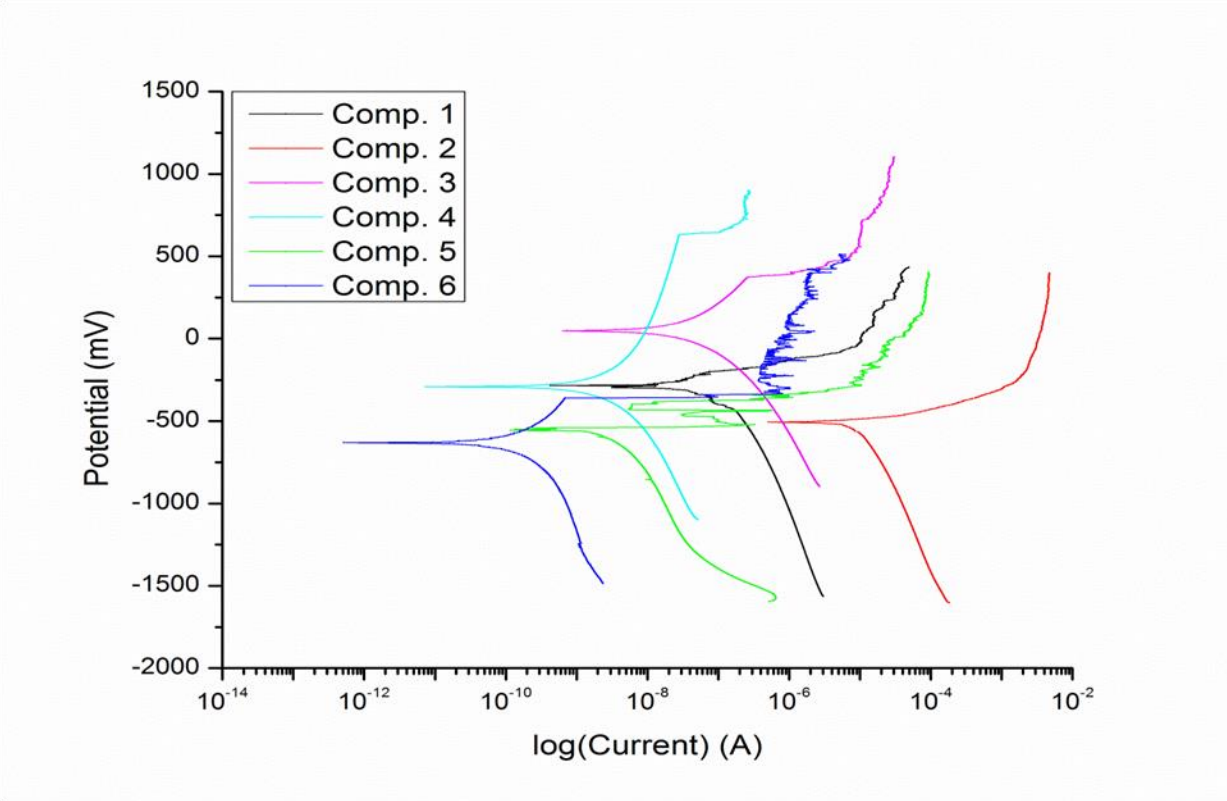

Figure 6.4: Polarization scans for coatings containing the composite pigments

The type of organic corrosion inhibitor also determines the magnitude of the noble shift in the corrosion potential. The values for the corrosion potentials and corrosion current are listed in Table 6.4. The strongest passivation effect was observed with the pigment doped with 4-hydroxybenzenesulfonic acid (composite 3). This passivation effect is believed to be short lived however as the accelerated wreathing tests showed the most blistering for the coatings containing this pigment. More work in studying the corrosion potential with respect to immersion time is needed to better understand how long the coatings can passivate the aluminum 2024 substrate. For all coatings containing Al-PPy composite pigments, the corrosion density was also shown to increase. This is due to the fact the Al-PPy composite pigments are electrically electrically

conductive thus allow an easier electrical pathway to occur between the substrate and the counter electrode and not due to a more porous coating.

Table 6.3: E_{corr} values for pigmented primers

Composite	E_{Corr} (mV)
Composite 1	-284
Composite 2	-505
Composite 3	46
Composite 4	-290
Composite 5	-560
Composite 6	-630

6.4.5. Electrochemical Impedance Spectroscopy

Bode plots are listed in Figures 6.5-7. The impedance for the primers Al-PPy composite pigments was about 2 orders of magnitude less than the impedance for primers containing unmodified aluminum flake. Analyzing these coatings traditionally would lead to the conclusion that these Al-PPy composite coatings are more porous and thus inferior. Visual assessments of Al-PPy composite pigment coatings that have undergone weathering tests however demonstrate the exact opposite and in fact the coatings containing Al-PPy composite pigments perform much better than the control versions. The low impedance of these coatings is determined to be due to the incorporation of the electrically conductive pigments. The low frequency AC signal applied during EIS favors the least resistive pathway through a material. In the case of organic coatings pigmented with Al-PPy composite pigments, the AC signal will traverse the coating through the pigments instead of the dielectric material. This effect has also been observed by others working with Al-PPy composite pigments.[31]

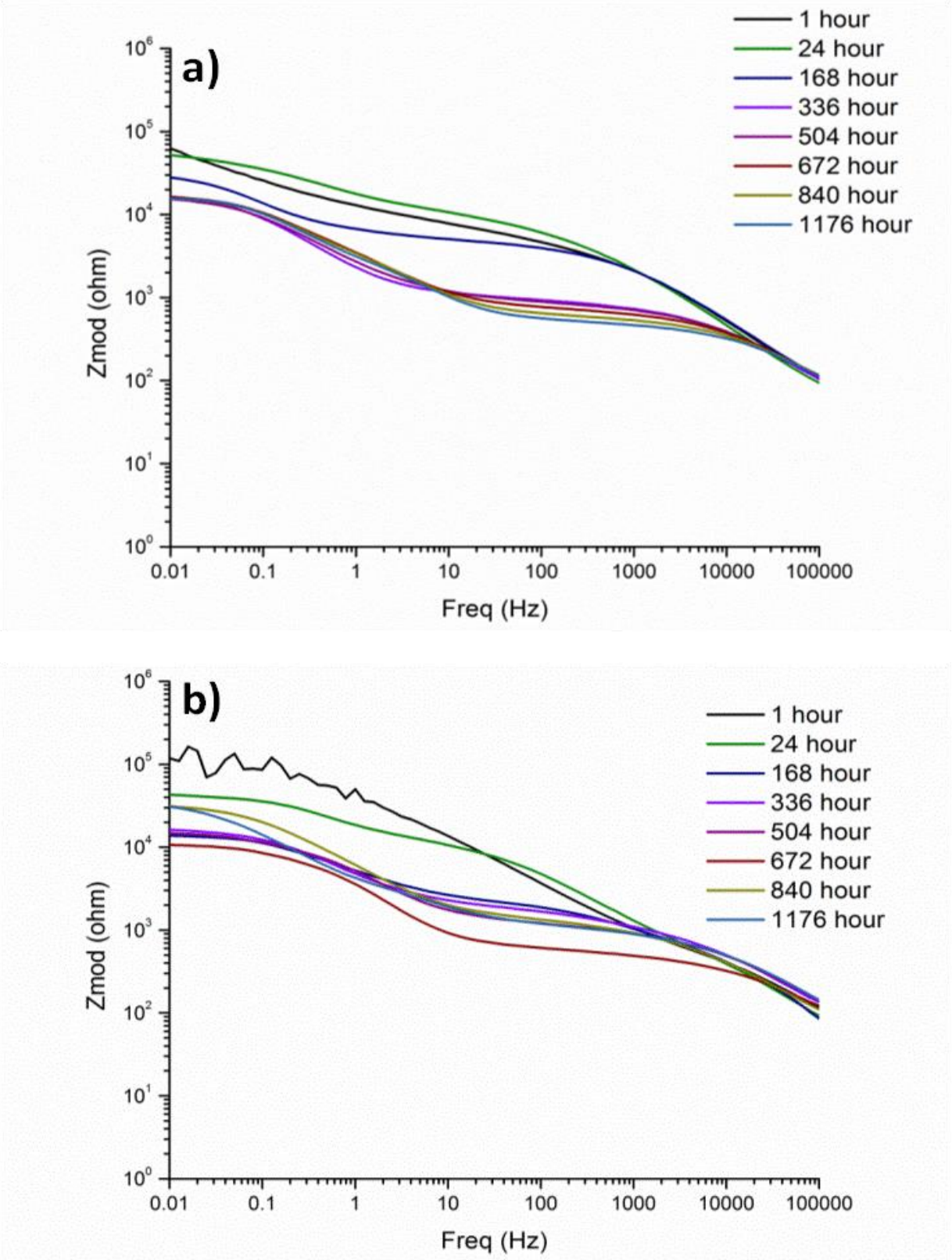

Figure 6.5: Bode plots for coatings containing composite 1 (a) and composite 2 (b).

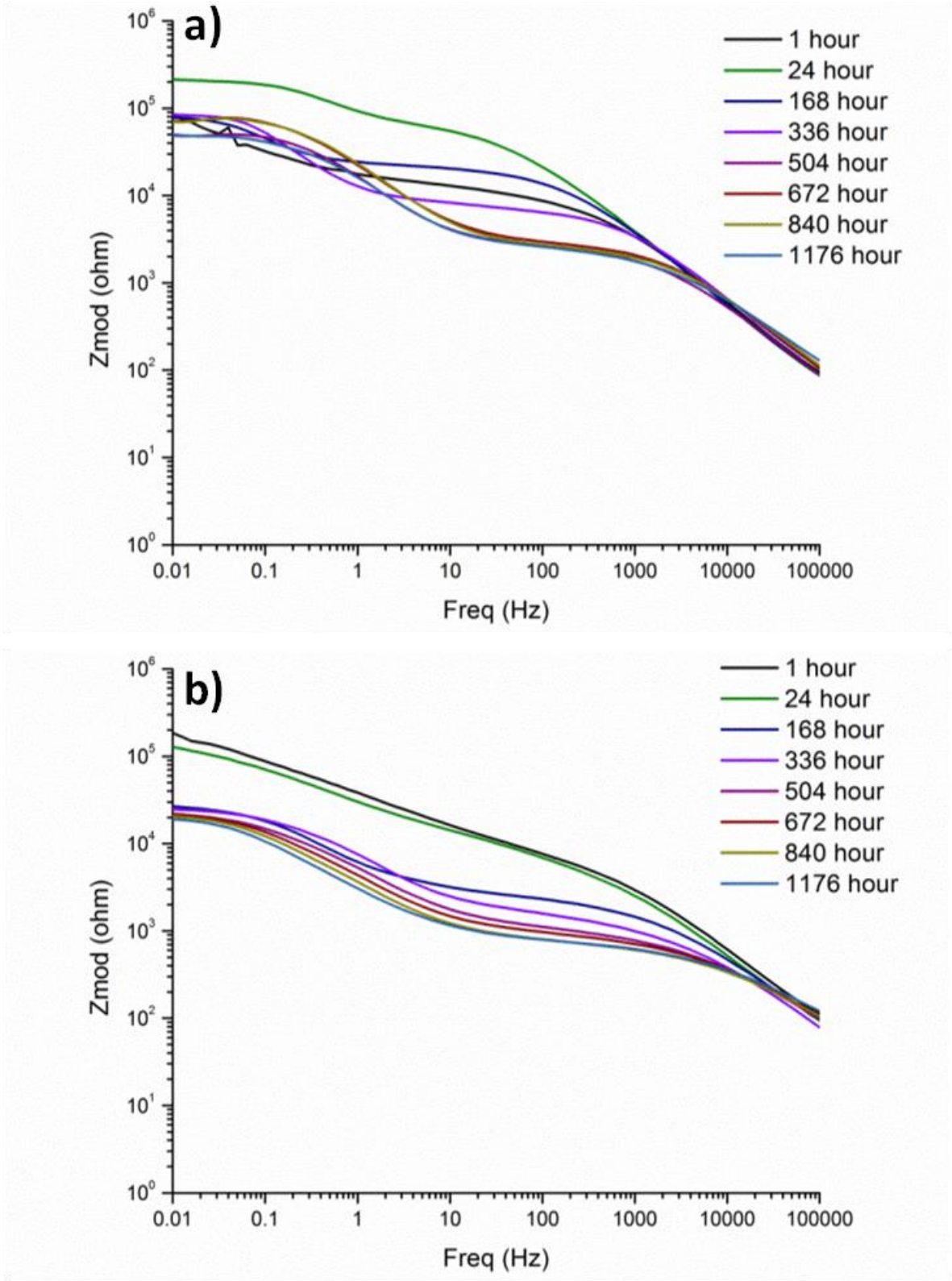

Figure 6.6: Bode plots for coatings containing composite 3 (a) and composite 4 (b).

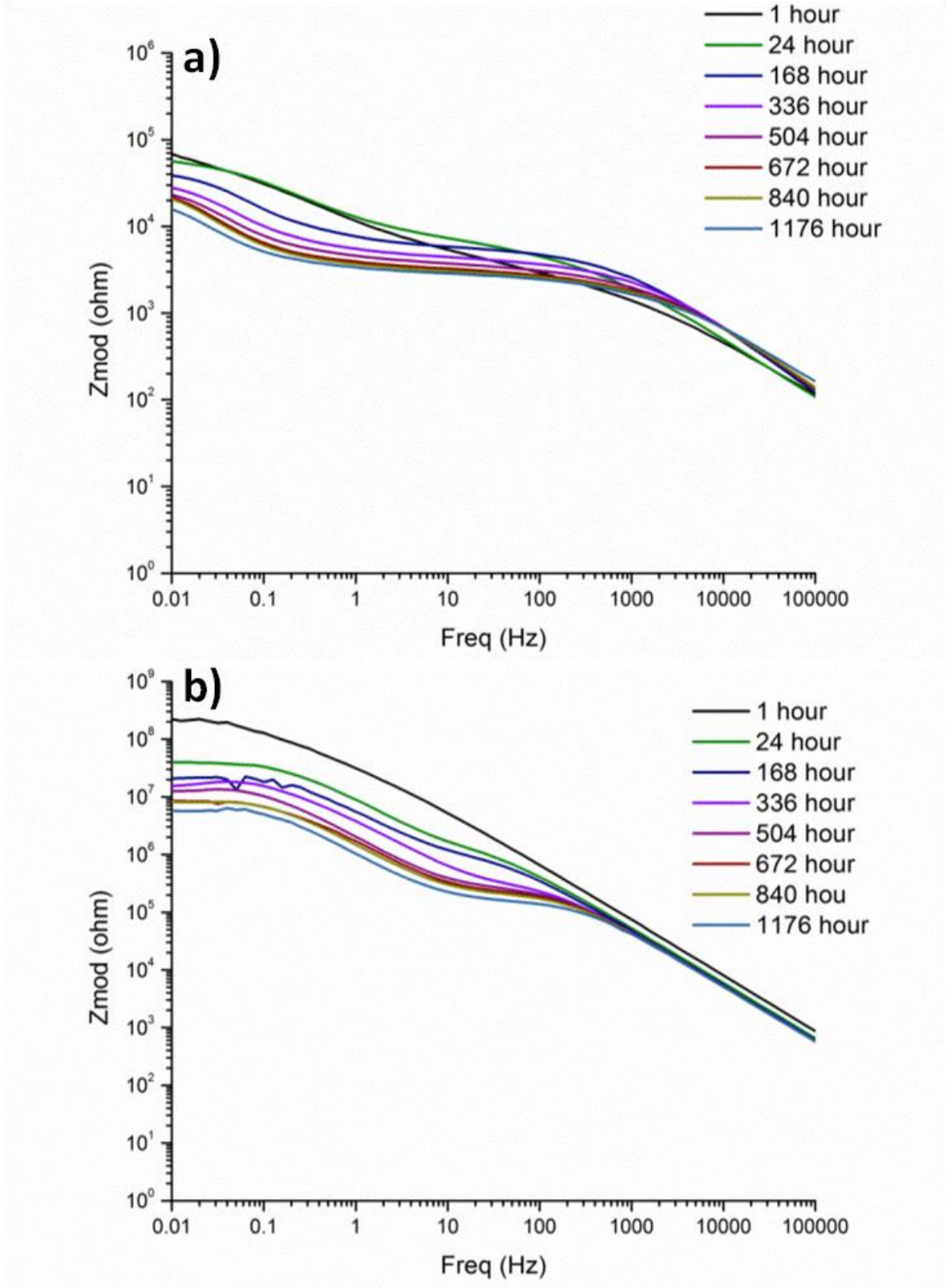

Figure 6.7: Bode plots for coatings containing composite 5 (a) and composite 6 (b).

The lower impedance values observed via EIS but superior performance in accelerated weathering tests indicated that the protection offered by coatings pigmented with Al-PPy composite pigments is not dependent on the barrier protective properties alone. Other mechanisms that could be involved in the improved corrosion protection are investigated further with SVET and galvanic coupling experiments.

In all samples after about 168 hours a two time constant system is observed. This means that in addition to the primer, electrolyte has reached the surface and an aluminum oxide layer developed. For coatings containing the pigment 1,2-dihydroxybenzene-3,5-disulfonate (composite 4) showed little to no change after 168 hours of immersion indicating the oxide layer that formed did not break down even after 1176 hours of immersion thus suggesting the Al-PPy composite pigment passivates the oxide layer preventing further breakdown and dissolution of the aluminum substrate. This theory correlates with the accelerated weathering tests where no blistering occurred even after 672 hours under prohesion conditions. Coatings containing the Al-PPy composite pigment doped with hydroquinonesulfonate (Composite 5) also displayed small changes after 168 hours at low frequency indicating good protection of the substrate.

Coatings containing the Al-PPy composite pigment doped with 4-hydroxybenzenesulfonic (Composite 3) acid showed an increase in the impedance after 24 hours. This impedance increase is believed to be development of an aluminum oxide film indicating poor corrosion protection. Further immersion in which a drop in impedance is observed is indicative of a breakdown of the oxide layer by the ingress of corrosive species further causing the dissolution of aluminum.

For the control coatings a sharp drop after 24 hours was visible. In addition to the noticeable decrease in impedance after 24 hours, two time constants are evident also indicating

electrolyte reached the substrate and an oxide layer was developing. As immersion time was extended a steady drop in impedance was observed until it dropped below 10^7 ohms. This further drop in impedance is the result of electrolyte permeating the oxide layer resulting in further dissolution of the Al-2024T3 substrate. This indicates that the coating with unmodified aluminum flake does not passivate the substrate, which demonstrates the need for depositing PPy onto the aluminum flakes to achieve an active coating.

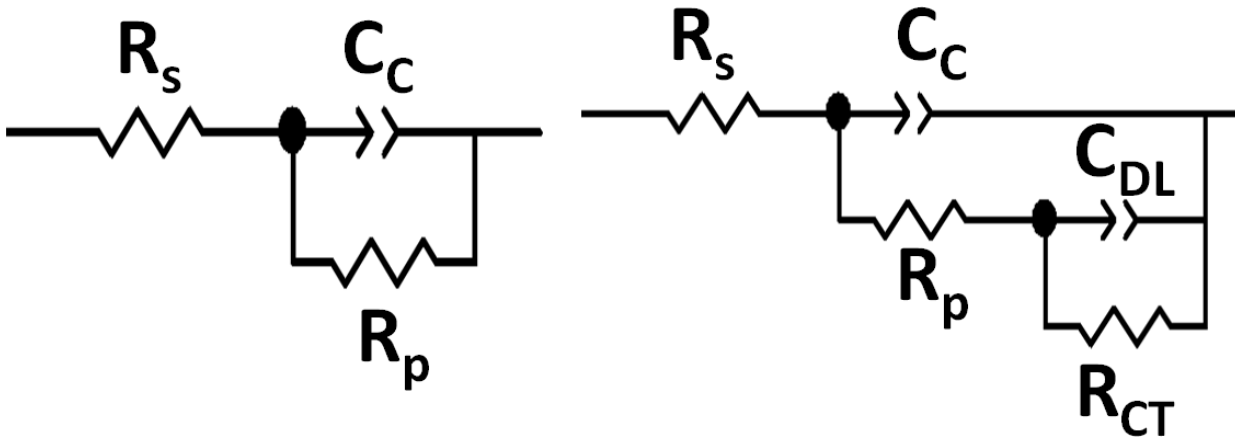

Figure 6.8: Equivalent circuit models used to model the EIS results of the coatings

To further analyze the corrosion inhibiting properties for these pigments the results from EIS were modeled to fit equivalent circuits. Figure 6.8 shows the circuit models used for modeling the EIS results. The typical Randle's cell on the left is the equivalent circuit used to model many coating systems. In this circuit R_s is the solution resistance of the electrolyte, C_c is the coating capacitance, and R_p is the pore resistance. This resistance is useful in determining the difficulty of the electrolyte to travel through the coating to the substrates surface. The other equivalent circuit model is used to explain a coating where electrolyte has permeated the coating and an oxide layer is developing. In this setup R_s, C_c, and R_p are the same as in the Randle's cell. C_{DL} is the double layer capacitance or the capacitance of the oxide layer that has developed. R_{CT} is the charge

transfer resistance which illustrates the difficulty of electrolyte permeating the oxide layer that has developed. It should be mentioned that aluminum oxide layers can act as a decent barrier to electrolyte ingress as they show excellent adhesion to aluminum metal.

Figure 9 is a graph of the R_p with respect to immersion time. For the coatings containing Al-PPy composite pigments a small increase is observed in the first few hours. It is suggested that this may be due to the fact that polypyrrole is first reduced from the oxidized (electrically conductive) form resulting is a less conductive coating. As electrolyte permeates the primer however the pore resistance of the coating decreases. The magnitude of this decrease is smaller in the coatings containing Al-PPy composite pigments due to the ability of the reduced PPy to consume dissolved oxygen resulting in slower corrosion rates.

From Figure 6.9 the coatings containing the Al-PPy composite pigments doped with anthraquinone-2-sulfonate (Composite 2) and 4-hydroxybenzenesulfonate (Composite 3) showed the largest drops in the pore resistance of all of the Al-PPy composite pigments. This is not surprising as the accelerated weathering studies showed these composite pigments displayed the worst corrosion protection of the pigments tested as shown in Figure 6.3. Coatings containing the FPPy pigment doped with hydroquinonesulfonate (Composite 5) displayed little to no change in the pore resistance even after 1176 hours indicating good protection of the substrate.

The control coatings that are pigmented with as received aluminum flake showed sharp decrease in the pore resistance after only 24 hours indicating the coating was porous and allowed electrolyte to permeate very quickly. The pore resistance continued to drop although at a much slower rate afterwards. This slower change in pore resistance after the initial drop is attributed to the development of both an oxide layer at the substrate surface, as well as an aluminum oxide layer on the aluminum flakes within the coating.

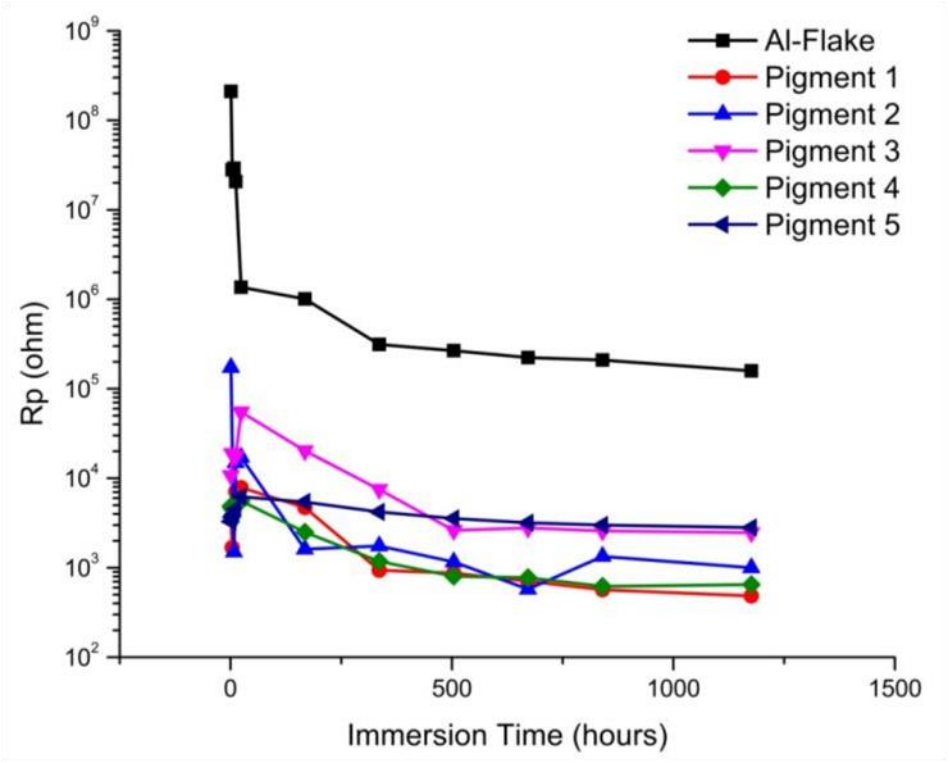

Figure 6.9: Pore resistance (R_p) for the pigmented coatings with respect to immersion time in DHS.

6.4.6. SVET Measurements

SVET experiments are useful for studying corrosion processes at a local level and yield information regarding the corrosion processes that occur, that cannot be obtained by the global electrochemical techniques such as EIS. Current density scans for coatings containing the pigments are displayed in Figures 6.10-11. For these SVET scans anodic peaks are a result of either anodic dissolution of aluminum or the oxidation of PPy. Cathodic peaks arise from the reduction of PPy or reduction of oxygen. In Figures 6.10 and 6.11 positive currents measured are indicative of anodic activity while negative currents indicated the presence of cathodic activity.

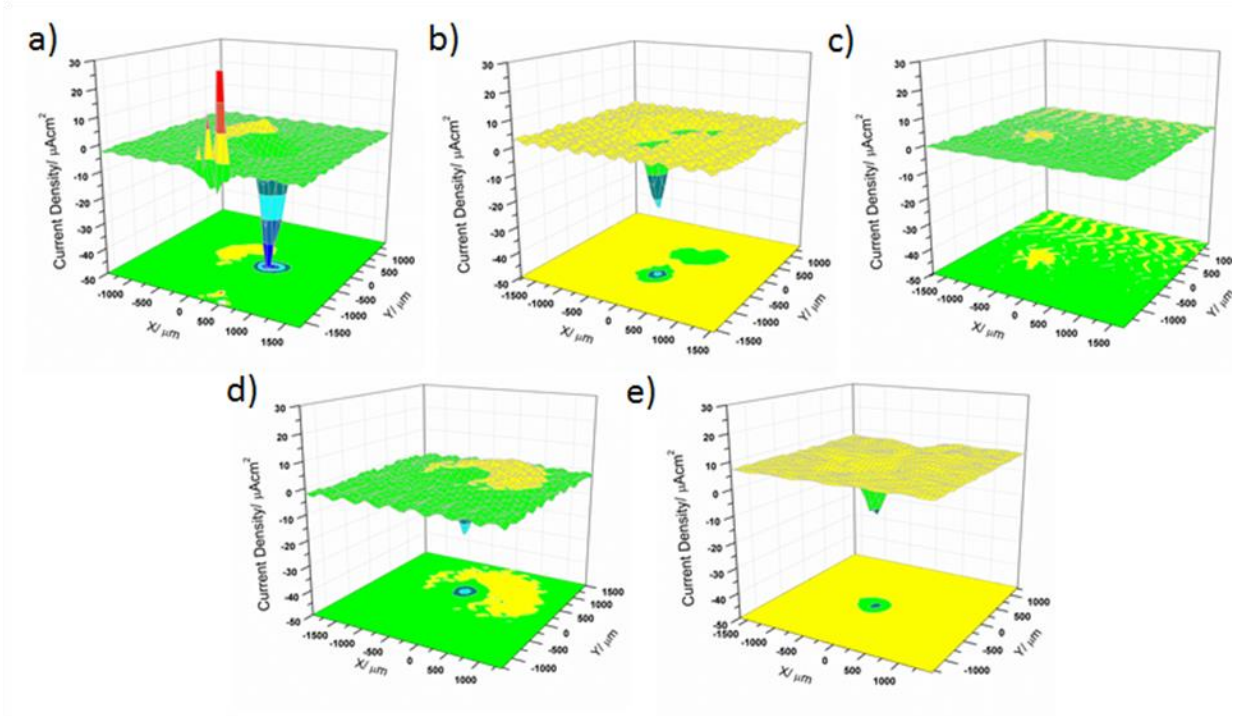

Figure 6.10: SVET images after 48 hours of immersion. Top – composite 1 (a), composite 2 (b), composite 3 (c). Bottom – composite 4 (d) and composite 5 (e).

Figure 6.10 provides scan results after 48 hours of immersion in 0.5% sodium chloride solution. For all coatings besides the coating containing the pigment doped with 4-hydroxybenzenesulfonate (Composite 3) a cathodic peak in the scribe was visible. This is a possible indication of galvanic protection, which has been witnessed in previous studies of these Al-PPy composite pigments. For all of these samples little to no current was apparent during the 0h scans. This lack of visible cathodic current is attributed to the induction time required for the coupling to take place. This induction time is discussed more during the galvanic coupling experiments. Outside of the scribe low levels (2-5 µA) of anodic current is slightly visible. This anodic current could be due to the oxygen scavenging mechanism that reduced PPy takes part in. Coatings with the pigment doped with 4,5-dihydroxynaphthalene-2,7-disulfonate (Composite 1)

shows a large anodic current away from the defect indicating large amounts of activity occurring there as well.

In Figure 6.11 are the SVET scan results for the initial (a) and 48 hours (b) for the control coatings pigmented with unmodified aluminum flake. These coatings display initially an anode and cathode in the scribe indicating corrosion has begun to occur. After 48 hours of immersion the scribe and parts around the scribe all show anodic current indicating further dissolution of the aluminum flake and substrate. These results indicate poor protection by the aluminum flake coatings compared to the cathodic protection of defects in coatings provided by coatings pigmented with these Al-PPy composite pigments.

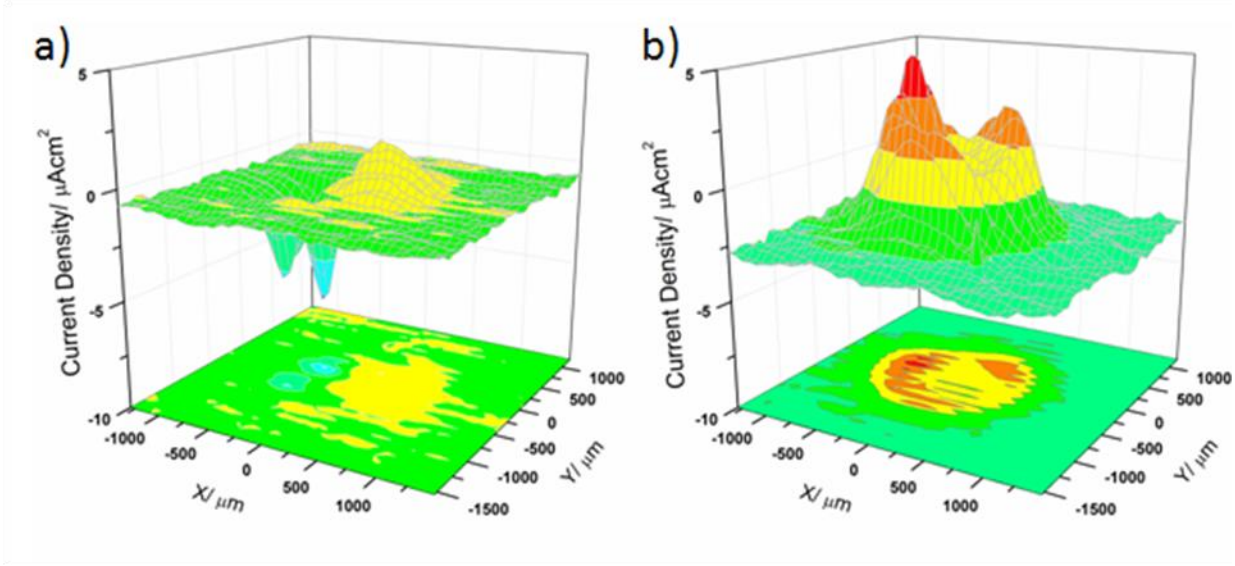

Figure 6.11: SVET images for coatings containing as recieved aluminum flake for 0 hour (a) and after 48 hours (b) immersion under 0.5% NaCl.

6.4.7. Galvanic Coupling Measurements

Previous work in the development of Al-PPy composite pigments demonstrated the ability of PPy to galvanically couple with the aluminum flake it is deposited onto. When the PPy comes into contact with electrolyte the PPy is reduced and the underlying aluminum flake is oxidized.

This activation effect has shown to cause the aluminum flakes in turn to act as a sacrificial pigment to protect the Al-2024T3 surface. During galvanic coupling experiments the DHS solution in the bare Al-2024T3 cell was aerated during testing to ensure oxygen was readily available at the surface of the substrate. For the cell connected to the coated substrate the solution was deaerated by purging with N_2. This experimental setup was designed to simulate the conditions of electrolyte that has permeated a coating to better understand the corrosion processes that occur.

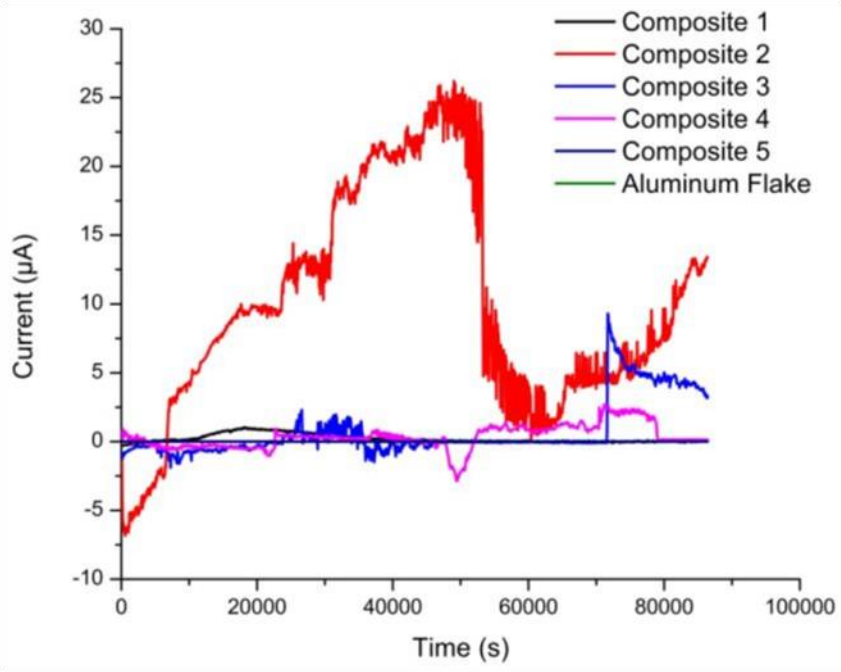

Figure 6.12: Galvanic coupling current generated between aluminum 2024T3 and aluminum flake-PPy coatings.

Figure 6.12 displays the results from the galvanic coupling experiments. Initially, all coating samples showed negative coupling potentials. This negative coupling current is attributed to the reduction of conductive PPy on initial immersion into electrolyte. Upon immersion in DHS, there is an initial inductance period until the coupling current begins to rise and show a positive coupling current indicating cathodic protection. From the scans presented in Figure 6.10 the only

coating showing significant coupling current within 24 hours of immersion were the coating with the dopant anthraquinone-2-sulfonate.

Coatings containing the pigment doped with 4,5-dihydroxynaphthalene-2,7-disulfonate (Composite 1) showed an increasing coupling current upon testing until a max current of about 1.5 µA was reached after about 20,000 seconds. The coupling current steadily decreased over the remaining testing cycle indicating a loss of cathodic protection. This is not surprising as the coatings containing this composite pigment demonstrated poor protection in the Prohesion testing.

The other coatings show coupling currents maxing around 1-2 µA after 24 hours but showed significant fluctuations over the 24 hour immersion period. This difference in the magnitude of coupling currents is believed to be attributed to the fact the pigment doped with anthraquinone-2-sulfonate had the highest level of PPy deposition onto the aluminum flake as observed by the SEM, as well as also had noticeable segments of a wire-like morphology of PPy deposited onto the aluminum flake unlike the other composite pigments synthesized.

Previous work by Jadhav et al. demonstrated composite pigments with the wire like morphology showed higher coupling currents than spherical PPy pigments as well as showing a lower induction period than spherical PPy pigments.[32] In those studies, spherical PPy pigments had an induction period of greater than 24 hours. Upon completion of the galvanic coupling experiments the aluminum 2024 substrates were washed and dried. An optical photograph in Figure 6.13 shows the surface differences.

The substrate examined with coatings containing as received aluminum flake showed noticeable amounts of white aluminum oxide as well as discoloration ranging from dark to light regions indicating corrosion has begun occurring. The substrates investigated with coatings containing Al-PPy composite pigments showed little to no discoloration even after 24 hours of

testing. This suggests that even though low levels of galvanic current were detected, the bare Al-2024T3 substrate was still protected. This result further confirms these pigments display an active mechanism in the protection of Al-2024T3 substrates. Future studies at longer immersion times should show increases in the coupling current as the induction period ends.

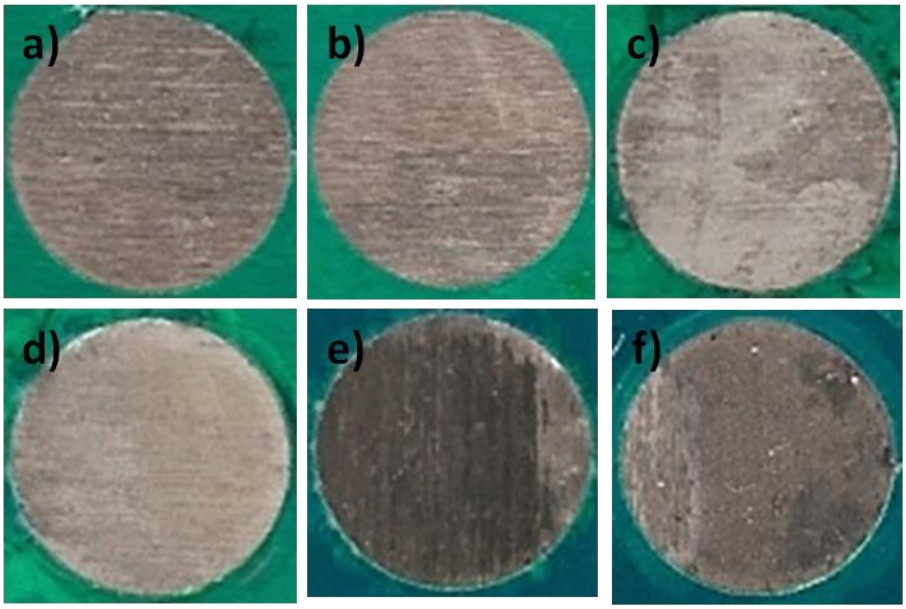

Figure 6.13: Optical micrograph for aluminum 2024T3 substrates upon completion of galvanic coupling experiment.

6.5. Conclusions

Al-PPy composite pigments were successfully synthesized and the organic corrosion inhibitors effectively doped the polypyrrole by the conformation from the EDS results. Morphology experiments indicated the deposition of PPy onto the aluminum flake and even unique wire morphology was observed on samples. Conductive AFM studies showed the PPy deposited onto the aluminum flake was in the oxidized form due to the conductivity observed. Pigmented epoxy primers were formulated and coated onto Al-2024T3 panels to study the corrosion protection afforded by the coatings. Electrochemical techniques indicated superior performance

for the coatings with Al-PPy pigments compared to the control coatings with unmodified aluminum flake. SVET results demonstrated cathodic protection for all composite pigments except for those doped with 4-hydroxybenzenesulfonate. Accelerated weathering tests indicated excelled performance for the pigments doped with 1,2-dihydroxybenzene-3,5-disulfonate and hydroquinonesulfonate. Galvanic coupling measurements shows long induction times and need to be further studied to find where the induction period ends.

6.6. Acknowledgements

The researchers would like to thank the Army Research labs for providing the funding under the grant number W911NF-11-2-0027.

6.7. References

1. Koch, G. H.; Brongers, M. P.; Thompson, N. G.; Virmani, Y. P.; Payer, J. H. *Corrosion cost and preventive strategies in the United States*; 2002.

2. Nakai, M.; Eto, T., New aspect of development of high strength aluminum alloys for aerospace applications. *Materials Science and Engineering: A* 2000, *285* (1), 62-68.

3. Chen, G.; Gao, M.; Wei, R., Microconstituent-induced pitting corrosion in aluminum alloy 2024-T3. *Corrosion* 1996, *52* (1), 8-15.

4. Kendig, M.; Jeanjaquet, S.; Addison, R.; Waldrop, J., Role of hexavalent chromium in the inhibition of corrosion of aluminum alloys. *Surface and Coatings Technology* 2001, *140* (1), 58-66.

5. Dayan, A.; Paine, A., Mechanisms of chromium toxicity, carcinogenicity and allergenicity: review of the literature from 1985 to 2000. *Human & Experimental Toxicology* 2001, *20* (9), 439-451.

6. Kasten, L.; Grant, J.; Grebasch, N.; Voevodin, N.; Arnold, F.; Donley, M., An XPS study of cerium dopants in sol–gel coatings for aluminum 2024-T3. *Surface and Coatings Technology* 2001, *140* (1), 11-15.

7. Voevodin, N.; Jeffcoate, C.; Simon, L.; Khobaib, M.; Donley, M., Characterization of pitting corrosion in bare and sol–gel coated aluminum 2024-T3 alloy. *Surface and Coatings Technology* 2001, *140* (1), 29-34.

8. Vreugdenhil, A.; Balbyshev, V.; Donley, M., Nanostructured silicon sol-gel surface treatments for Al 2024-T3 protection. *Journal of Coatings Technology* 2001, *73* (915), 35-43.

9. Voevodin, N.; Grebasch, N.; Soto, W.; Kasten, L.; Grant, J.; Arnold, F.; Donley, M., An organically modified zirconate film as a corrosion-resistant treatment for aluminum 2024-T3. *Progress in Organic Coatings* 2001, *41* (4), 287-293.

10. Nanna, M. E.; Bierwagen, G. P., Mg-rich coatings: a new paradigm for Cr-free corrosion protection of Al aerospace alloys. *JCT research* 2004, *1* (2), 69-80.

11. Chiang, C.; Fincher, C.; Park, Y.; Heeger, A.; Shirakawa, H.; Louis, E.; Gau, S.; MacDiarmid, A. G., Electrical conductivity in doped polyacetylene. *Physical Review Letters* 1977, *39* (17), 1098-1101.

12. Spanggaard, H.; Krebs, F. C., A brief history of the development of organic and polymeric photovoltaics. *Solar Energy Materials and Solar Cells* 2004, *83* (2), 125-146.

13. Rogers, J.; Katz, H., Printable organic and polymeric semiconducting materials and devices. *Journal of Materials Chemistry* 1999, *9* (9), 1895-1904.

14. Wang, G.; Zhang, L.; Zhang, J., A review of electrode materials for electrochemical supercapacitors. *Chemical Society Reviews* 2012, *41* (2), 797-828.

15. Zarras, P.; Anderson, N.; Webber, C.; Irvin, D.; Irvin, J.; Guenthner, A.; Stenger-Smith, J., Progress in using conductive polymers as corrosion-inhibiting coatings. *Radiation Physics and Chemistry* 2003, *68* (3), 387-394.

16. Tallman, D. E.; Spinks, G.; Dominis, A.; Wallace, G. G., Electroactive conducting polymers for corrosion control. *Journal of Solid State Electrochemistry* 2002, *6* (2), 73-84.

17. Spinks, G. M.; Dominis, A. J.; Wallace, G. G.; Tallman, D. E., Electroactive conducting polymers for corrosion control. *Journal of Solid State Electrochemistry* 2002, *6* (2), 85-100.

18. Nguyen Thi Le, H.; Garcia, B.; Deslouis, C.; Le Xuan, Q., Corrosion protection and conducting polymers: polypyrrole films on iron. *Electrochimica acta* 2001, *46* (26), 4259-4272.

19. Lu, W.-K.; Elsenbaumer, R. L.; Wessling, B., Corrosion protection of mild steel by coatings containing polyaniline. *Synthetic Metals* 1995, *71* (1), 2163-2166.

20. Kalendová, A.; Veselý, D.; Stejskal, J., Organic coatings containing polyaniline and inorganic pigments as corrosion inhibitors. *Progress in Organic Coatings* 2008, *62* (1), 105-116.

21. Selvaraj, M.; Palraj, S.; Maruthan, K.; Rajagopal, G.; Venkatachari, G., Polypyrrole as a protective pigment in organic coatings. *Synthetic Metals* 2008, *158* (21), 888-899.

22. Li, P.; Tan, T.; Lee, J., Corrosion protection of mild steel by electroactive polyaniline coatings. *Synthetic Metals* 1997, *88* (3), 237-242.

23. Tallman, D. E.; Levine, K. L.; Siripirom, C.; Gelling, V. G.; Bierwagen, G. P.; Croll, S. G., Nanocomposite of polypyrrole and alumina nanoparticles as a coating filler for the corrosion protection of aluminium alloy 2024-T3. *Applied Surface Science* 2008, *254* (17), 5452-5459.

24. Truong, V.-T.; Lai, P.; Moore, B.; Muscat, R.; Russo, M., Corrosion protection of magnesium by electroactive polypyrrole/paint coatings. *Synthetic Metals* 2000, *110* (1), 7-15.

25. Liu, H.; Ye, H.; Zhang, Y.; Tang, X., Preparation and characterization of poly (trimethylolpropane triacrylate)/flaky aluminum composite particle by in situ polymerization. *Dyes and Pigments* 2008, *79* (3), 236-241.

26. Mahmoudian, M.; Basirun, W.; Alias, Y.; Ebadi, M., Synthesis and characterization of polypyrrole/Sn-doped TiO< sub> 2</sub> nanocomposites (NCs) as a protective pigment. *Applied Surface Science* 2011, *257* (20), 8317-8325.

27. Sathiyanarayanan, S.; Azim, S. S.; Venkatachari, G., A new corrosion protection coating with polyaniline–TiO< sub> 2</sub> composite for steel. *Electrochimica acta* 2007, *52* (5), 2068-2074.

28. Hosseini, M.; Raghibi-Boroujeni, M.; Ahadzadeh, I.; Najjar, R.; Seyed Dorraji, M., Effect of polypyrrole–montmorillonite nanocomposites powder addition on corrosion performance of epoxy coatings on Al 5000. *Progress in Organic Coatings* 2009, *66* (3), 321-327.

29. Qi, X.; Vetter, C.; Harper, A. C.; Gelling, V. J., Electrochemical investigations into polypyrrole/aluminum flake pigmented coatings. *Progress in Organic Coatings* 2008, *63* (3), 345-351.

30. Yan, M.; Vetter, C. A.; Gelling, V. J., Electrochemical investigations of polypyrrole aluminum flake coupling. *Electrochimica acta* 2010, *55* (20), 5576-5583.

31. Jadhav, N.; Vetter, C. A.; Gelling, V. J., Characterization and Electrochemical Investigations of Polypyrrole/Aluminum Flake Composite Pigments on AA 2024-T3 Substrate. *ECS Transactions* 2012, *41* (15), 75-89.

32. Jadhav, N.; Vetter, C. A.; Gelling, V. J., The effect of polymer morphology on the performance of a corrosion inhibiting polypyrrole/aluminum flake composite pigment. *Electrochimica acta* 2013, *102*, 28-43.

33. Gelling, V. J.; Wiest, M. M.; Tallman, D. E.; Bierwagen, G. P.; Wallace, G. G., Electroactive-conducting polymers for corrosion control: 4. Studies of poly (3-octyl pyrrole) and poly (3-octadecyl pyrrole) on aluminum 2024-T3 alloy. *Progress in Organic Coatings* 2001, *43* (1), 149-157.

CHAPTER 7. SUMMARY

ECPs are seen as a suitable replacement to traditional metallic materials in a variety of areas such as printable electronics, anti-static technologies, and corrosion inhibition. With regards to printable electronics, ECPs offer a more cost effective route to the development of electrically conductive inks that could be utilized in the advancement of inkjet printing of simplistic circuit boards and furthering the development of flexible electronics. The goal of the first two chapters in this work was to determine the efficacy of photopolymerization of pyrrole to polypyrrole. This system's main benefits were due to the lack of dispersion issues of pigment particles as well as long term stability due to the requirement of UV-light to induce polymerization. Combining pyrrole with UV-curable resins allowed the development of composites with enhanced physical and electrical properties. The resulting coatings however, were only able to obtain semi-conductor like electrical properties thus limiting them to possible anti-static uses. In addition, these coating systems were not protective of Al 2024T3 due to the silver inclusions that resulted during the photopolymerization mechanism.

For corrosion inhibition, two different routes in utilizing PPy as a corrosion inhibiting pigment were also investigated. The first route traveled was to functionalize PPy as a reactive pigment thus forming chemical bonds with the coating matrix. This was thought to help improve the barrier protection properties of UV-Curable coatings. Initial tests with different reactive surfactants (surfmers) helped uncover the most optimum surfer for improved physical properties. EIS and accelerated weathering techniques further proved that the enhancement of physical properties showed a direct correlation in the barrier protective properties of these coatings. Further ladder studies were conducted to try to find the optimum reaction parameters in the synthesis of

PPy_BisomerSEM. These studies concluded that a wide window with regards to pH is available for the synthesis with little to no effect on the protective properties of the pigment.

Lastly, Jadhav's work at NDSU was continued on to study how Al-flake/PPy composite pigments doped with organic corrosion inhibitors helped protect Al-2024T3. Advanced electrochemical studies with SVET demonstrated cathodic protection for all composite pigments except for those doped with 4-hydroxybenzenesulfonate. In, addition accelerated weathering studies demonstrated that primers containing pigments doped with 1,2-dihydroxybenzene-3,5-disulfonate and hydroquinonesulfonate proved to provide the best protection of Al 2024T3.

In summation, a variety of techniques were utilized PPy as a functional pigment in organic coating matrices. The aforementioned work allows new coating systems based of environmentally friendly materials that could one day act as suitable replacements to currently utilized technologies.

CHAPTER 8. FUTURE WORK

With the amount of diversity with respect to the experiments above there is quite a few different avenues that could investigated for future work. With regards to photopolymerization of ECPs, there are numerous other ECP precursors that have not yet been studied. From the list only thiophene has been shown in literature to not photopolymerize in the presence of silver salts. In addition, only free radical polymerized resins were used in conjunction with pyrrole for these coatings thus other technologies such as cationic UV-curable systems could also be implemented. Initial studies in the use of cationic photoinitiators such as iodonium and diphenyl sulfonium salts were looked at as possible photo-oxidants of pyrrole. These studies however only showed the successful synthesis of pyrrole oligomers and had very low yields of PPy (1-2 wt%).

Crosslinkable ECPs can also be developed from the traditional ECP precursors due to the convention chemical oxidation mechanism that was used. Polyaniline (PANI) would be an attractive choice due to the ability to synthesize color shifting pigments. This could lead to the development of UV-curable pH/chemical sensors, as well as primers that can indicate where corrosion is occurring due to the inherent nature of PANI.

Lastly, Al-Flake/PPy composited with organic corrosion inhibiting anions should be investigated further for real world corrosion protection. Accelerated weathering techniques do not correlate directly to real world tests; thus these coatings should be subjected to a South-Florida like environment with high humidity to see how they protect over the course of several years. In addition, studying these coatings over a variety of chromate pretreatments would give the best real world indication of how these primers stack up to conventional primer technologies.

Also other composite pigments derived from PANI and Thiophene should also be looked at for the corrosion protection of Al 2024T3. PANI would be an ideal candidate for smart primer

technology as if we can get the protective properties observed on the SVET and GC experiments, we would be one step close to a primer that signals where corrosion is occurring.